The impact of lee waves on the Southern Ocean circulation and its sensitivity to wind stress

Luwei Yang

Grad. Dip. Mar. Sci., B.Sc.

Institute for Marine and Antarctic Studies
University of Tasmania

Submitted in fulfilment of the requirements for the degree of
Doctor of Philosophy

October 2019

To my parents.

Declaration

Declaration of originality

This thesis contains no material which has been accepted for a degree or a diploma by the University or any other institution, except by way of background information and duly acknowledged in the thesis, and to the best of my knowledge and belief, no material previously published or written by another person except where due acknowledgment is made in the text of the thesis, nor does the thesis contain any material that infringes copyright.

Signed:
Luwei Yang
PhD Candidate
Institute for Marine and Antarctic Studies (IMAS)
University of Tasmania
Date: October 25, 2019

Statement of co-authorship

The following people and institutions contributed to the publication of work undertaken as part of this thesis:

Luwei Yang (Candidate), University of Tasmania, ARC Centre of Excellence for Climate System Science

Maxim Nikurashin (Primary Supervisor), University of Tasmania, ARC Centre of Excellence for Climate Extremes.

Andy Hogg (Co-supervisor), Australian National University, ARC Centre of Excellence for Climate Extremes.

Bernadette Sloyan (Co-supervisor), CSIRO Oceans and Atmosphere.

Author details and their roles:

Paper 1 Energy Loss from Transient Eddies due to Lee Wave Generation in the Southern Ocean.

Located in Chapter 2

Luwei Yang was the primary author and contributed 65% to the planning execution and preparation of the research project and subsequent paper.

Maxim contributed to the collection of the topographic data, Andy the collection of the global ocean model data, and Bernadette the collection of the observational data. Luwei did all the calculations and drafted the paper. All the authors contributed to the analysis and interpretation of the research data and contributed to the interpretation of the work by critically revising the paper.

We the undersigned agree with the above stated "proportion of work undertaken" for the above published peer-reviewed manuscripts contributing to this thesis:

Signed:	Signed:
Dr. Maxim Nikurashin	**Prof. Neil Holbrook**
Supervisor	Head, Centre for Oceans & Cryosphere
Institute for Marine and Antarctic Studies	Institute for Marine and Antarctic Studies
University of Tasmania	University of Tasmania
Date: October 25, 2019	Date: October 25, 2019

Authority of access

Luwei Yang

October 2019

Acknowledgements

During my PhD journey, I have gradually grown to be a mature researcher. I have also learned a lot beyond scientific skills and knowledge, such as how to make friends with stress and how to maintain work-life balance. All these would not have happened without the support from my supervisors, colleagues, friends, and family. Therefore I would like to thank them for being there for me, offering help for me to overcome frustrations, and celebrating my achievements with me. I feel very lucky that I was never alone during this journey and I am truly grateful for their company.

I would like to thank my primary supervisor, Max Nikurashin, for being such an amazing supervisor for last four years. I came to Australia on my own not knowing any friend, it was Max who picked me up from the airport, helped me with paperwork, and introduced me to other students and colleagues. It was Max who first made me feel welcome in an unfamiliar environment. Because of his kind help, I was able to adjust to the new environment and delve into my research project in a very early stage. I was also constantly inspired by Max's enthusiasm towards science, which was such a delight in the days when I was lack of motivation. Other than the tremendous help he provided for me to write this thesis, I also appreciate his guidance, encouragement, and patience over the years. Apart from his contribution to my PhD research, I am also thankful for the advice he gave me on my career based on his own experience.

I am also grateful to my co-supervisor, Andy Hogg. Thanks to Andy for joining the team, attending our fortnight video-conferences, and hosting me for my one-week visits at the Australian National University (ANU). Thank Andy for his regular contributions to my research despite the geographical distance. The computational resources offered by Andy and technical support I received from his group, especially from Angus and Aidan, were invaluable to my PhD research and this thesis, especially on the challenging parts like implementing parameterisations. Thank Andy also for introducing me to his lovely group at ANU, where I had opportunities to have conversations with Alice Barthel, Angus Gibson, Callum Shakespeare, Cat Vreugdenhil, Josué Moreno, Mainak Mondol, Navid Constantinou, and Taimoor Sohail about their research. I would also like to thank Andy's group for their hospitality. It was always sad and hard to say goodbye to the group. Thank Andy for taking

me to the group retreat in Kosciuszko National Park, which was an extremely excellent experience.

My thanks also go to my co-supervisor, Bernadette Sloyan. Thank Bernadette for always being very generous with her time. Thank Bernadette for always reminding me of my priorities and timeline when I was overwhelmed. Thank Bernadette for our inspiring conversations when I had low self-confidence. Thank Bernadette for our conversations where I got to know my strengths and weaknesses. Thank Bernadette for offering me an opportunity to volunteer in a GO-SHIP voyage, where I saw the amazing views of the South Pacific Ocean, learned a lot about ocean observations, and realised the hardship every crew member has to endure. With this experience, I am more appreciative of the effort that goes into collecting observational data and its value.

I would also like to thank the visitors to the group, Andrew Stewart, Ali Mashayek, David Munday, and Scott Bachman, with whom I had illuminating discussions; I would also like to thank Xuebin Zhang and Russell Fiedler from CSIRO, who kindly offered help when I got stuck running my configuration to a steady state. A special thank to Molly, a psychologist who helped me in a very professional yet empathetic way when I was so frustrated that I wanted to give up; the counselling sessions I had with her really helped me to relax from stress, rebuild my self-confidence, and make my determination.

Thanks to my wonderful friends at IMAS, Ajitha Cyriac, Ana Berger, Asher Riaz, Chen Zhao, Doreen Warjri, Gabi Pilo, Jiale Lou, Ram Patel, Wilma Huneke, Yu Hong, and Tze Low, with whom I went hiking, camping, and travelling, with whom I had relaxing lunch breaks, coffee breaks, and endless chats. The friendship definitely helped me to survive in PhD. I would also like to thank my roomies Claire Kavic and Yusra Saleem, who made our share house feel like a home and made me less homesick.

I would like to thank my parents for always supporting me from the northern hemisphere. I am really thankful for the time, money, and effort they invested to guarantee that I received good education from a very young age. I appreciate that they let me choose my own career path, encourage me to dream big yet take small steps to achieve my goals.

Abstract

The westerly wind over the Southern Ocean has been strengthening and shifting poleward for the last few decades. It remains an outstanding problem to understand the response of the Antarctic Circumpolar Current (ACC) and Southern Ocean Meridional Overturning Circulation (MOC) to the changing wind conditions, noting that the local changes in the Southern Ocean will have remote impacts on global ocean and climate through the interbasin connection and the exchange of heat and carbon with the atmosphere. The response of the Southern Ocean circulation to the changing wind is regulated by the energetic eddy field, which acts to transfer momentum, heat, and tracers horizontally and to transfer momentum vertically. These eddy effects are particularly important for the Southern Ocean in the latitudinal band of Drake Passage. Therefore, the sensitivity of the Southern Ocean circulation to wind stress is usually explored using eddy-permitting and eddy-resolving global ocean models, where eddy generation is well resolved. However, eddy-resolving models do not fully represent the dynamics of eddy energy dissipation. A potential route of eddy energy dissipation occurs in the deep ocean where deep-reaching eddies interact with small-scale topography, generating internal lee waves. It is suggested that lee waves sustain mixing in the deep Southern Ocean and apply a drag on the time-mean flow of the ACC. In this study, we evaluate the role of lee waves for the dissipation of transient eddies in the Southern Ocean and investigate the impacts of lee waves on the Southern Ocean circulation and its response to changes in wind stress.

Using linear lee wave theory, abyssal hill topographic datasets, and bottom velocity from a global eddy-resolving model, we estimate the contribution of lee waves to the dissipation of transient eddies. The results show that the energy dissipation of the eddy field due to lee wave generation (0.12 TW) exceeds its dissipation due to bottom friction in the turbulent bottom boundary (0.05 TW), and that lee waves make a stronger contribution to the dissipation of transient eddies (0.12 TW) than to the dissipation of the time-mean ACC (0.04 TW).

We then develop an energetically consistent lee wave drag and mixing parameterisation and use it in an idealised, eddy-resolving model of the Southern Ocean to investigate the impact of lee waves on the ACC and MOC and their response to changes in wind stress. The results show that adding lee waves to the model increases the baroclinic transport of the ACC

by over 60 Sv (by 40%). The results are explained by the eddy kinetic energy (EKE) balance in which the EKE dissipation by the lee wave drag is compensated by the enhanced EKE generation through baroclinic instability of the ACC, and hence isopycnal slope, leading to an increase in the ACC transport. We find that the lee-wave-driven mixing plays a minor role in the baroclinic ACC transport increase but has a significant impact on the overturning circulation and deep stratification. The parameterisation of lee waves significantly alters the sensitivity of the baroclinic ACC transport and lower overturning circulation to wind stress. The baroclinic ACC transport increases with wind stress in the presence of lee waves, in contrast to the reference case where the eddy saturation is reproduced without lee waves. The lower overturning circulation increases considerably with wind stress, contrary to the decrease found in the reference case without lee waves. We also find a coupling between lee wave drag and lee-wave-driven mixing, through bottom stratification and bottom kinetic energy. The coupling effect leads to a nonlinear combination of the effect from each component and demonstrates that both drag and mixing effects need to be parameterised to properly represent the impact of lee waves on the Southern Ocean circulation.

Our results show that lee waves are an important player in the eddy energy balance in the Southern Ocean and regulate the strength of the ACC, MOC, and how they respond to the changing climate. These findings suggest that the presence of lee waves in global eddy-resolving ocean models can improve the representation of the eddy field, the Southern Ocean circulation and its sensitivity to changing climate. Hence, lee waves need to be parameterised in the global ocean models.

Table of contents

List of figures

List of tables

Chapter 1

Introduction

The eddy field plays an important role in the Southern Ocean by transferring momentum, heat, and tracers horizontally and vertically (Olbers et al., 2004). The eddy energy generation mechanisms are well-understood and captured by global eddy-resolving ocean models, however, the processes governing the eddy energy loss and subsequent energy transfer to small-scale turbulence and mixing remain uncertain (Ferrari and Wunsch, 2009). A potential route to dissipation may occur in the deep ocean where deep-reaching eddies interact with rough small-scale topography, generating internal lee waves (Bell, 1975; Ferrari and Wunsch, 2009; Naveira Garabato et al., 2004; Nikurashin and Ferrari, 2010b; Nikurashin et al., 2013; Sheen et al., 2014; Sloyan, 2005; St. Laurent et al., 2012). These lee waves have been suggested to extract energy from eddies to sustain water mass transformation in the Southern Ocean (de Lavergne et al., 2016; Meyer et al., 2015; Nikurashin and Ferrari, 2013) and apply a drag on the time-mean flow of the Antarctic Circumpolar Current (ACC) (Naveira Garabato et al., 2013). For the last few decades, the westerly winds over the Southern Ocean have been observed to increase (Böning et al., 2008), leading to a stronger eddy field (e.g., Hogg et al., 2015; Meredith and Hogg, 2006). Modelling studies have suggested that the strengthening of the eddy field results in a nearly insensitive ACC transport and less sensitive Meridional Overturning Circulation (MOC) under the changing climate (Abernathey et al., 2011; Böning et al., 2008; Dufour et al., 2012; Farneti et al., 2010, 2015; Morrison and Hogg, 2013). Given the potentially significant energy loss from eddies to lee waves at rough topography, the response of the Southern Ocean circulation to varying winds might also be regulated by lee waves through the eddy field. However, these processes have not been completely implemented in global ocean models and therefore the effects of lee waves on the Southern Ocean circulation remain poorly understood. In this thesis, we parameterise lee waves into an eddy-resolving ocean model and study the impact of lee waves on the Southern Ocean circulation and its sensitivity to changes in wind stress.

1.1 The role of the Southern Ocean in the global circulation and climate

The Southern Ocean plays an important role in the global ocean circulation and climate (Rintoul, 2018; Rintoul et al., 2001; Rintoul and Naveira Garabato, 2013). The importance of the Southern Ocean has been linked to two aspects of its circulation. Firstly, the lack of a lateral boundary at the latitude of the Drake Passage permits the existence of a strong eastward ACC, which connects three main ocean basins and isolates Antarctica from the warm water to the north (Rintoul and Naveira Garabato, 2013). Secondly, the interbasin connection provided by the Southern Ocean and the strong atmospheric forcing in this region result in a global MOC. The Southern Ocean overturning rate exerts a major control on heat and carbon exchange between the deep ocean, which has a huge heat and carbon storing capacity, and atmosphere, which largely influences the biosphere and human activities (Frölicher et al., 2015; Talley et al., 2016). The special structure of the ACC and the MOC makes the Southern Ocean unique in the global ocean circulation and climate.

The ACC has a distinct structure in the global ocean circulation and plays a pivotal role in the Southern Ocean dynamics. The ACC is a generic description for a set of deep zonal circumpolar fronts (Orsi et al., 1995) driven by westerly winds (Allison et al., 2010; Gill, 1968) and surface buoyancy fluxes (Hogg, 2010; Rintoul et al., 2001). The circumpolar structure leads to the following roles of the ACC in the Southern Ocean dynamics. Firstly, the ACC acts as a barrier between the high latitudes and the warm water flowing poleward from subtropical gyres in the western boundary currents (e.g., the East Australian Current, Agulhas Current, and Brazil Current). This results in the isolation and cooling of Antarctica (Rintoul et al., 2001). Secondly, steered by large topographic features, the ACC forms standing meanders upstream and downstream of major topographic features (Ivchenko, 1996). Standing meanders provide bottom form stress that largely balances the wind stress at the surface (Masich et al., 2015; Munk and Palmén, 1951). Standing meanders are important in setting local dynamics that modifies the stratification, bottom speed, and the vertical structure of the mean flow in the Southern Ocean (Thompson and Naveira Garabato, 2014). Standing meanders have also been suggested by Thompson and Naveira Garabato (2014) and shown by Dufour et al. (2012) and Bishop et al. (2016) to drive an overturning circulation that moderates the increase in the wind-driven overturning following recent trends in wind stress over the Southern Ocean. Thirdly, the instability of the ACC generates a strong transient eddy field. The transient eddy field redistributes heat and other properties across the ACC (e.g., Griffies et al., 2015; Hausmann and Czaja, 2012; Patel et al., 2019; Phillips and Rintoul, 2000; Watts et al., 2016), transfers momentum downwards (Olbers et al., 2004), and controls

the response of the ACC and the MOC to changing climate (e.g., Farneti and Delworth, 2010; Farneti et al., 2010; Gent, 2015; Hallberg and Gnanadesikan, 2006; Meredith and Hogg, 2006; Morrison and Hogg, 2013; Munday et al., 2013; Viebahn and Eden, 2010). Standing and transient eddies are not evenly distributed along the ACC and are characterised by local hotspots (Fig. 1.1), highlighting the importance of local dynamics on the Southern Ocean (e.g., Rintoul, 2018; Tamsitt et al., 2016; Thompson and Naveira Garabato, 2014).

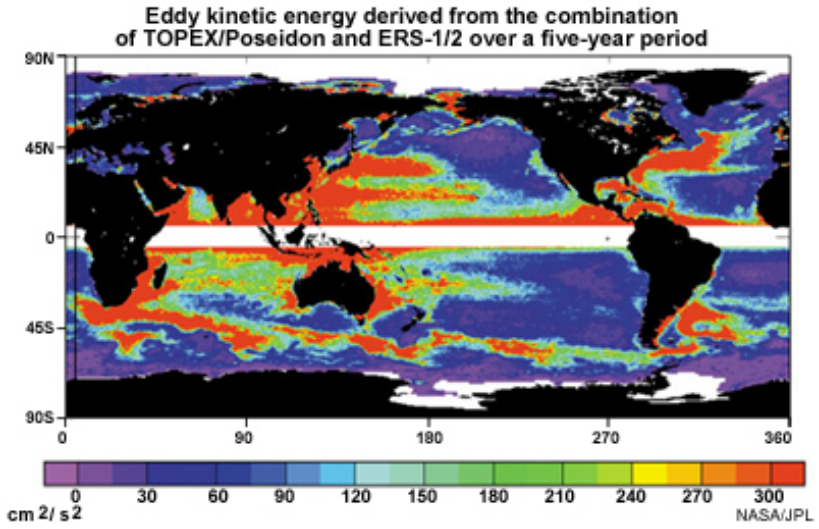

Fig. 1.1 Global eddy kinetic energy (EKE) derived from the combination of TOPEX/Poseidon and ERS-1/2 over a five-year period (source: https://www.eumetsat.int/jason/print.htm). Several EKE hotspots can be seen in the Southern Ocean.

The Southern Ocean limb of the MOC, simplified as a double-celled structure (Fig. 1.2), also plays a significant role in the Southern Ocean dynamics (Lumpkin and Speer, 2007; Marshall and Speer, 2012; Sloyan and Rintoul, 2001a,b; Speer et al., 2000). The double-celled structure is a result of a complex interaction of wind and buoyancy forcing, eddies, stratification, and topography (Rintoul and Naveira Garabato, 2013, and references therein). Driven by atmospheric forcings and partly compensated by the eddy field (e.g., Hallberg and Gnanadesikan, 2006), the upper cell consists of a wind-driven overturning circulation and an eddy-induced overturning circulation. The net overturning is referred to as the residual-mean circulation (Marshall and Radko, 2003). Driven by deep water formation near Antarctica and diapycnal mixing in the abyssal ocean (Lumpkin and Speer, 2007; Sloyan and Rintoul, 2001b), the lower cell is regulated primarily by the surface buoyancy and wind forcing, sea ice formation, and the breaking of internal waves in the ocean interior (Marshall and Speer, 2012; Nikurashin and Ferrari, 2013). While the upper cell is largely adiabatic in the ocean interior with the residual overturning circulation following isopycnals, the lower cell is intrinsically diabatic with mixing and water mass transformation taking place in the abyssal

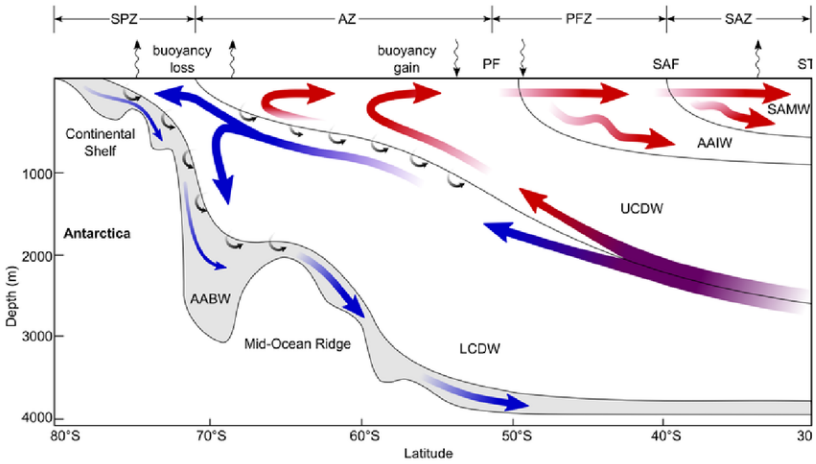

Fig. 1.2 A schematic view of the MOC in the Southern Ocean (Speer et al., 2000).

ocean (de Lavergne et al., 2016; Kunze, 2017; Lumpkin and Speer, 2007; Marshall and Speer, 2012; Sloyan and Rintoul, 2001a). The strength of both cells is believed to be controlled by the transient eddy field under the changing atmospheric conditions (Marshall and Speer, 2012; Sheen et al., 2014). However, the lower overturning circulation remains poorly measured and understood (Cessi, 2019). Recently, the 3D structure of the Southern Ocean overturning circulation is better depicted via observations and idealised modelling (Ferrari et al., 2017; Talley, 2013; Thompson et al., 2016). It is also shown that the overturning circulation is constrained by the distribution of bottom topography (de Lavergne et al., 2017).

In summary, the Southern Ocean circulation (the ACC and the MOC) is controlled by the balance amongst wind and buoyancy forcing, eddies, stratification, and topography (Rintoul and Naveira Garabato, 2013, and references therein). While the ACC and the MOC are two different components of the Southern Ocean circulations governed by different dynamics, they are not independent from each other. In addition to both circulations being forced by wind and buoyancy forcing, they are connected through eddies; eddies are generated from the instability of the ACC and contribute to the saturation of the ACC transport as westerlies increase (e.g., Farneti et al., 2010; Meredith and Hogg, 2006); eddies also induce the overturning circulation, which opposes and compensates changes in the wind-driven overturning circulation in response to increasing winds (e.g., Hallberg and Gnanadesikan, 2006; Morrison and Hogg, 2013).

1.2 Eddy control of the Southern Ocean circulation under the changing climate

The observations have shown that the wind stress above the Southern Ocean has been increasing over the last few decades and shifting poleward, indicated by the positive phase of the Southern Annular Mode (Böning et al., 2008; Thompson and Solomon, 2002). Given the role of the Southern Ocean in global climate, such as heat and carbon uptake as discussed in section 1.1, the response of the Southern Ocean circulation to changing wind stress has a big impact on the global climate.

Recent studies have shown that the increasing energy input to the Southern Ocean by winds only leads to slight changes in both ACC transport and overturning circulation (e.g., Bishop et al., 2016; Farneti and Delworth, 2010; Farneti et al., 2010; Gent, 2015; Hallberg and Gnanadesikan, 2006; Meredith and Hogg, 2006; Morrison and Hogg, 2013; Munday et al., 2013; Viebahn and Eden, 2010). The extra energy input in the ocean is verified to generate a stronger eddy field (Meredith and Hogg, 2006; Morrison and Hogg, 2013). The insensitivity of the ACC and the upper MOC, referred to as *eddy saturation* (Straub, 1993) and *eddy compensation* (Viebahn and Eden, 2010), respectively, imply that the eddy field regulates the response of the Southern Ocean circulation to changes in wind stress.

The regulation of the eddy field on the ACC is understood via its generation, through both baroclinic and barotropic instability (Constantinou, 2018; Marshall et al., 2017). The baroclinic control on the ACC transport is well understood and is considered as the main reason for the eddy saturation phenomenon (e.g., Marshall et al., 2017). As wind stress increases, the extra energy input to the Southern Ocean is stored as the available potential energy (APE) in the sloping isopycnals, which is then converted to EKE due to baroclinic instability. The release of APE flattens isopycnals and thereby keeps the transport unchanged. Recently, Constantinou (2018) argued that the eddy saturation can occur even in the barotropic flow, when the baroclinicity was absent. The two important factors for the eddy saturation to occur in the barotropic model were geostrophic contours and the height of topography. The author found eddy saturation in the barotropic flow when geostrophic contours were open and the height of topography satisfied the conditions to excite barotropic-topographic instability. Both baroclinic control and barotropic control maintain the transport by allowing the eddy generation and removing extra energy input from the wind.

The regulation of the eddy field on the upper overturning circulation is achieved through the diabatic eddy flux (Karsten and Marshall, 2002). Stronger winds tend to accelerate the wind-driven overturning circulation; however, a stronger eddy field generated by a more

baroclinic ACC leads to a stronger eddy-induced overturning circulation, i.e., eddy thickness fluxes of isopycnal layers, which opposes the wind-driven overturning circulation.

The regulation of the eddy field on the lower overturning circulation is achieved through diapycnal mixing. Theories predicted that the lower overturning circulation weakens with wind stress (Ito and Marshall, 2008; Nikurashin and Vallis, 2011). However, as suggested by Saenko et al. (2012) and shown by (Stanley and Saenko, 2014), the lower overturning circulation increased with wind stress if a fraction of eddy energy was provided for diapycnal mixing in the ocean interior. In the presence of the energy link between the eddy and mixing fields, an increase in eddy energy leads to an intensification of turbulent mixing and therefore a strengthening of the lower overturning circulation.

Given the role of the eddy field in the sensitivity of the Southern Ocean circulation to changes in wind stress, it is important to represent the eddy field accurately. The simulation of eddy energy generation has been improved by increasing the horizontal resolution. A higher horizontal resolution leads to a better-resolved eddy field and thus lowers the sensitivity of the zonal transport to increasing wind stress (Hallberg and Gnanadesikan, 2001, 2006; Tansley and Marshall, 2001). The horizontal resolution of a model has been found to significantly affect the structure of the overturning circulation and the extent of eddy compensation (Farneti et al., 2010; Hallberg and Gnanadesikan, 2006; Morrison and Hogg, 2013; Munday et al., 2013). Additionally, a typical 2-3 year delay of the eddy response found in observations (Meredith et al., 2004) and modeling studies (Meredith and Hogg, 2006; Screen et al., 2009) also means that non-eddy-resolving models are unable to reproduce eddy behaviors on a longer timescale, such as the eddy flux of heat. Hogg et al. (2008) found that the eddy heat flux exceeded the Ekman heat flux and thus warmed the ocean in the longer term, despite the instantaneous cooling following the increased wind stress. By examining the poleward heat flux using model runs at coarse to eddy-resolving resolutions, Screen et al. (2009) found that the poleward heat flux was efficiently enhanced in the high-resolution runs as the eddy-driven temperature response was better captured, which led to the warming south of the Polar Front on the longer timescales.

As coarse-resolution models do not resolve eddies, the eddy-induced along-isopycnal diffusivity is parameterised as per Gent and McWilliams (1990). By introducing eddy parameterisations, coarse resolution models are able to capture the eddy compensation phenomenon as eddy-resolving models do (Farneti and Gent, 2011; Gent and Danabasoglu, 2011; Hofmann and Morales Maqueda, 2011). The problem with eddy parameterisations is that, while the eddy compensation is achieved with a temporal-and-spatial varying eddy transfer coefficient, the eddy saturation is destroyed as isopycnal slopes are deliberately changed in order to have an eddy-induced overturning circulation that counteracts the wind-

driven overturning circulation. However, as discussed Treguier et al. (2010), low resolution models also fail to reproduce the processes of water mass transformation near Antarctica that might be as important in setting the ocean response as wind forcing.

Eddy energy is also determined by how and where eddy energy is removed. Current representation of eddy energy dissipation mechanisms is very poor in the global eddy-permitting and eddy-resolving ocean models. Improving our understanding of eddy energy dissipation mechanisms and implementing parameterisations to remove eddy energy in the ocean remain challenging; however, the parameterisations of eddy energy dissipation mechanisms potentially have an impact on the eddy energy balance and, through the eddy field, on the Southern Ocean circulation and its sensitivity to changes in wind stress.

1.3 The generation of internal lee waves by geostrophic flows

A potential dissipation route for geostrophic eddies in the abyssal Southern Ocean is the generation of lee waves by the interaction of geostrophic flows and small-scale topography. Topographic obstacles of horizontal scale of 1-10 km and with steepness satisfying the sub-critical condition (the topographic slope is smaller than the internal wave slope) permit strong bottom flow to go over the topography to generate lee waves. By disturbing the isopycnals above topography, an internal wave signal can propagate upward. The net topographic form drag and energy loss from background flow resulting from lee wave generation are predicted by linear lee wave theory (Bell, 1975).

Previous studies estimated the global energy conversion rate from geostrophic flows to internal lee waves using model outputs and current meter data, and found that the generation of internal lee waves was dominated by the Southern Ocean (Nikurashin and Ferrari, 2011; Scott et al., 2011; Wright et al., 2014). Nikurashin and Ferrari (2011) estimated a global energy conversion rate of 0.2 TW from geostrophic flows to internal lee waves and to which the Southern Ocean contributed more than 50%. Scott et al. (2011) produced higher generation rates of internal lee waves (0.34-0.49 TW), which were also dominated by the Southern Ocean. These two offline estimates were based on the same theory (Bell, 1975), but used bottom geostrophic velocity fields from different eddy-resolving ocean models, different topography datasets, and different background stratification. Regardless of the differences, both studies agreed that the generation of internal lee waves at the small-scale topography was an important source for turbulent mixing in the Southern Ocean and suggested that this process was a significant energy sink for geostrophic flows. Geostrophic flows can be

decomposed into the time-mean ACC flow and the transient geostrophic eddy field, with the latter dominating oceanic kinetic energy. Gille et al. (2000) demonstrated that EKE tended to be lower where the bottom topography was rough suggesting a higher dissipation rate of EKE over rough bathymetry. Therefore, it was suggested that the geostrophic eddy field dominates the generation of internal lee waves in the Southern Ocean.

Analyses from observations in the Southern Ocean were in agreement with estimates from global ocean models. The hotspots of the generation of lee waves were characterized by the enhanced turbulent kinetic energy dissipation ($\varepsilon \sim 10^{-8}$ W kg^{-1}) and the elevated diapycnal diffusivity ($\kappa \sim 10^{-4}$ m^2 s^{-1}), with respect to their background values ($\varepsilon \sim 10^{-10}$ W kg^{-1}; $\kappa \sim 10^{-5}$ m^2 s^{-1}). Naveira Garabato et al. (2004) found intense mixing rates above the rough sea floor of Drake Passage, the South Scotia Ridge, and the eastern Scotia Sea. Sloyan (2005) found enhanced diffusivities in the ACC over complex topography. The calculations in St. Laurent et al. (2012) showed that the diapycnal diffusivity along the Phoenix Ridge was one order of magnitude higher than the hydrographic section slightly upstream, where the amplitude of abyssal hills was smaller. This implied that the enhanced mixing might come from the breaking of lee waves generated over rough topography. The annual-mean internal wave energy radiation predicted in the western Scotia Sea by Brearley et al. (2013) was 5.3 mW m^{-2}, which was sufficient to support the dissipated power calculated from the ADCP. This was similar to the section-averaged western Drake Passage value (3.1 mW m^{-2}) computed by Sheen et al. (2013). In contrast to the Southeast Pacific where seafloor was relatively smooth, Sheen et al. (2013) found larger mid-depth turbulent dissipation rates, enhanced levels of turbulent mixing and a more energetic bottom-generated internal wave field in the Scotia Sea where bathymetry was complex with a series of topographic ridges. Watson et al. (2013) used the results from their tracer release experiment starting at 2000 km upstream of Drake Passage to show that diapycnal processes were also important for the Southern Ocean overturning at mid-depths, in addition to contributions of isopycnal stirring. Contrasted with the Southeast Pacific (from the tracer releasing site to the entrance of the Drake Passage), diapycnal mixing rates at mid-depths in the Drake Passage were 20 times larger and lee wave generation rates were 30 times greater. The consistency in scale implied that the source of mixing might come from breaking internal lee waves. Their measurements also suggested that even the limited sources of high dissipation were enough to produce substantially increased average mixing rates. By analyzing the observations from SOFine experiment north of the Kerguelen Plateau, Waterman et al. (2013) predicted the regional-mean energy radiation for the SOFine region was 15 mW m^{-2}, which lied in between the values characterizing the Drake Passage and southeast Pacific, 30 mW m^{-2} and 3 mW m^{-2} respectively (Nikurashin and Ferrari, 2010a). They also noticed that the internal lee wave

near-bottom dissipation rates were much lower than the generation rates and attributed this difference to the nonlocal balance and nonlinear wave-mean flow interactions. The suppression of internal wave breaking in the SOFine region was further studied in Waterman et al. (2014), the local inconsistency between dissipation and generation of internal waves was discussed in Waterhouse et al. (2014). Using hydrographic profiles from Electromagnetic Autonomous Profiling Explorer (EM-APEX) floats, Meyer et al. (2016) also found the horizontal propagation of internal waves near the Kerguelen Plateau. In addition, Meyer et al. (2015) found enhanced mixing of 10^{-3} m^2 s^{-1} due to the local dissipation of internal waves generated by the ACC fronts and rough small-scale topography; their mixing estimate near the Kerguelen Plateau, if extended to the entire Southern Ocean, implied a water mass transformation of 17 Sv in the upper overturning circulation.

Recently, numerical simulations have been used to study the mismatch between the local generation (estimated) and dissipation (observed) rate of internal waves, as discussed in Waterhouse et al. (2014). The simulations revealed the additional conditions, which should be taken into consideration to yield a better estimation of lee wave energy flux. Nikurashin et al. (2013) found that 80% of wind energy input was converted from eddies to smaller-scale motions and only 20% of that can radiate away into the ocean interior to sustain mixing. Nikurashin et al. (2014) compared 2D and 3D simulations and demonstrated that the generation rate was lower in the 3D case because of the finite-amplitude topography effects. Except the finite-amplitude effects, the anisotropy of topography was suggested to make a difference as well (Scott et al., 2011).

Global estimates revealed the overall importance of lee waves as an important energy dissipation mechanism for the geostrophic time-mean flow. Recent observations in the Southern Ocean and high-resolution regional numerical simulations showed that the turbulent energy dissipation rate and diapycnal diffusivity were regulated by the eddy field through the generation and breaking of lee waves, both locally or remotely. However, it remains unclear that the relative contribution of the time-mean and eddy fields into generating lee waves, and how important lee waves are to the dissipation of the time-mean and eddy fields compared with other dissipation mechanisms.

1.4 Parameterisations of internal lee waves in the ocean general circulation models

The preceding discussions motivate parameterisations of lee waves in eddy-resolving ocean models. In the presence of lee waves, a greater dissipation from the eddy field and an

enhanced mixing in the abyssal ocean are anticipated. In this section, ideas regarding how to parameterise lee waves, the previous attempts to include lee waves into ocean and climate models, and the drawbacks of those parameterisations are discussed.

An effective way to represent internal lee waves in ocean and climate models is to add both lee wave drag, a momentum term, and lee-wave-driven mixing to the background flow (Naveira Garabato et al., 2013). The work done by lee wave drag would extract energy from the background flow and subsequently sustain turbulent mixing when lee waves break within the bottom 1000 m above the seafloor.

Previous studies have already implemented and assessed various parameterisation schemes for representing the impacts of lee waves in the idealised channel models and realistic global ocean models (Broadbridge et al., 2016; Trossman et al., 2013, 2016). Motivated by the potential mixing driven by the breaking of internal lee waves and the following impacts exerted on the large-scale circulation, Trossman et al. (2013) analysed the mechanical energy budget of the total flow using an eddy resolving ocean model with and without lee wave drag. Their lee wave drag was defined as a representation of both topographic blocking and the generation of lee waves arising from geostrophic flow impinging upon rough topography, which was different from the definition in Naveira Garabato et al. (2013). They found that the inclusion of lee wave drag reduced the energy dissipation rate of the total flow associated with both bottom drag and lee wave drag because of a resultant weaker bottom velocity field. They utilised two different wave drag schemes, Bell (1975) and Garner (2005), which were further compared in Trossman et al. (2015). The impact of lee wave drag on the eddy field was discussed in Trossman et al. (2016); Trossman et al. (2016) investigated the impact of lee wave drag on eddy field using a momentum-sink based parameterisation based on Garner (2005) and compared modelled eddies to observations. The eddy statistics they chose were the sea surface height variance and geostrophic surface kinetic energy. They found that the total energy dissipation due to bottom drag and lee wave drag in the simulations with lee wave drag was greater than that in the simulations having only bottom drag. However, they did not discuss the impacts of the implemented wave drag on the large-scale circulation (e.g., the volume transport and the overturning circulation in the Southern Ocean). Broadbridge et al. (2016) adopted a mixing parameterisation into an idealised model with a double-cell overturning. They found that the mixing driven by the breaking of lee waves sustained the lower overturning cell and underpinned the sensitivity of the lower cell to changes in wind stress. They admitted that a momentum-based parameterisation might be a better choice for representing lee waves.

Parameterisations of lee-wave-driven mixing have also been implemented in climate models and the sensitivity of lee-wave-induced effects to changing climate has been dis-

cussed (Melet et al., 2015, 2014). Melet et al. (2014) employed a mixing parameterisation representing effects of lee waves and found its impact on the ocean state. The mixing parameterisation in Melet et al. (2014) was based on a global map of energy conversion into lee waves (Nikurashin and Ferrari, 2011). Melet et al. (2014) argued that because the spatial pattern of lee-wave-driven mixing was notably different from that of tidal mixing and the lee-wave-driven mixing significantly modified the temperature and stratification fields in the Southern Ocean, the lee-wave-driven mixing should also be parameterised in climate models in addition to the tidal mixing. While the intensity of mixing was enhanced to include the effects of breaking lee waves, this increased level of mixing was not accompanied with an equivalent amount of energy loss from the resolved background flow. Therefore, a physical link between the large-scale motion and the small-scale mixing was still missing in their study. Moreover, results in Melet et al. (2014) may be quantitatively subject to the limitations of estimates provided by Nikurashin and Ferrari (2011). Nevertheless, they argued that their motivation was to assess the impacts of the lee-wave-driven mixing rather than to examine the realistic cases. Melet et al. (2015) estimated the energy flux into lee waves and assessed its time variability from a climate model. They found that the global energy flux into lee waves had been decreasing over time. There was an annual cycle of lee wave energy flux in the Southern Ocean with maximum values in austral winter. The change in bottom velocity was the reason of both long-time decreasing and annual variability.

Most parameterisations that have been used are the mixing parameterisations which allow the study of the impacts of lee-wave-driven mixing but not the self-regulating physics connecting large-scale sources and small-scale sinks. Trossman et al. (2016) used a momentum sink-based parameterisation to represent the drag effect of lee waves, but they did not include the mixing effect.

1.5 Potential impacts of lee waves

Most global ocean and climate models used to study eddy saturation and eddy compensation do not include effects of lee waves. If internal lee waves extract a significant amount of energy from the mesoscale eddy field, they are expected to be more energetic as westerlies increase; there will be more energy available for the mixing associated with the breaking of a stronger internal lee wave field, which will strengthen the overturning circulation. Therefore, ocean models without internal lee waves might overestimate the eddy field and its impact, meanwhile underestimate the intensity of diapycnal mixing and its contribution to water mass transformation and the overturning circulation in the Southern Ocean. There are three reasons why the presence of internal lee waves may be important in the study of the

sensitivity of the Southern Ocean circulation to changes in wind stress. Firstly, given the importance of eddies in the Southern Ocean, an overestimation of the eddy energy might lead to, for example, a larger eddy heat flux and thus a warmer Southern Ocean (Hogg et al., 2008; Screen et al., 2009). Secondly, given the regulation of lee waves on diapycnal mixing (section 1.3), the absence of lee waves would affect the deep ocean-atmosphere exchange of heat and carbon because of the reduced diapycnal mixing and hence the reduced lower overturning circulation rate. Thirdly, the reduced diapycnal mixing might also lead to an underestimation of the upper overturning circulation, as implied by Meyer et al. (2015). It is suggested that the parameterisation of internal lee waves would provide a more realistic model to study the response of the Southern Ocean circulation to changing winds in the climate. The necessity to consider lee waves in the Southern Ocean sensitivity study has been reinforced by observational evidence along a hydrographic transect in the Drake Passage (Sheen et al., 2014), where abyssal mixing was proved to be modulated by eddies over rough topography through the breaking of lee waves. Sheen et al. (2014) believed that the dynamics linking eddies with mixing through lee waves was common to all ACC regions where rough topography was present.

In order to improve the modelled Southern Ocean eddy field and the lower overturning circulation in the Southern Ocean, numerical simulations were used to explore the potential impacts of lee waves on the sensitivity of the Southern Ocean circulation to changes in wind stress. Broadbridge et al. (2016) showed the response of the lower overturning circulation to wind forcing perturbations, and suggested that it was regulated by diapycnal mixing induced by the breaking of lee waves generated by the simulated eddies impinging on small-scale topography. The regional process-studying model they used took some simplifications but was still able to capture the features of the Southern Ocean. However, the applicability to the Southern Ocean where the local dynamics is important (Dufour et al., 2012; Rintoul, 2018; Thompson and Naveira Garabato, 2014) needs further consideration.

1.6 Objectives and outline

The eddy field plays a key role in regulating the Southern Ocean circulation and its sensitivity to changes in wind stress, which will further impact the global ocean circulation and climate. The simulation of the eddy field in the Southern Ocean depends on the representation of both eddy generation and eddy dissipation mechanisms. With increasing horizontal resolution of the global ocean models, eddy generation is better captured and it leads to an improved representation of the eddy heat flux, the momentum and tracers redistribution in the ACC, and the sensitivity of the Southern Ocean circulation to changes in wind stress. However, the

eddy dissipation mechanisms are not well quantified and represented in the eddy-resolving global ocean models. To simulate a realistic eddy field and its impact on the Southern Ocean, the representation of eddy energy dissipation is as important as that of eddy energy generation. One of the energy dissipation routes from the eddy field to turbulent mixing is through the generation and breaking of internal lee waves. Lee waves act as an energy sink for the eddy field as well as an energy source for the mixing. Through their control on the eddy field and turbulent mixing, lee waves can potentially regulate the strength of the lower overturning circulation and its sensitivity to changes in wind stress. However, current lee wave parameterisation schemes do not include all the potential lee wave effects. Our objective is to quantify the role of lee waves in dissipating eddy energy in the Southern Ocean, develop a physical lee wave parameterisation scheme, and use it to investigate the regulation of lee waves on the Southern Ocean circulation under varying wind stress through the eddy field.

In chapter 2, we will quantify the energy extraction from the eddy field by lee waves using an eddy-resolving global ocean model to assess the importance of lee wave generation as an eddy energy dissipation mechanism. We compare it with the energy dissipation of the eddy field in the TBBL due to the frictional processes. We also compare the relative contribution of the time-mean and transient eddy fields to the generation of lee waves.

In chapter 3, we will investigate the regulation of the bottom frictional drag on the Southern Ocean circulation and its sensitivity to changes in wind stress in an eddy-resolving idealised channel configuration, which is an intermediate step we take prior to the parameterisation and exploration of the impact of lee waves.

In chapter 4, we will develop and implement a lee wave parameterisation into an eddy-resolving idealised channel configuration to better understand the role of lee waves in regulating the Southern Ocean circulation and its response to increasing wind stress. The lee wave drag effects and their comparisons with the bottom frictional drag effects (chapter 3) are shown and discussed. The mixing effects are understood in the context of previous studies (Broadbridge et al., 2016; Saenko et al., 2012; Stanley and Saenko, 2014).

We summarise the key findings, discuss the implications of the results, and comment on the future work in chapter 5.

Chapter 2 has been removed for copyright or proprietary reasons.

It has been published as: Yang, L., Nikurashin, M., Hogg, A. M., Sloyan, B. M., 2018. Energy loss from transient eddies due to lee wave generation in the Southern Ocean, Journal of physical oceanography, 48(12), 2867-2885

Chapter 3

Bottom frictional control of the Southern Ocean circulation and its sensitivity to winds

3.1 Introduction

Yang et al. (2018) (chapter 2) showed that lee waves extracted a significant amount of energy from transient eddies and thus acted as an energy sink for the eddy field in the Southern Ocean. Since the eddy field has been long recognised to regulate the Southern Ocean circulation under a changing climate (Bishop et al., 2016; Farneti and Delworth, 2010; Farneti et al., 2010; Gent, 2015; Hallberg and Gnanadesikan, 2006; Meredith and Hogg, 2006; Morrison and Hogg, 2013; Munday et al., 2013; Viebahn and Eden, 2010), lee waves could potentially modify this regulation through extracting the momentum and energy from the eddy field. However, the modulation on the Southern Ocean circulation and its sensitivity to changes in wind stress by lee waves has not been extensively studied because the connection between lee waves and large-scale flow is not well established in eddy-resolving ocean models. As the role of lee-wave-driven mixing for global ocean and climate has been addressed (Melet et al., 2015, 2014), we first seek to understand how lee wave drag affects the Southern Ocean circulation and its response to changing climate, and then the combined effects of lee wave drag and lee-wave-driven mixing.

Lee wave drag has been derived from linear theory (Bell, 1975), it has a complex nonlinear dependence on bottom flow and stratification (Eq. 2.2). Various simplified formula have been put forward that can be used for its parameterisation in global ocean models (Naveira Garabato et al., 2013; Nikurashin and Ferrari, 2010a; Pedlosky, 2013). Depending on how

the multi-scale small-scale topography is represented and assumptions made, lee wave drag has been shown to scale linearly (Pedlosky, 2013) or quadratically (Naveira Garabato et al., 2013) with velocity, and it acts against the bottom flow analogous to bottom frictional drag. Therefore, as an intermediate step to understand the impacts of lee waves, we first explore how bottom frictional drag affects the Southern Ocean circulation.

Recently, Marshall et al. (2017) investigated how the linear bottom frictional drag controlled the Antarctic Circumpolar Current (ACC) transport using an idealised periodic channel model and found that, counterintuitively, the zonal transport increased with increased linear drag coefficient. Marshall et al. (2017) proposed a theory which predicted that the baroclinic transport scaled linearly with the eddy energy damping rate, which was believed to be dominated by the dissipation due to bottom drag in global ocean models (Arbic et al., 2009) [1]. Marshall et al. (2017)'s theory is based on the eddy kinetic energy (EKE) balance: when the eddy energy is dissipated at a higher rate due to an increase in the linear drag coefficient, the flow becomes more baroclinic and more eddies are generated to balance the increased dissipation. The increased baroclinicity of the flow leads to a larger baroclinic transport relative to the seafloor.

The applicability of Marshall et al. (2017)'s theory and implied changes to the Southern Ocean circulation may not be circumpolarly consistent at all time scales, for the following reasons. First, their model configuration represents an idealised Southern Ocean, with a topographic barrier (a single Gaussian ridge of 1000 km wide and 1500 m tall) that occupies only 10% of the domain in the horizontal. The Southern Ocean topography has a broad spectrum of length scales and orientation and covers a significant fraction of the area. Second, they adopt a diffusive northern boundary condition, which means the diffusivity in the thin sponge layer is enhanced to a level that is equal to the effect of weak background diffusivity acting throughout the ocean basin to the north of the Southern Ocean. This type of boundary condition allows the stratification in the north to vary following the changes in the Southern Ocean, which approximates the response of the global ocean at long time scales (Talley, 2013). At shorter time scales, where the ocean basins have not yet adjusted to changes in the Southern Ocean due to their slow response (Allison et al., 2011), restoring boundary condition is more appropriate (e.g., Abernathey et al., 2011; Morrison and Hogg, 2013). Third, their conclusion that the zonal transport increases with increased drag coefficient and is independent of wind stress is made based on the assumption that the EKE dissipation rate scales linearly with the domain-integrated EKE. This assumption holds when bottom

[1] This statement is not contradictory with the findings in chapter 2. In most global ocean models, dissipation in TBBL remains a dominant eddy energy sink because lee waves are not resolved or fully parameterised.

frictional drag is linear. However, it remains unclear whether their theory holds if the bottom friction is parameterised as a quadratic drag.

It is unclear whether Marshall et al. (2017)'s theory is dependent on the parameterisation of the bottom friction. We focus on this particular question because the use of a linear or quadratic bottom frictional drag in a model is associated with the physical processes that remove the momentum and energy from the flow near the seafloor and therefore should be based on physical laws. By contrast, the choice of topography and northern boundary conditions are somewhat influenced by the question the model is addressing.

Linear bottom frictional drag typically represents the momentum loss in the bottom Ekman layer, whereas the quadratic bottom frictional drag represents the momentum loss due to turbulent bottom boundary layer (TBBL) processes (e.g., Gill, 1982). Both linear and quadratic drag are operating in the ocean; however, neither the Ekman layer nor the TBBL (the thickness of which is on the order of 10-100 m) is resolved by global ocean models. The frictional processes at the seafloor are more commonly parameterised as a quadratic drag in global ocean models (e.g., Griffies, 2012). Quadratic drag has also been shown to behave differently from linear drag and its use in ocean models tends to yield a more realistic eddy field in terms of its energetics, vertical structure and horizontal scales (Arbic and Scott, 2008). It is expected that the dynamics would not be identical when linear drag is replaced with quadratic drag, therefore it is uncertain whether the findings in Marshall et al. (2017) are robust for an ocean damped by quadratic drag. Understanding of the similarities and differences between the role of linear and quadratic drag is fundamental to inferring the impacts of complex bottom processes on the circulation.

The purpose of this chapter is to understand the bottom frictional control of the Southern Ocean circulation and its sensitivity to changes in wind stress, following and extending previous work (Marshall et al., 2017). We revisit the theory proposed in Marshall et al. (2017) on the control of the ACC by the linear bottom frictional drag (section 3.2.1) and extend their theory by considering an ocean where the eddy energy is damped by the quadratic bottom frictional drag (section 3.2.2). We then, for the first time, provide a theoretical prediction of the frictional control of the Meridional Overturning Circulation (MOC) (section 3.2.3). We set up an idealised channel configuration representing the Southern Ocean and use it to study the regulation of the Southern Ocean circulation by bottom frictional drag in the absence of lee waves, which is described in more detail in section 3.3.1. This model configuration will then be used to study the role of lee waves for the Southern Ocean circulation and its sensitivity to changes in wind stress in chapter 4. To understand the control of the circulation by the types and strengths of bottom drag through eddy energy dissipation in

an eddy-resolving configuration, we conduct two sets of experiments, one with the linear bottom frictional drag and the other the quadratic bottom frictional drag, respectively.

This chapter is organised as follows; First, we test the robustness of Marshall et al. (2017)'s results on frictional control of the ACC using a more complex topography (section 3.4.1). Then, we extend Marshall et al. (2017)'s work by studying how the quadratic bottom frictional drag affects the zonal transport (section 3.4.2). Third, we examine whether and how the sensitivity of the ACC to changes in wind stress is affected by bottom drag (section 3.4.3). Fourth, we explore how the linear and quadratic bottom frictional drag modify the MOC in the Southern Ocean (section 3.5). Finally, we discuss how our results are affected by differing northern boundary condition in the model (section 3.6).

3.2 Theory: Regulation of the ACC and the MOC by bottom frictional drag

The ACC transport has been suggested to be regulated by a number of processes that can affect the meridional density gradient (Allison et al., 2011), such as mesoscale eddy processes (e.g., Karsten et al., 2002), diapycnal mixing (e.g., Munday et al., 2011), and the formation rate of the Antarctic Bottom Water (Antarctic Bottom Water (AABW)) (e.g., Gent et al., 2001). An extension of Gnanadesikan (1999)'s model has suggested that the ACC transport is set by wind forcing, eddy diffusivity, and the pycnocline depth at the northern boundary of the ACC (Allison et al., 2011). Using an interhemispheric three-layer model, Shakespeare and Hogg (2012) predicted that the ACC transport was regulated by both wind stress and the magnitude of southern surface buoyancy flux. While previous studies have focused on the control of surface forcing and interior parameters on the strength of the ACC transport, whether bottom drag also plays a role in setting the ACC transport has only been discussed very recently (Marshall et al., 2017).

Motivated by the impact of bottom-intensified lee waves on the lower branch of the overturning circulation in the Southern Ocean (e.g., Broadbridge et al., 2016; Melet et al., 2014), we also investigate how the strength of the lower overturning circulation is sensitive to bottom drag. The lower cell consists of the subduction and export of AABW, the diffusive processes driven by diapycnal mixing that lead to the upwelling branch in the interior, and the adiabatic southward return branch driven by wind (Marshall and Speer, 2012; Visbeck, 2007). In a steady state, the generation and the diapycnal transformation of the AABW must balance; therefore, a stronger diapycnal mixing requires increased formation and subduction of AABW into the deep ocean, which leads to a larger residual lower overturning. The

strength of the lower cell is therefore related to both AABW formation and export (Purkey and Johnson, 2012), which has been shown to be regulated by the easterly wind over the Antarctic continental slope (Stewart and Thompson, 2012), surface buoyancy fluxes (Jansen and Nadeau, 2016; Snow et al., 2016), and the intensity of mixing in the deep ocean (e.g., Ito and Marshall, 2008; Nikurashin and Vallis, 2011), which is enhanced by the breaking internal waves over the rough topography and long tracer residence time adjacent to mixing hotspots (Mashayek et al., 2017). The lower overturning cell can also be modulated by wind and eddy diffusivity, which measures the along-isopycnal advection of buoyancy by the eddy field through their effect on the stratification.

The lower cell and AABW transport, although distant from the surface westerly wind over the Southern Ocean, has been found to increase with wind when a certain fraction of EKE is allowed to contribute to and therefore regulate the diapycnal mixing in the deep ocean (Saenko et al., 2012; Stanley and Saenko, 2014). However, there has been no study, to our knowledge, that has investigated how bottom drag might affect the lower MOC in the Southern Ocean.

3.2.1 Dependence of the ACC transport on linear drag coefficient

In Marshall et al. (2017)'s theory, the control of the linear bottom frictional drag on the ACC transport is derived from an eddy energy budget. The authors make two assumptions to connect the ACC transport with the eddy energy; first, the ACC transport is baroclinicly dominated; second, eddies are generated primarily due to baroclinic instability in the Southern Ocean.

Eddy generation in the Southern Ocean results from the mixed barotropic-baroclinic instability (Barthel et al., 2017; Youngs et al., 2017), with the baroclinic instability dominating (e.g., Rintoul and Naveira Garabato, 2013). The eddy energy generation rate due to baroclinic instability in an ocean of uniform stratification and shear is (Marshall et al., 2012),

$$\text{eddy energy source} = \alpha_1 \frac{|f|}{N} \frac{\partial \overline{u}}{\partial z} \text{EKE}, \tag{3.1}$$

where α_1 is a non-dimensional parameter representing eddy geometrical characteristics (defined in section 4 in Marshall et al., 2012), f is the Coriolis parameter, N is the buoyancy frequency, $\overline{u}$ is the zonal- and time-mean flow representing the ACC, EKE is the vertical integral of the local eddy kinetic energy, $E = \frac{1}{2}(u'^2 + v'^2)$,

$$\text{EKE} = \int_{-H}^{0} E dz,$$

where $u' = u - \overline{u}$ and H is the depth of the ocean. EKE generation is linearly proportional to the vertical shear of horizontal velocity $\overline{u}$, whose depth integral is the ACC transport.

The eddy energy dissipation rate, the contribution of all eddy energy dissipation mechanisms, is assumed to scale linearly with EKE (Marshall et al., 2017),

$$\text{eddy energy sink} = \lambda\ \text{EKE}, \tag{3.2}$$

where λ is the eddy energy damping rate.

In steady state, the EKE generation rate is balanced by its dissipation rate,

$$\alpha_1 \frac{|f|}{N} \frac{\partial \overline{u}}{\partial z} = \lambda, \tag{3.3}$$

from which we obtain a prediction for the baroclinic ACC transport,

$$T = \lambda \frac{N}{|f|} \frac{H^2 L}{2\alpha_1}, \tag{3.4}$$

assuming the velocity vanishes at the bottom and taking the mean velocity as $\frac{1}{2} H \frac{\partial \overline{u}}{\partial z}$ and the width L. This prediction shows that the transport T linearly depends on the eddy energy damping rate λ.

The response of the transport to an increase in the eddy energy dissipation rate λ can be summarised as follows. When the eddy energy dissipation rate λ is increased because of a larger drag coefficient, the EKE balance is perturbed with more EKE being dissipated by bottom drag. To compensate for the increase in EKE dissipation and re-establish a steady state for EKE, a higher eddy generation rate is required. The circulation responds to this requirement by increasing the vertical shear of the ACC (i.e., steepening the isopycnals), so that eddy generation increases via baroclinic instability. A larger vertical shear, when integrated (twice) in depth from the bottom to the top of the ocean, results in a larger baroclinic transport relative to the seafloor.

In the linear drag case, the baroclinic ACC transport (Eq. 3.4) depends on the bottom drag coefficient through the eddy energy damping rate λ and is independent of wind stress, the latter is known as an eddy saturation state. Marshall et al. (2017) have found that the total transport increases with increased linear drag coefficient and verified the insensitive response of the transport to changing wind stress using a model with a linear bottom frictional drag.

3.2.2 Dependence of the ACC transport on quadratic drag coefficient

Following Marshall et al. (2017), we extend their theory to study how the ACC transport is controlled by the strength of the quadratic bottom frictional drag and investigate the sensitivity of the ACC to changes in wind stress when the quadratic bottom frictional drag is used. Here, we focus on the eddy energy dissipation and discuss the balance established when bottom frictional drag changes from linear to quadratic.

If eddies are damped by the quadratic bottom frictional drag $\boldsymbol{\tau}_{\text{TBBL}}$, as discussed in chapter 2,

$$\boldsymbol{\tau}_{\text{TBBL}}(\mathbf{u}) = -\rho_0 C_d |\mathbf{u}|\mathbf{u}, \tag{3.5}$$

where C_d is the quadratic drag coefficient (non-dimensional), bottom eddy energy dissipation becomes,

$$\mathbf{u}_b' \boldsymbol{\tau}_{\text{TBBL}}(\mathbf{u}_b') = \rho_0 C_d |\mathbf{u}_b'|^3 \propto (\frac{1}{2}\rho_0 |\mathbf{u}_b'|^2)^{\frac{3}{2}}, \tag{3.6}$$

which no longer scales linearly with the bottom eddy energy. If a quadratic drag relationship is applied to the entire domain, Eq. (3.2) is modified to

$$\text{eddy energy sink} = \lambda_{\text{TBBL}}\, \text{EKE}^{\frac{3}{2}}, \tag{3.7}$$

where λ_{TBBL} is the eddy damping rate when the quadratic bottom frictional drag is used in the TBBL. Replacing the linear bottom frictional drag with a quadratic formula demonstrates that locally, the eddy energy dissipation might not be linearly dependent on the eddy energy integral. Over the entire domain, when more energy dissipation processes are considered, the linear relationship between the eddy energy dissipation and eddy energy integral (Eq. 3.2) remains questionable.

With the new eddy energy sink expression (Eq. 3.7), the eddy energy balance (Eq. 3.3) becomes

$$\alpha_1 \frac{|f|}{N}\frac{\partial \overline{u}}{\partial z} = \lambda_{\text{TBBL}}\, \text{EKE}^{\frac{1}{2}}, \tag{3.8}$$

and the ACC transport is rewritten as

$$T = \lambda_{\text{TBBL}}\, \text{EKE}^{\frac{1}{2}} \frac{N}{|f|}\frac{H^2 L}{2\alpha_1}, \tag{3.9}$$

which is a function of eddy energy damping rate λ_{TBBL} and EKE. In this case, the baroclinic transport still increases with the eddy energy damping rate λ_{TBBL}, although the relationship is quantitatively altered due to the presence of the EKE integral (Eq. 3.9). In addition, the transport is also affected by EKE and therefore depends on the dynamics that governs EKE.

Marshall et al. (2017) have derived a scaling for EKE based on the zonal momentum budget of the upper ocean and a relationship between the eddy form stress and the eddy energy; they found that EKE is set by the westerly wind stress with an offset due to residual overturning.

The dependence of EKE on wind alters Marshall et al. (2017)'s theory for the quadratic drag case in that the transport depends not only on bottom drag but also on surface wind stress. The modulation of the transport by residual overturning through EKE is not as significant as that by wind (shown later). The expression for baroclinic transport (Eq. 3.9) could be further written (not shown) and simplified as,

$$T = T(\lambda_{\mathrm{TBBL}}, \tau_w^x). \tag{3.10}$$

Compared with the linear drag case (Eq. 3.4) where the transport is only a function of eddy energy damping rate λ, in the quadratic case, the transport is also a function of wind stress. This additional dependence on wind indicates that the transport is no longer eddy saturated.

3.2.3 Dependence of the MOC on bottom drag

The response of the lower overturning circulation to bottom drag is understood in the context of Ito and Marshall (2008) and Nikurashin and Vallis (2011)'s theory on how the diapycnal mixing and eddy diffusivity controls the strength of the lower overturning circulation. In this section, we will first revisit the scaling of the mixing-driven lower overturning proposed in Ito and Marshall (2008), and then combine it with the relationship for isopycnal slope to describe changes in the lower overturning circulation in response of bottom drag. Finally, we depict a full picture by connecting the response of the eddy field, the slope of the isopycnals, the lower overturning circulation, and the ACC following an increase in the drag coefficient.

In the transformed Eulerian-mean framework, the residual overturning circulation, Ψ_{res}, is the sum of the wind-driven Eulerian mean circulation, $\overline{\Psi}$, and the eddy-driven circulation, Ψ^*,

$$\Psi_{\mathrm{res}} = \overline{\Psi} + \Psi^*. \tag{3.11}$$

The wind-driven overturning circulation $\overline{\Psi}$ is associated with the wind-driven Ekman upwelling and downwelling arising from the wind-stress curl over the Southern Ocean. It acts to steepen the isopycnals, and is linearly dependent on wind stress,

$$\overline{\Psi} = -\frac{\tau_{\mathrm{w}}^x}{\rho_0 f}, \tag{3.12}$$

where τ_w^x is the surface wind stress along the latitudinal direction, ρ_0 is the reference density, and f is the Coriolis parameter. The eddy-driven overturning circulation Ψ^* is associated with the slumping effects of eddies on the isopycnals in the Southern Ocean. It opposes the wind-driven overturning circulation and is often parameterised as (Gent and McWilliams, 1990)

$$\Psi^* = K s_\rho, \tag{3.13}$$

where K is the eddy diffusivity of buoyancy and s_ρ is the slope of the isopycnals.

The residual overturning circulation Ψ_{res} advects the mean buoyancy $\overline{b}$ described by its advection-diffusion equation (Ito and Marshall, 2008; Marshall and Radko, 2003; Nikurashin and Vallis, 2011):

$$J_{y,z}(\Psi_{res}, \overline{b}) = \frac{\partial}{\partial z}(\kappa \frac{\partial \overline{b}}{\partial z}), \tag{3.14}$$

where $J_{y,z}(\Psi_{res}, \overline{b}) = (\Psi_{res})_y \overline{b}_z - (\Psi_{res})_z \overline{b}_y = \mathbf{v}_{res} \cdot \nabla \overline{b}$, $\mathbf{v}_{res} = (v_{res}, w_{res}) = (-\partial_z \Psi_{res}, \partial_y \Psi_{res})$ is the residual velocity, and κ is the diapycnal diffusivity. The physical interpretation of the buoyancy advection-diffusion equation is that, in the steady state, for the equatorward flowing branch of the lower overturning circulation, the amount of dense water being advected northward is exactly the amount of water that is being converted by diffusion into lighter waters. Assuming that $|\overline{b}_z| \gg |\overline{b}_y|$, we can neglect the horizontal advection term on the left hand side of Eq. (3.14) and rewrite the equation as

$$\frac{\partial \Psi_{res}}{\partial y} \frac{\partial \overline{b}}{\partial z} = \frac{\partial}{\partial z}(\kappa \frac{\partial \overline{b}}{\partial z}). \tag{3.15}$$

Replacing terms in Eq. (3.15) with their characteristic scales, we obtain,

$$\Psi_{res} = \frac{\kappa}{h/l} = \frac{\kappa}{s_\rho}, \tag{3.16}$$

where h and l are the characteristic depth and length scales, respectively, of the isopycnals in the Southern Ocean. Combining Eq. (3.11), (3.12), (3.13) and (3.16), we obtain

$$-\frac{\tau_w^x}{\rho_0 f} + K s_\rho = \frac{\kappa}{s_\rho}, \tag{3.17}$$

which is a scaling relationship for the mixing-driven lower overturning circulation in the Southern Ocean. This agrees with the conceptual framework proposed by Gnanadesikan (1999) and is similar to the ones used in Ito and Marshall (2008) and Nikurashin and Vallis (2011).

Nikurashin and Vallis (2011) have proposed a theory for the overturning circulation, where the stratification of the lower overturning circulation is set by the wind and eddy field in the Southern Ocean and the overturning circulation is driven by diapycnal mixing acting on this stratification. The westerly wind over the Southern Ocean and the eddy field in the Southern Ocean sets the slope of isopycnals and therefore the deep stratification. The diapycnal mixing in the ocean interior transforms bottom water into light waters and sets the rate of lower overturning circulation in the Southern Ocean.

As in Nikurashin and Vallis (2011), we assume that the strength of the residual overturning circulation is much weaker than that of the wind-driven overturning circulation, $\Psi_{\text{res}} \ll \overline{\Psi}$, and the wind-driven overturning circulation is largely balanced by the eddy-driven overturning circulation, $\overline{\Psi} \sim \Psi^*$. Then, to the leading order, the slope of isopycnals is set by the balance between the wind steepening effects and eddy flattening effects,

$$\frac{\tau_{\text{w}}^x}{\rho_0 f} = K s_\rho, \tag{3.18}$$

from which we can predict the slope of isopycnals as

$$s_\rho = \frac{\tau_{\text{w}}^x}{\rho_0 f K}. \tag{3.19}$$

We have understood that, from sections 3.2.1 and 3.2.2, the use of a larger bottom drag coefficient leads to an increase in the vertical shear, which generates eddies at a higher rate to match the increased eddy dissipation rate, and also an increase in the isopycnal slope. The increase in the isopycnal slope s_ρ predicts a drop in the eddy diffusivity K, through Eq. (3.19).

According to the mixing-length theory (Taylor, 1922), the eddy diffusivity scales with the eddy length scale L_e and the eddy energy EKE, as $K \approx L_e \text{EKE}^{1/2}$, implying that the more energy there is in the eddy field, the more efficient it is at flattening isopycnals. Therefore, a decrease in the eddy diffusivity K following the increase in the drag coefficient and the steepening of isopycnals indicates a reduction in EKE.

We summarise how bottom drag affects the lower residual overturning circulation through regulating EKE. As the drag coefficient increases, the EKE balance is perturbed; as the eddy dissipation rate becomes larger, EKE decreases. The decrease in EKE weakens the eddy diffusivity according to the mixing-length theory and therefore weakens the eddy-driven overturning circulation (Eq. 3.13). A weaker eddy-driven overturning circulation allows the wind to steepen isopycnals and therefore increase the baroclinicity of the flow via the thermal wind relation, so that more eddies can be generated to compensate the increased

EKE dissipation rate associated with a larger drag coefficient. Note that at the end of the adjustment, in the new steady state, the isopycnals are steeper than they are in the original state (the state before the drag coefficient is increased) because the system relies on them to constantly produce an EKE generation rate that is larger than that in the original state. With steeper isopycnals, the lower overturning circulation is weaker, as predicted by Eq. (3.16), which means the eddy-driven overturning required in the new steady state is not as strong as it is in the original state, given the same wind-driven overturning circulation. Even though both EKE generation and dissipation rates increase responding to a larger drag coefficient, the EKE reservoir actually reduces.

3.3 Model configuration and experiments

3.3.1 Model configuration

We use the Modular Ocean Model, version 6 (MOM6; https://github.com/NOAA-GFDL/MOM6). We set up a periodic channel configuration on β-plane, whose domain size is $L_x \times L_y \times L_z = 4000$ km $\times$ 2500 km $\times$ 4 km (Fig. 3.1), with 10 km horizontal resolution. There

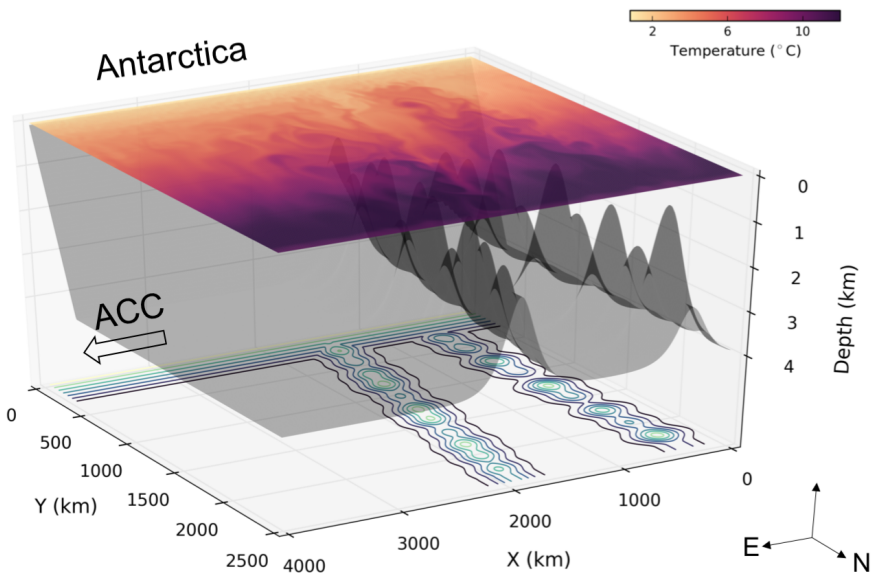

Fig. 3.1 The gray surface indicates the topography used in the model configuration, whose height contours are projected onto the x-y plane. The colour at the surface shows a snapshot of surface temperature.

are 72 vertical layers, divided by the vertical grid spacing that ranges from 5 m at the surface to 98 m above the bottom. Key parameters of the configuration are listed in Table 3.1.

Table 3.1 Key parameters used in the control experiment.

Symbol	Value	Description
L_x, L_y	4000 km, 2500 km	Domain size
L_{sponge}	100 km	Sponge width
H	4000 m	Domain depth
Δx, Δy	10 km	Horizontal grid spacing
Δz	5 - 98 m	Vertical grid spacing
Δt	1200 s	Time step
ρ_0	1035.0 kg m^{-3}	Reference density
f_0	-1.1570$\times10^{-4}$ s^{-1}	Reference Coriolis parameter
β	1.5$\times10^{-11}$ s^{-1} m^{-1}	Meridional gradient of Coriolis parameter
r_b	3$\times10^{-4}$ m s^{-1}	Linear bottom frictional drag coefficient
τ_0	0.2 N m^{-2}	Wind stress magnitude
$\tau_{surface}$	0.5 m day^{-1}	Surface restoring rate
κ_H	1×10^{-5}	Background diapycnal diffusivity
A_v	1×10^{-4}	Background kinematic viscosity
A_4	1×10^{10}	Biharmonic viscosity

The model is forced by the surface wind stress (Fig. 3.2a), the surface temperature restoring (Fig. 3.2a), and a sponge layer located in the northernmost 100 km of the domain (2400 km $\leqslant$ Y $\leqslant$ 2500 km, Fig. 3.2b, c). In this configuration, the salinity is set as a constant, 35 psu, throughout the domain, and the density is only a function of temperature. The surface wind stress takes the form of

$$\tau_{\mathrm{w}}^{x} = \tau_0 \sin(\pi y/L_y),\ \tau_{\mathrm{w}}^{y} = 0, \tag{3.20}$$

where the peak wind stress τ_0 = 0.2 N m^{-2} in the reference case. The surface buoyancy flux is determined by how fast the surface temperature is restored to a prescribed profile (Fig. 3.2a); that is, the controlling factors for the buoyancy exchange are the difference between the ocean temperature and surface restoring temperature and the temperature restoring rate. The surface restoring temperature (red line in Fig. 3.2a) is a function of latitude, i.e., zonally uniform. The surface temperature restoring profile follows

$$\mathrm{T_{surf}} = \begin{cases} 12 \times y/2000, & 0 \leqslant y \leqslant 2000 \text{ km}; \\ 12, & 2000 \text{ km} \leqslant y \leqslant 2500 \text{ km}. \end{cases} \tag{3.21}$$

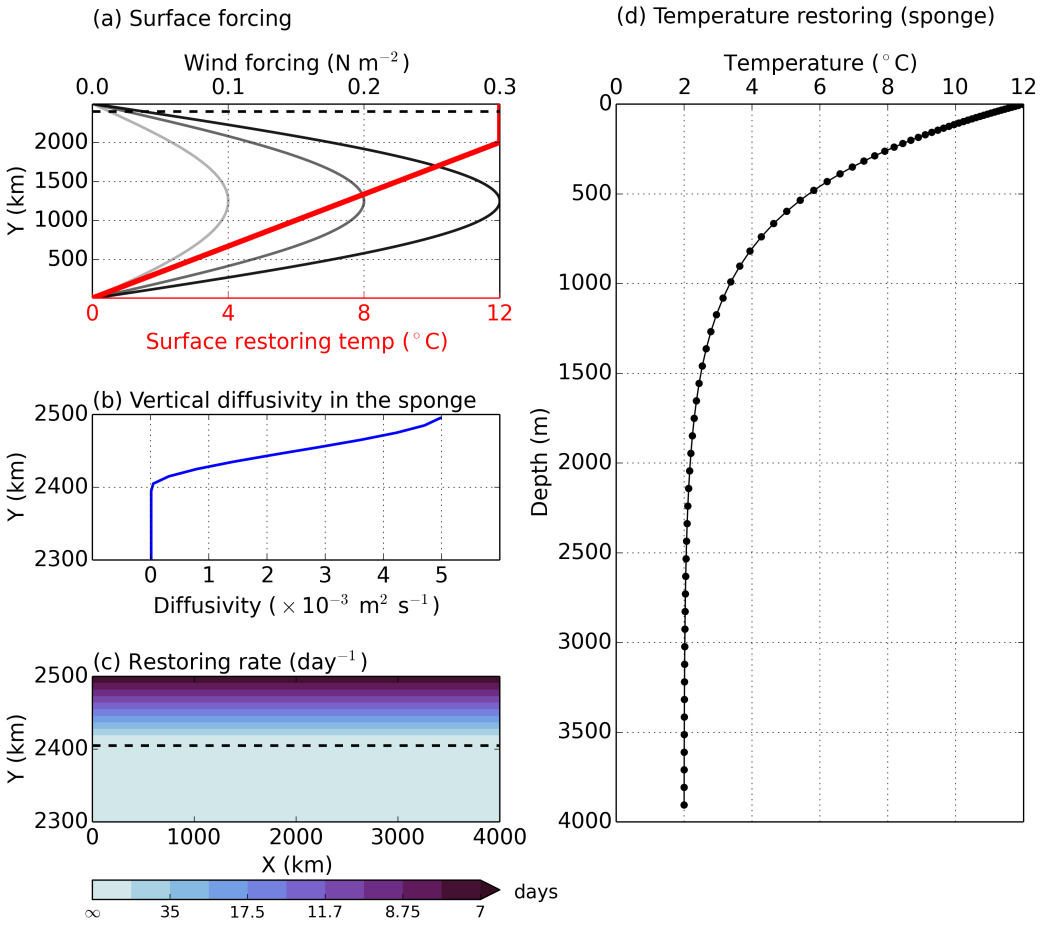

Fig. 3.2 External forcing and boundary conditions. (a) Surface forcing consists of wind forcing (black lines), which is a sinusoidal function of latitude, and the temperature restoring (red line). (b) When the diffusive boundary condition is used in the sponge layer, the vertical diffusivity in the sponge layer is increased up to 5×10^{-3} m^2 s^{-1} with respect to the background value of 1×10^{-5} m^2 s^{-1}. When the restoring boundary condition is applied in the sponge layer, the temperature is restored at the rate shown by (c) to a vertical profile shown in (d).

In the northern sponge layer, similar to Hogg (2010), we increase the vertical diffusivity (Fig. 3.2b) to represent the downward flux of heat, equivalent to the cold water upwelling, due to the interior mixing occurring in the ocean basins to the north of the Southern Ocean. The maximum diffusivity in the sponge layer is 5×10^{-3} m^2 s^{-1} (Fig. 3.2b). The adoption of an enhanced diffusivity in the sponge layer guarantees a physically closed lower overturning circulation in an idealised model that has a solid wall in the north. Note that in this case, the upper overturning circulation is virtually non-existent. The advantage of adopting a diffusive boundary condition is that the isopycnals can move vertically within the sponge layer; given

the relative fast restoring at the surface, the freedom provided by the sponge layer allows the isopycnal slope and therefore the baroclinic transport to vary. The diffusive boundary condition can also represent the propagation of signals from the Southern Ocean northward and therefore reflects the control of the Southern Ocean processes on the stratification in the ocean basins to the north (Hall and Visbeck, 2002; Kamenkovich and Radko, 2011; Wolfe and Cessi, 2010). We argue that this diffusive boundary condition simulates a long timescale and represents the response of adjacent basins to changes in the Southern Ocean. At shorter timescales, in which the stratification in the north edge of the Southern Ocean has not adjusted to changes in the Southern Ocean, a restoring boundary condition is commonly used to ensure a fixed stratification profile (e.g., Abernathey et al., 2011; Morrison and Hogg, 2013).

Motivated by the behaviour and response of the stratification in the northern edge of the Southern Ocean at different timescales, we conduct another set of experiments using the quadratic bottom frictional drag and a restoring northern boundary condition, which restores the temperature to the vertical profile (Fig. 3.2d)

$$\mathrm{T}_{\mathrm{sponge}} = (\mathrm{T}_{\mathrm{surf}} - 2)(e^{z/h} - e^{-H/h})/(1 - e^{-H/h}) + 2, \quad 2400\ \mathrm{km} \leqslant y \leqslant 2500\ \mathrm{km}, \quad (3.22)$$

where $\mathrm{T}_{\mathrm{surf}}$ is the surface restoring temperature, z (< 0, directing upward) is the vertical coordinate, h = 500 m is the scale height, and H = 4000 m is the maximum ocean depth. The temperature inside the sponge is restored to the profile (Fig. 3.2d; Eq 3.22) on a timescale of 7 days (Fig. 3.2c). The vertical temperature distribution (Fig. 3.2d) is chosen to represent the stratification at the northern boundary of the Southern Ocean.

The energy is dissipated in the model through the work done by bottom frictional drag and interior viscosity. The bottom frictional drag either takes a linear or a quadratic expression. The background kinematic viscosity is 10^{-4} m^2 s^{-1} and the background biharmonic horizontal viscosity is 10^{10} m^4 s^{-1}.

The topography consists of a slope at the southern boundary representing the Antarctic slope and two meridional ridges with bumps located in the western half of the domain (Fig. 3.1).

3.3.2 Experiments

Reference case

The reference case uses the linear bottom frictional drag with a drag coefficient of $r_b = 3 \times 10^{-4}$ m s^{-1} and the diffusive boundary condition. The reference case simulation reproduces

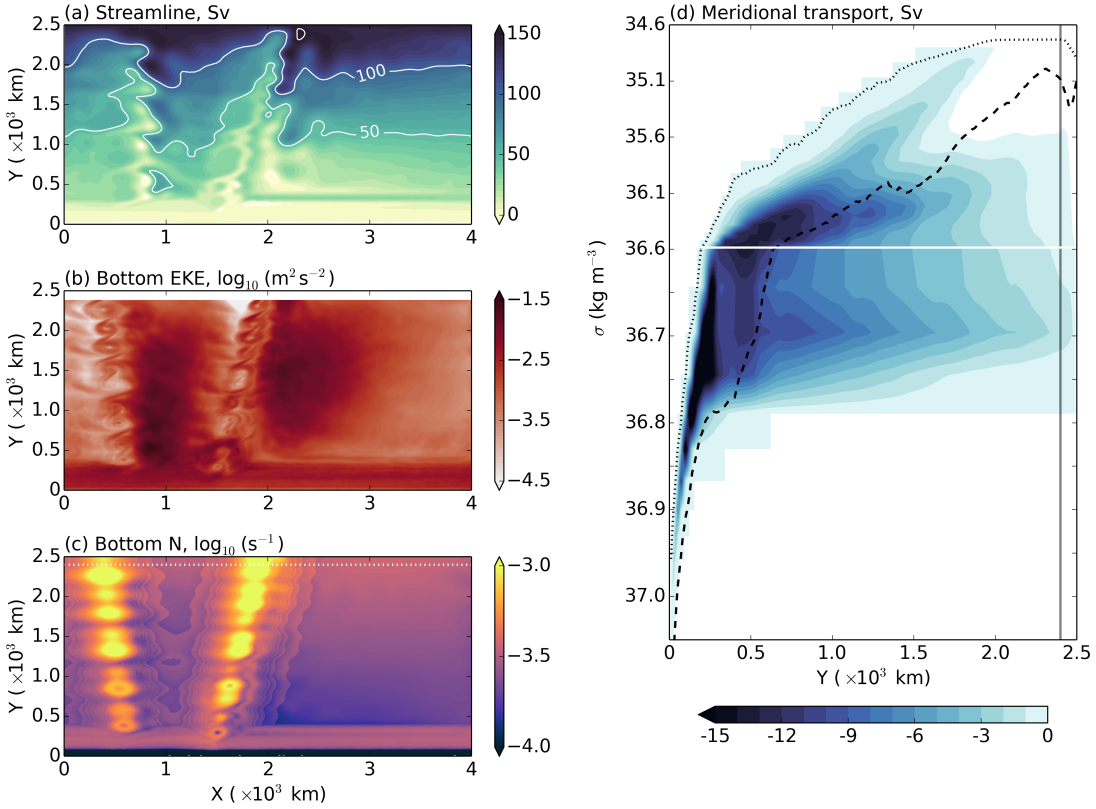

Fig. 3.3 Diagnostics for the reference case. (a) Streamlines in units of Sv. White contours mark the streamline of 50 and 100 Sv. (b) Bottom-500m-averaged EKE, $\log_{10}$ scale, in units of $m^2\ s^{-2}$. (c) Bottom-500m-averaged stratification, $\log_{10}$ scale, in units of s^{-1}. (d) MOC streamfunction in units of Sv. The dotted and dashed black lines represent the minimum and maximum density, respectively, that ever occurred at the surface. The white block (2400 km $\leqslant$ Y $\leqslant$ 2500 km) in (b), white dotted line in (c), and grey vertical line in (d) indicate the position of the sponge layer. The white line in (d) marks the density level of 36.6 kg m^{-3}, below which the density coordinate is stretched.

not only the large-scale circulation in the Southern Ocean, but also bottom velocity and stratification fields that are characteristic of lee wave generation sites in the Southern Ocean (chapter 2). As the lee wave parameterisation closely relies on the bottom velocity and stratification fields, we mainly look at the EKE and stratification fields in the bottommost 500 m from model output.

The total zonal transport is 141.5 Sv (1 Sv = 10^6 m^3 s^{-1}), which is in the observed Drake Passage range, 136.7 $\pm$ 6.9 Sv (Meredith et al., 2011). As the theory discussed in section 3.2.1 predicts the baroclinic transport, we hereafter calculate and show the baroclinic transport using the density field based on the thermal wind relation. Complex topographic features (Fig. 3.1) used in the model configuration steers the zonal flow and permits a

meandering structure of the flow (Fig. 3.3a). Due to the diffusive boundary condition, only the lower overturning circulation is produced in the reference case (Fig. 3.3d). The strength of the lower overturning circulation is 5.3 Sv (at Y = 1600 km), it scales up to roughly 26.5 Sv given a circumpolar perimeter at the latitude of 55°S, which is comparable to the total production of AABW (29 Sv; Talley, 2013). Therefore our channel is a good representation of a sector in the Southern Ocean. The stretched density coordinate shows that the lower overturning circulation occupies a small density range (roughly from 36.6 to 36.8 kg m^{-3}), which, in depth space, fills up the deep ocean below 2 km (solid lines in Fig. 3.4). Bottom

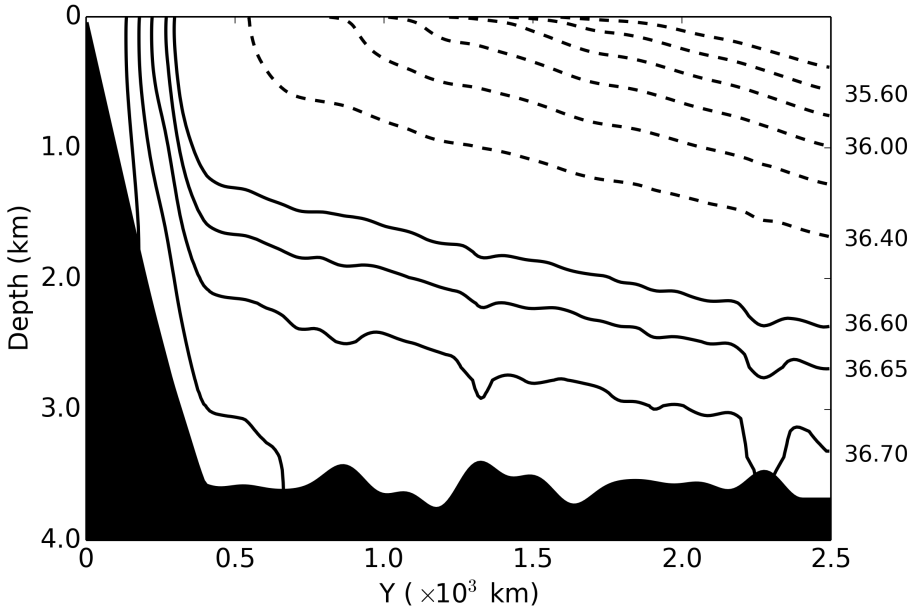

Fig. 3.4 Zonal- and time-mean density structure for the reference case. Dashed contours show density levels ranging from 35.4 kg m^{-3} to 36.4 kg m^{-3} with an interval of 0.2 kg m^{-3}. Solid contours represent density levels ranging from 36.60 kg m^{-3} to 36.80 kg m^{-3} with an interval of 0.05 kg m^{-3}.

EKE reproduced in the reference case (Fig. 3.3b) has a similar magnitude to that in the global ocean model (Fig. 2.4c) and shows clear hotspots downstream of the topography. Bottom EKE varies from $10^{-3.5}$ to $10^{-1.5}$ m^2 s^{-2} (Fig. 3.3b). Bottom EKE can be as large as 10^{-2} m^2 s^{-2}, which indicates the bottom eddy flow can be as strong as 0.1 m s^{-1}. Bottom stratification is strong over the topography in the shallow ocean and weak over the flat area in the abyss (Fig. 3.3c). Bottom stratification is estimated to be lower than $10^{-3.5}$ s^{-1} in most of the domain, with an average of 3×10^{-4} s^{-1} (Fig. 3.3c), which is lower than typical observed and modelled value (10^{-3} s^{-1}) in the abyssal Southern Ocean, especially in lee

wave generation sites (Nikurashin and Ferrari, 2011; Scott et al., 2011; Yang et al., 2018). Lower bottom stratification than expected in the idealised setup is also found in Broadbridge et al. (2016). We acknowledge that a lower stratification limits the frequency band (Eq. 2.1) of radiating lee waves and constrains the lee wave generation; however, the bottom stratification in our model is not unrealistic.

Perturbation experiments

We have designed two sets of experiments (Table 3.2): one with the linear drag coefficient varying from 1×10^{-4} m s^{-1} to 6×10^{-4} m s^{-1} and the other with the quadratic drag coefficient varying from 1×10^{-3} to 6×10^{-3}. Both sets of perturbation are forced by the wind stress with a peak value of 0.2 N m^{-2} and the diffusive boundary condition in the northern sponge layer. We have also set up additional runs with the restoring boundary condition when the quadratic bottom frictional drag is used (Table 3.2). These runs enable us to consider if the northern boundary condition predetermines the results; without extending the model domain to include ocean basins in the north, we also hope to see if the use of different boundary condition helps to reproduce the response of the ocean at different timescales (section 3.6).

Table 3.2 Perturbation experiments under the peak wind stress of 0.2 N m^{-2}. The reference case discussed above is indicated by text 'Ref.'.

Bottom frictional drag	Drag coefficient	Northern boundary condition (b.c.)	
Linear	$r_b = 1 \times 10^{-4}$ m s^{-1}	diffusive	
	$r_b = 2 \times 10^{-4}$ m s^{-1}	diffusive	
	$r_b = 3 \times 10^{-4}$ m s^{-1}	diffusive	(Ref.)
	$r_b = 4 \times 10^{-4}$ m s^{-1}	diffusive	
	$r_b = 5 \times 10^{-4}$ m s^{-1}	diffusive	
	$r_b = 6 \times 10^{-4}$ m s^{-1}	diffusive	
Quadratic	$C_d = 1 \times 10^{-3}$	diffusive	restoring
	$C_d = 2 \times 10^{-3}$	diffusive	restoring
	$C_d = 3 \times 10^{-3}$	diffusive	restoring
	$C_d = 4 \times 10^{-3}$	diffusive	
	$C_d = 4.5 \times 10^{-3}$		restoring
	$C_d = 5 \times 10^{-3}$	diffusive	
	$C_d = 6 \times 10^{-3}$	diffusive	restoring

We have perturbed the surface wind stress for the linear ($r_b = 3 \times 10^{-4}$ m s^{-1}) and quadratic ($C_d = 3 \times 10^{-3}$) drag experiments with a diffusive boundary condition. The peak wind stress has been changed from 0.2 N m^{-2} to 0.1 N m^{-2} and 0.3 N m^{-2}.

The model is initialised from a state of rest; the initial temperature field has the same vertical structure as the restoring temperature profile used in the sponge layer (Fig. 3.2d). The model is spun up for 200 years until it reaches a steady state. When parameters are changed, the model was run from a previously equilibrated state for another 50 years, and the last 5 years of output are diagnosed and used for averaging.

3.4 Sensitivity of the ACC transport to changing bottom drag coefficient and wind stress

3.4.1 Linear bottom drag coefficient

We first evaluate the sensitivity of the baroclinic transport and domain-averaged EKE to the linear bottom drag coefficient in a model configuration with the topography (Fig. 3.1) that is more complex than the one used in Marshall et al. (2017). We exclude the southernmost 500 km (Antarctic slope area) for the integration of baroclinic transport and EKE to focus on the ACC.

The results show that, under the same wind stress, increasing the linear bottom drag coefficient from 1×10^{-4} m s^{-1} to 6×10^{-4} m s^{-1} leads to an increase of over 100% of the baroclinic transport (Fig. 3.5a) and a nearly 12% decrease in the domain-averaged EKE (Fig. 3.5b). The increase in the baroclinic transport is nearly linear with the drag coefficient,

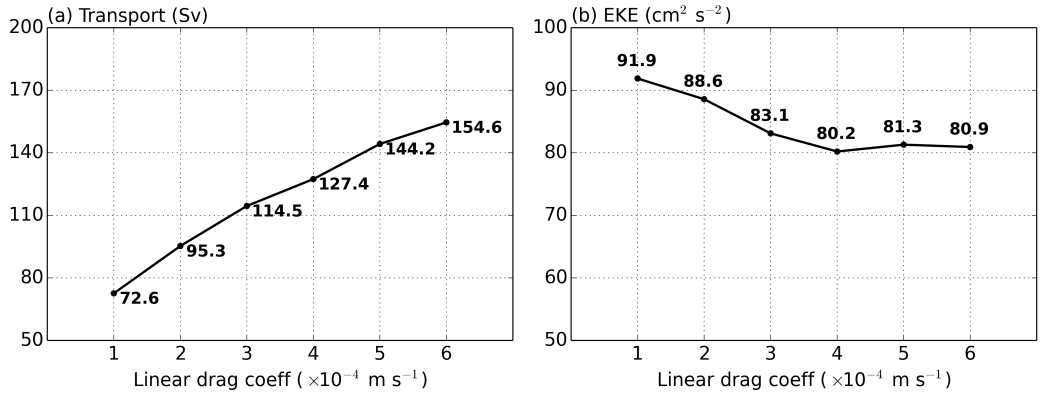

Fig. 3.5 (a) Baroclinic transport excluding the southernmost 500 km and (b) domain-averaged EKE as a function of the linear drag coefficient.

which is consistent with Eq. (3.4). As the linear drag coefficient increases, the eddy energy is dissipated at a higher rate. The increase in the eddy energy dissipation rate needs to be balanced by an increase in the eddy energy generation rate, which is achieved by a larger vertical shear. The larger vertical shear leads to an increase in the baroclinic transport and a greater generation rate of eddies that eventually matches the increased dissipation rate due to a larger drag coefficient. The vertical shear of the ACC is related to isopycnal slopes through geostrophy. As a result, increasing the drag coefficient results in the steepening of isopycnals (Fig. 3.6a), which is also consistent with the MOC dynamics discussed in section 3.2.3.

With a larger drag coefficient, the EKE reservoir experiences a net loss (Fig. 3.5b), consistent with the dynamics that we have discussed in sections 3.2.2 and 3.2.3: EKE is set primarily by the wind stress and regulated by the residual overturning circulation; while the wind is independent of the drag coefficient, the residual overturning circulation decreases with the drag coefficient.

The sensitivity of the baroclinic transport and domain-averaged EKE to the linear drag coefficient, produced in our model with a more realistic topography, is consistent with the theoretical scaling and modelling results in Marshall et al. (2017), despite the difference (e.g., vertical resolution, topography) in the model.

3.4.2 Quadratic bottom drag coefficient

Marshall et al. (2017)'s theory predicts that the ACC transport scales linearly with the eddy energy damping rate (Eq. 3.4). This prediction relies on the assumption that the eddy energy sink is linearly proportional to the eddy energy integral (Eq. 3.2), which might not be the case in the ocean (section 3.2.2). Using a quadratic drag relationship (Eq. 3.7), we have shown that the ACC transport still scales linearly with the eddy energy damping rate (and therefore the quadratic drag coefficient), but also depends on EKE (Eq. 3.9). Here, we test the sensitivity of the ACC transport to the quadratic drag coefficient (Eq. 3.9) and compare this sensitivity with that in the linear case.

As before, we calculate the baroclinic transport excluding the slope area from each quadratic drag coefficient experiment and examine its sensitivity to the quadratic drag coefficient (Fig. 3.7a). It is found that the baroclinic transport also increases with the drag coefficient when the quadratic bottom frictional drag is used, which is consistent with our theoretical prediction (Eq. 3.9). The explanation is similar: the increase in the quadratic drag coefficient leads to a higher eddy energy dissipation rate, which is compensated by a larger eddy energy generation rate provided by a more baroclinic flow (equivalent to the steeper isopycnals shown in Fig. 3.6b), assuming baroclinic instability as the main eddy generation mechanism, and the integration of which gives a stronger baroclinic transport.

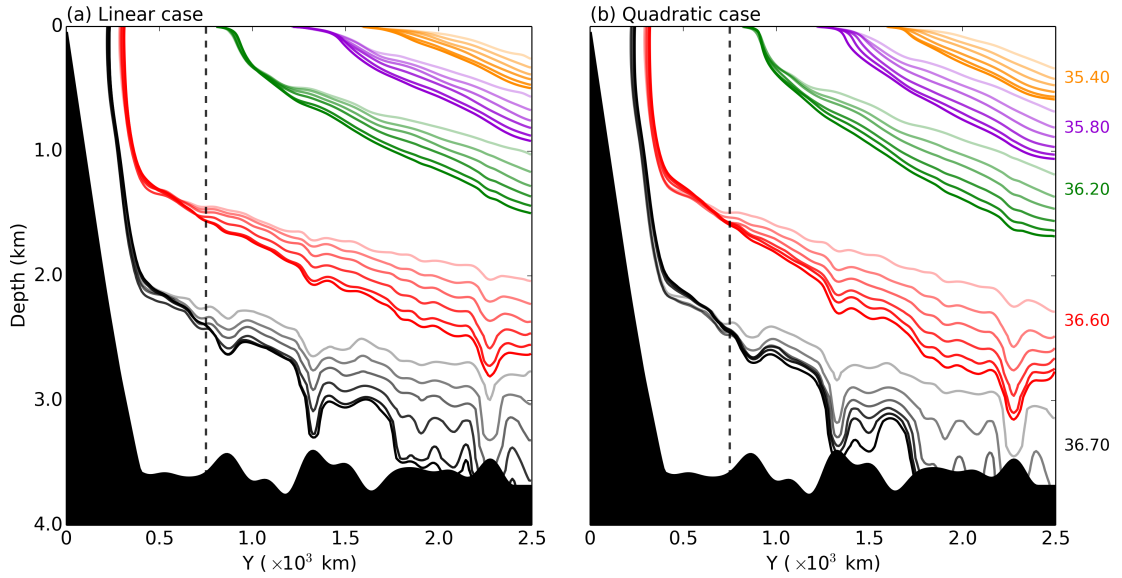

Fig. 3.6 Zonal- and time-mean density structure for the (a) linear and (b) quadratic drag experiments. The colours represent different density levels; from top to bottom, orange, purple, green, red, and black colours represent the density level of 35.4 kg m^{-3}, 35.8 kg m^{-3}, 36.2 kg m^{-3}, 36.6 kg m^{-3}, and 36.7 kg m^{-3}, respectively. The six lines of each colour, from light to dark, in (a) correspond to the linear drag coefficient of 1×10^{-4} m s^{-1}, 2×10^{-4} m s^{-1}, 3×10^{-4} m s^{-1}, 4×10^{-4} m s^{-1}, 5×10^{-4} m s^{-1}, 6×10^{-4} m s^{-1}, respectively (Table 3.2). The six lines of each colour, from light to dark, in (b) correspond to the quadratic drag coefficient of 1×10^{-3}, 2×10^{-3}, 3×10^{-3}, 4×10^{-3}, 5×10^{-3}, 6×10^{-3}, respectively (Table 3.2). The black dashed vertical lines mark the latitude where the characteristic value of the lower overturning circulation streamfunction is chosen.

Note that in Fig. 3.7a, the linear drag case has the same x-axis with the quadratic drag case; this is because the linear drag coefficient, r_b, is modelled in MOM6 as a multiplication of a non-dimensional drag coefficient, C_d, and a constant, 0.1, in units of m s^{-1}. When we change the type of bottom frictional drag from linear to quadratic, C_d is held the same.

We also compare the sensitivity of the baroclinic transport to the drag coefficient in the quadratic case with that in the linear case. Qualitatively, both linear and quadratic drag cases show an increase in the baroclinic transport with the drag coefficient. Here, the quadratic drag experiments produce higher transport than linear drag experiments because we did not tune the drag coefficient to ensure that the baroclinic transport was the same in the reference experiment of each case. The difference in the baroclinic transport between the linear and quadratic drag cases is not important because our focus is on the sensitivity of the baroclinic transport to the drag coefficient. We note that both linear and quadratic drag cases produce a

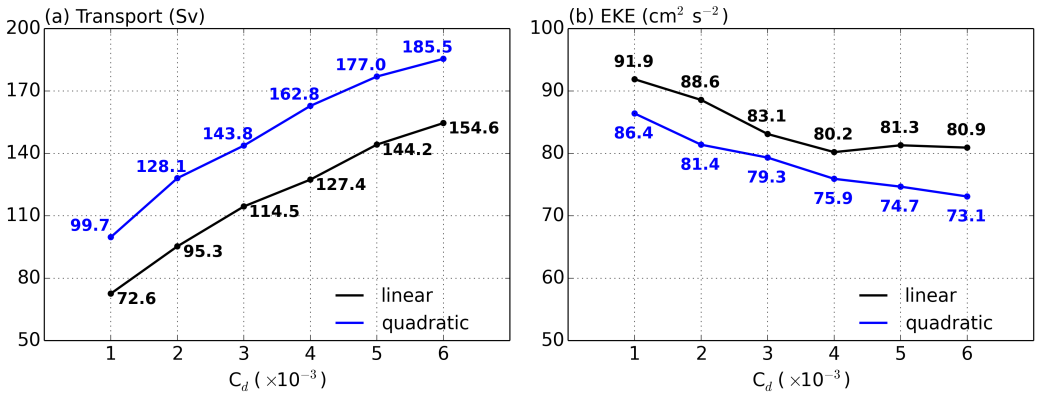

Fig. 3.7 (a) Baroclinic transport excluding the southernmost 500 km and (b) domain-averaged EKE as a function of the linear and quadratic drag coefficient.

reasonable total transport over the entire domain in their reference experiment, which are 141.5 Sv and 172.4 Sv, respectively.

The domain-averaged EKE in each experiment agrees with the predicted theoretical scaling (Fig. 3.7b). The quadratic drag case shows a decrease by approximately 15% in the domain-averaged EKE (Fig. 3.7b). The decrease in EKE is suggested to be a result of the weakening of the residual overturning circulation (section 3.2.3). The approximately same percentage of decrease in EKE in the linear and quadratic drag cases suggests that the regulation of the residual overturning circulation on EKE is independent of the type of bottom drag.

Based on the extension of Marshall et al. (2017)'s theory (section 3.2.2), we infer a more general control on the baroclinic transport than originally proposed by Marshall et al. (2017): any changes in the bottom that amplify the dissipation of the eddy field, either via the use of a larger drag coefficient (regardless the type of the drag being linear or non-linear), or through adding another form of drag (e.g., lee wave drag) that has a drag coefficient that is comparable to or larger than the bottom drag coefficient, will likely increase the baroclinic transport through enhancing the baroclinicity controlled by the EKE budget.

3.4.3 Wind stress

In section 3.2.2, we have proposed that the baroclinic transport becomes dependent on wind stress in the quadratic drag case, which implies that the baroclinic transport is no longer eddy saturated. Here, we test the sensitivity of the baroclinic transport to the increasing wind stress for the linear and quadratic drag cases, respectively, aiming to reproduce the eddy saturation

in the linear case (Eq. 3.4) and verify the breakdown of the eddy saturation in the quadratic case (Eq. 3.10).

We calculate the baroclinic transport excluding the slope area for the linear ($r_b = 3 \times 10^{-4}$ m s^{-1}) and quadratic ($C_d = 3 \times 10^{-3}$) drag experiments, for different values of peak wind stress τ_0. We find that the baroclinic transport is insensitive to wind stress in the linear

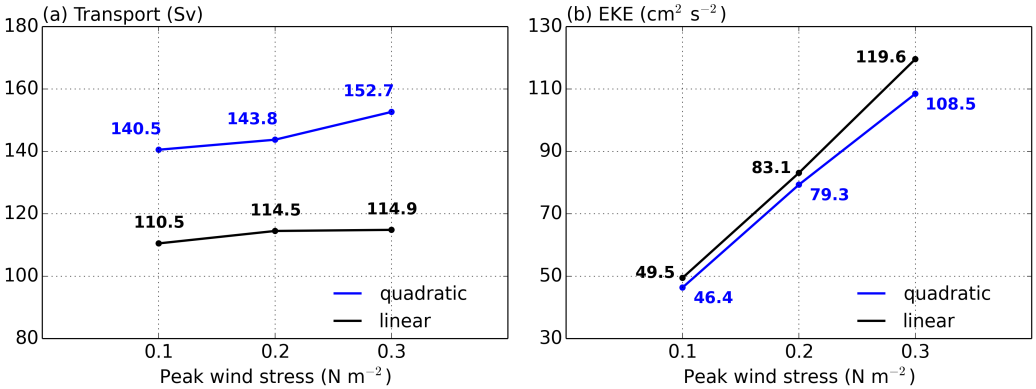

Fig. 3.8 Sensitivity of the (a) baroclinic transport and (b) domain-averaged EKE (excluding the slope area) to wind stress in the linear and quadratic cases, indicated by the black and blue lines, respectively.

drag case and becomes sensitive to wind stress in the quadratic case (Fig. 3.8a). This is consistent with our theoretical scalings (Eq. 3.4 and 3.10). The eddy saturation produced in the linear drag case demonstrates that the baroclinic transport is independent of wind stress, where the steepening of isopycnals due to the increasing wind is perfectly balanced by the isopycnal flattening due to the stronger eddy field. With the quadratic bottom frictional drag, the baroclinic transport increases with wind stress. This implies that there is a net steepening of isopycnals that is not balanced by the eddy flattening of isopycnals. Consistently, EKE does not increase as much with wind stress in the quadratic drag case as in the linear drag case (Fig. 3.8b).

In our simulations, when the wind stress increases, isopycnals deepen in both linear and quadratic cases (Fig. 3.9) because of a stronger wind-driven Ekman transport, a thicker surface mixed layer, and the freedom of isopycnals to move in the vertical direction in the northern sponge layer. Isopycnals steepen in the quadratic drag case while they retain their slope in the linear drag case, which is clearly seen in isopycnals 35.60 and 36.00 kg m^{-3} in the upper ocean (Fig. 3.9), where the slope of isopycnals determines the baroclinic transport.

We have shown that the response of the baroclinic transport to wind stress is modulated by the bottom drag parameterisation. While we are able to reproduce the eddy saturation in Marshall et al. (2017) in the linear drag case, we also find that the baroclinic transport

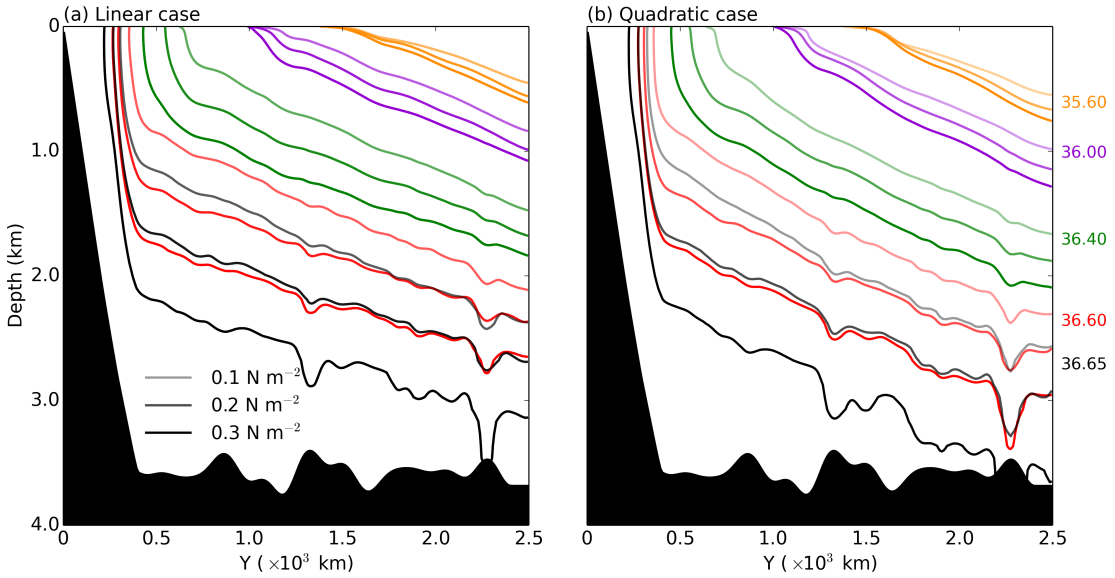

Fig. 3.9 Time- and zonal-mean isopycnals in the (a) linear and (b) quadratic cases, which are from experiments where the drag coefficient is $r_d = 3 \times 10^{-4}$ m s^{-1} and $C_d = 3 \times 10^{-3}$, respectively. The colours represent different density levels; from top to bottom, orange, purple, green, red, and black colours represent the density level of 35.60 kg m^{-3}, 36.00 kg m^{-3}, 36.40 kg m^{-3}, 36.60 kg m^{-3}, and 36.65 kg m^{-3}, respectively. For each colour, the darker the line, the larger the wind stress. There are three lines for each colour in corresponding to the peak wind stress of 0.1 N m^{-2}, 0.2 N m^{-2}, and 0.3 N m^{-2}.

increases with wind stress in the quadratic drag case. The dependence of the baroclinic transport on wind stress in the quadratic case arises from the nonlinear dependence of the eddy energy sink on eddy energy using equations in section 3.2.2.

3.5 Sensitivity of the lower MOC to bottom drag

To examine the sensitivity of the lower overturning circulation to the bottom drag coefficient, we calculate the streamfunction of the lower overturning circulation for each drag coefficient in the linear and quadratic drag cases. The streamfunction of the overturning circulation is calculated by vertically integrating the meridional velocity from the bottom to different layers above in density space, then time averaging and zonally integrating over the Southern Ocean (e.g., Hallberg and Gnanadesikan, 2006; Ito and Marshall, 2008). Three drag coefficients from each case are shown to illustrate the strength and spatial distribution of the lower overturning circulation (Fig. 3.10, 3.11). The lower overturning cell is strongly diabatic (Fig.

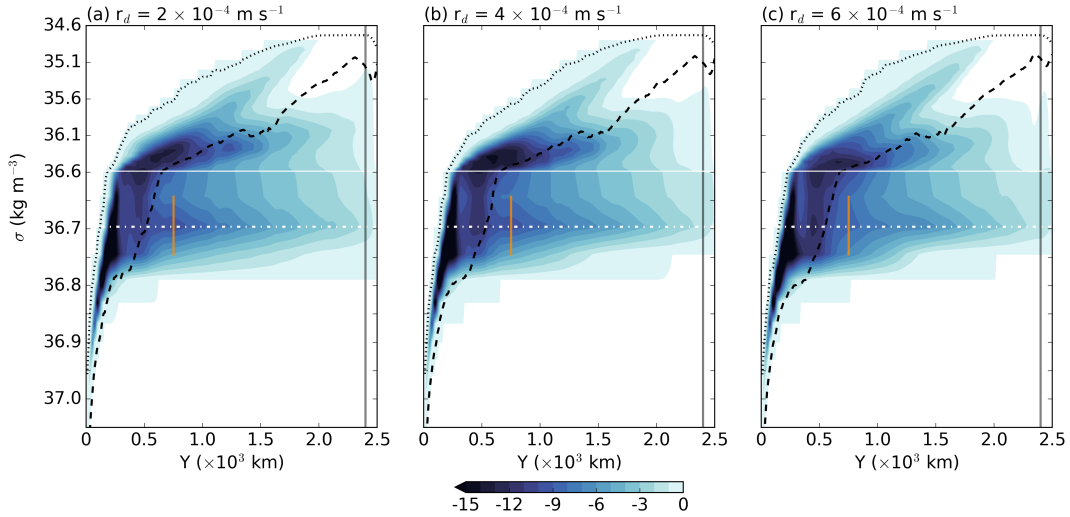

Fig. 3.10 Lower overturning circulation streamfunction (Sv) in the linear drag case for the drag coefficient of (a) $r_d = 2 \times 10^{-4}$ m s^{-1}, (b) $r_d = 4 \times 10^{-4}$ m s^{-1}, and (c) $r_d = 6 \times 10^{-4}$ m s^{-1}. The dotted and dashed black lines represent the minimum and maximum density, respectively, that ever occurred at the surface. The area between the dotted and dashed black lines indicates the surface mixed layer. The grey vertical line indicates the location of the sponge layer. The white dash dotted horizontal lines indicate the density layer (ρ = 36.7 kg m^{-3}) where the maxima of the lower overturning circulation streamfunction occur. Along the white dash dotted horizontal lines, the values of the streamfunction at the latitude marked by the orange vertical lines (Y = 750 km) are chosen as the characteristic values of the lower overturning circulation streamfunction.

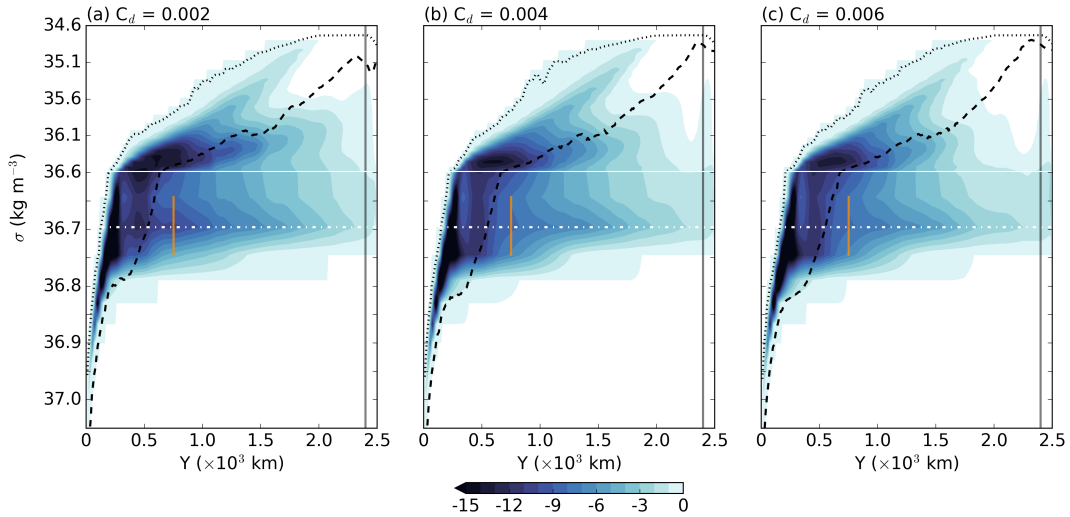

Fig. 3.11 Same as Fig. 3.10, but for the quadratic drag case.

3.3d, Fig. 3.10, and Fig. 3.11): streamfunction contours cross multiple isopycnals in the interior, which indicates that the bottom water is slowly transformed into lighter waters as it moves northwards. The lower overturning circulation reaches its maximum at the density level of ρ = 36.7 kg m^{-3} (the isopycnals in depth space are shown in Fig. 3.6) in both linear and quadratic drag cases and, along this density level, decreases northward as the bottom water is transformed by the mixing (Fig. 3.10, 3.11). The structure of the lower overturning circulation is not significantly different for the linear and quadratic drag cases (Fig. 3.10, 3.11).

We evaluate the sensitivity of the lower overturning circulation to the increasing drag coefficient by comparing values along the density level of ρ = 36.7 kg m^{-3} at the latitude of Y = 750 km. The latitude chosen here is outside of the surface mixed layer (Figs. 3.10 and 3.11) and also includes the majority of the lower overturning circulation and therefore gives a representative value of the lower overturning circulation streamfunction. The strength of the lower overturning circulation slightly decreases with the drag coefficient in both linear and quadratic drag cases (Fig. 3.12). The decrease in the lower overturning circulation

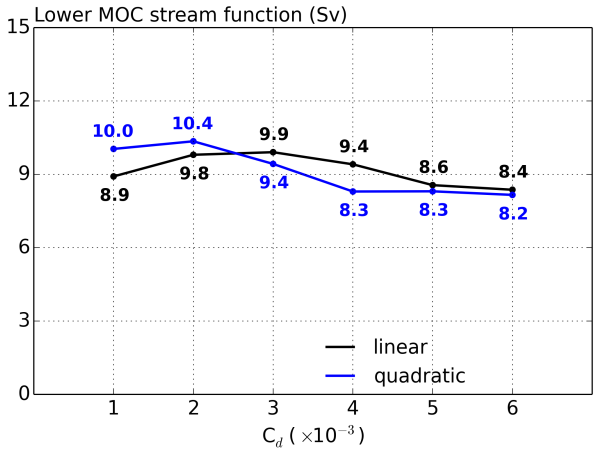

Fig. 3.12 Lower overturning circulation streamfunction as a function of the drag coefficient. Black (blue) lines are values along the density level ρ of 36.7 kg m^{-3} at the latitude Y of 750 km.

in the quadratic drag case is up to 20% (from C_d = 0.002 to 0.006). The decrease in the lower overturning circulation with the drag coefficient is associated with the change in the isopycnal slope and explains the change in EKE, as discussed in section 3.2.3.

Here, in addition to reproducing the increase in the isopycnal slope to larger drag coefficients predicted theoretically by Marshall et al. (2017), we develop a physical understanding of the adjustment processes in the system when the drag coefficient is increased, which con-

nects EKE, the isopycnal slope, the lower overturning circulation, and the ACC baroclinic transport. The use of a larger drag coefficient leads to a larger eddy energy dissipation rate and therefore reduces EKE. When the EKE responds initially with the drag coefficient, the isopycnal slopes have not yet changed significantly as the adjustment of density layers in the ocean happens at a much longer timescale. Therefore, the reduction in EKE leads to a smaller eddy diffusivity and weakens the eddy-driven overturning circulation (Eq. 3.13). The weakening of the eddy-driven overturning circulation then results in the tilting of the isopycnals (Fig. 3.6) because now the wind-driven overturning circulation is stronger than the eddy-driven overturning circulation. The steepening of the isopycnals is accompanied by an increasing vertical shear (through the thermal wind relation), which increases the eddy energy generation rate to match the increased eddy energy dissipation rate and strengthens the baroclinic transport (Fig. 3.7a). The isopycnals get steeper gradually during the adjustment and remain at a slope that is larger than their original slope so that they continue to support the eddy generation at a higher rate to balance the increased eddy dissipation. In the new steady state, the steeper isopycnals yield a weaker residual overturning circulation (Eq. 3.16, Fig. 3.12) and therefore a decreased EKE (Fig. 3.7b), despite that the eddies are generated and dissipated equally at a higher rate. A weaker residual overturning circulation also requires a weaker eddy-driven overturning circulation to oppose the wind-driven overturning circulation, which is likely to be the case here given the increased slope but decreased EKE.

3.6 Sensitivity of results to the choice of northern boundary condition

The purpose of using the enhanced diffusivity or temperature restoring in the sponge layer is to represent the response of the ocean basins north of the Southern Ocean to changes in the Southern Ocean at different timescales (section 3.3.1). Using a diffusive boundary condition, we are able to produce results that are consistent with Marshall et al. (2017) in the linear drag case and also extend their theory to consider the quadratic drag case. In this section, we investigate the response of the baroclinic transport to increased quadratic bottom drag coefficient at a shorter timescale, i.e., in the experiments with a restoring northern boundary condition.

With a temperature restoring northern boundary condition, the baroclinic transport is reduced significantly, and is much less sensitive to the quadratic drag coefficient (Fig. 3.13a). The baroclinic transport is strongly constrained because the isopycnals are fixed at the surface and northern boundaries by the temperature restoring boundary conditions (Fig. 3.14a).

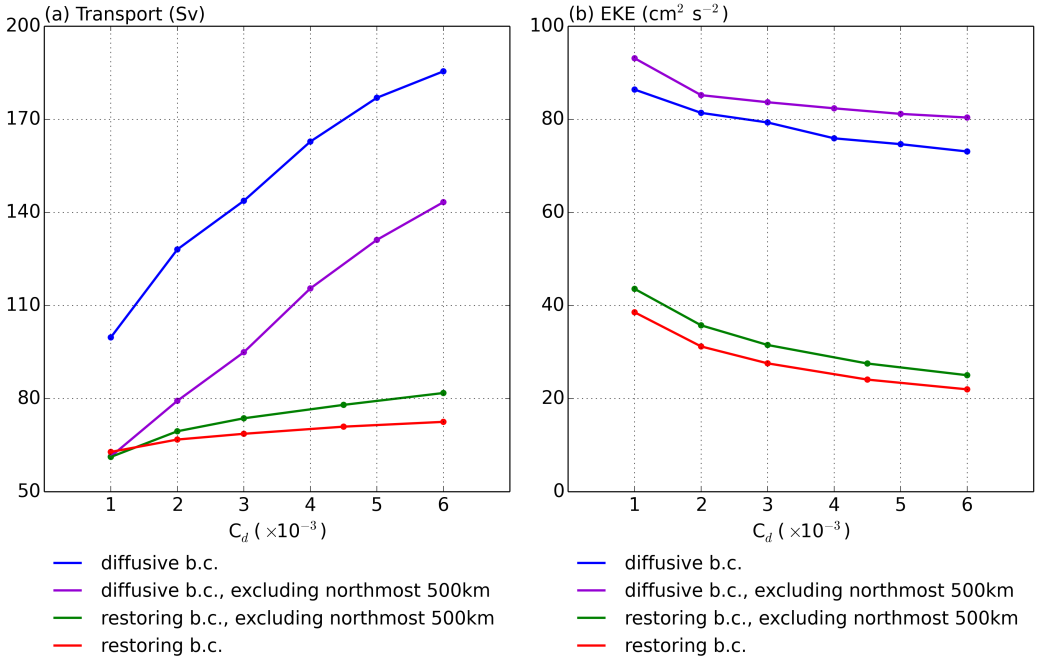

Fig. 3.13 (a) Baroclinic transport and (b) domain-averaged EKE as a function of the quadratic drag coefficient. Blue line represents the case where a diffusive boundary condition is used in the sponge layer; red line represents the case where a restoring boundary condition is used; the green and purple lines represent the transport calculated excluding the northernmost 500 km of the domain in the restoring and diffusive boundary condition cases, respectively.

The impact of boundary conditions is seen by varying the drag coefficient (Fig. 3.15); increasing the drag coefficient does not alter the position of the isopycnals (Fig. 3.15a). In contrast, when a diffusive boundary condition is used, increasing the drag coefficient leads to a deepening and tilting of the isopycnals (Fig. 3.15b). The comparison between the use of a restoring and a diffusive boundary condition demonstrates that the temperature restoring condition strongly inhibits the displacement of the isopycnals at the northern boundary.

To put these results in the context of the theory presented in this chapter, we define two regions of the domain: the transitional region (Y = 2000 - 2500 km) and the interior region (Y = 0 - 2000 km). The transitional region (marked in red boxes in Fig. 3.14) is where the isopycnals tilt in the opposite direction compared with the rest of the domain for the restoring case, in contrast with the isopycnals in the same region in the diffusive case. In this region, there is a westward flow, indicated by the blue colour marked in the red box in Fig. 3.14a, which results from the northward uptilting isopycnals in the restoring case. In the interior of the restoring case, the isopycnals are tilting in the same direction as those in the diffusive case. The transitional region arises from the need to match the (Southern Ocean) interior,

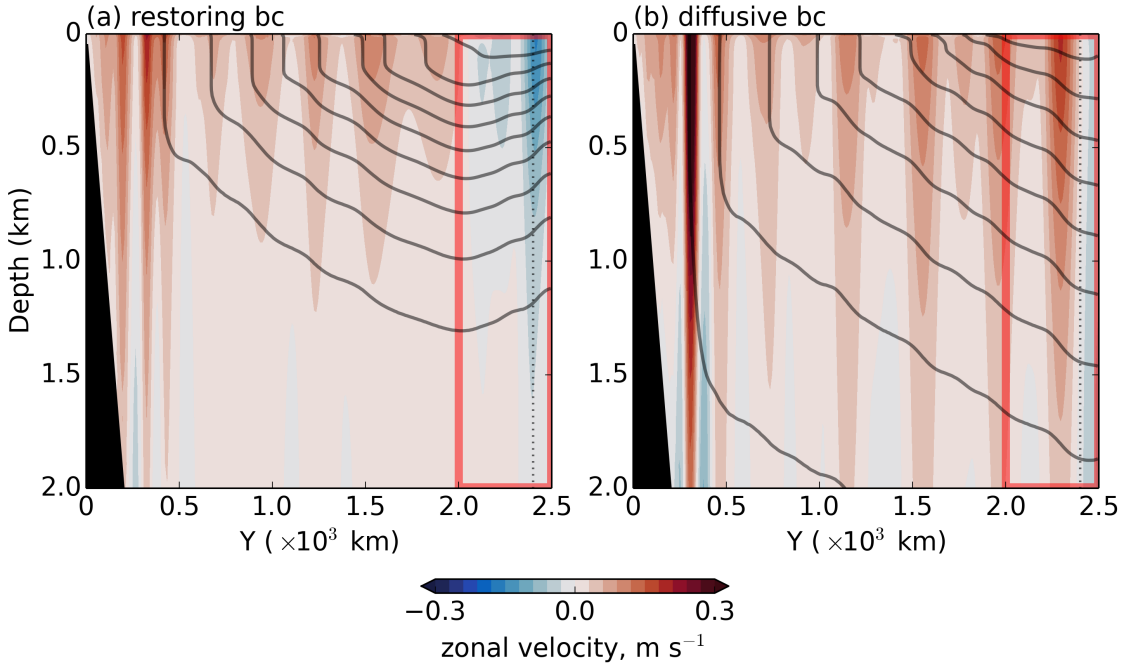

Fig. 3.14 Time averaged isopycnals (contours) and zonal velocity (colours) at X = 3500 km over the final year from the experiments with the (a) restoring boundary condition and (b) diffusive boundary condition. Both experiments use a quadratic bottom frictional drag. The grey lines represent the isopycnals ranging from 1035.0 to 1036.6 kg m^{-3} with an interval of 0.2 kg m^{-3}. Red boxes in (a) and (b) highlight the different control of the boundary condition on the height and the shape of the isopycnals. The grey dotted vertical lines indicate the position of the sponge layer.

governed by the wind, eddies, and bottom drag dynamics described in section 3.2.2, to the restoring boundary condition in the sponge layer.

To illustrate the effects of the transitional layer on the flow to its south and its sensitivity to the increasing drag coefficient, we exclude this area and repeat our calculations and compare results with those calculated using the entire domain. In the restoring case, excluding the northernmost 500 km (about 1/5 in meridional direction) of the domain, we found that the baroclinic transport is higher than that calculated using the entire domain and also increases with the drag coefficient (Fig. 3.13a). The transport is higher in the interior because we have now excluded the return flow in the transitional layer that partly cancels the eastward flow when integrated in the meridional direction. The increase of transport in the interior implies that the control of bottom drag is inherent in the system. Although the increase in the baroclinic transport is still found in the interior of the domain, the transport has been significantly reduced by using a temperature restoring boundary condition with respect to the case with a diffusive boundary condition (Fig. 3.13a). The transport in the restoring case

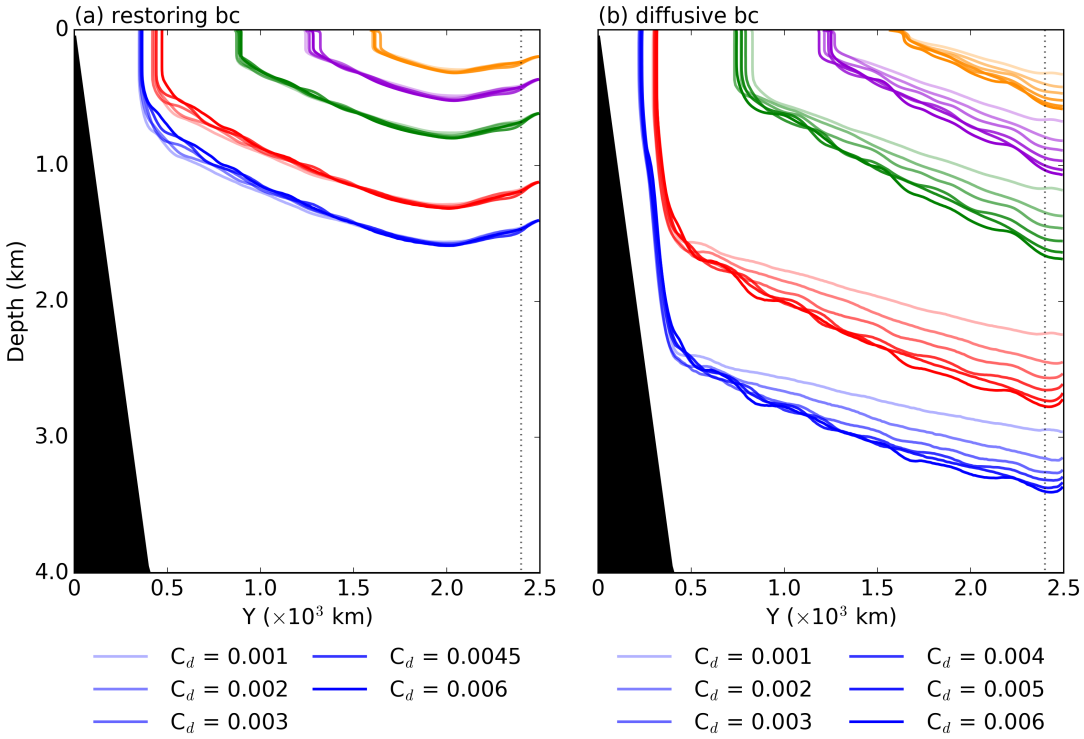

Fig. 3.15 Time averaged isopycnals at X = 3500 km over the final year from the experiments with the (a) restoring boundary condition and (b) diffusive boundary condition. The colours represent different density levels; from top to bottom, orange, purple, green, red, and blue lines represent the density level of 1035.4 kg m^{-3}, 1035.8 kg m^{-3}, 1036.2 kg m^{-3}, 1036.6 kg m^{-3}, and 1036.7 kg m^{-3}, respectively. For each colour, the darker the line, the larger the drag coefficient. There are five lines for each colour in (a), corresponding to the quadratic drag coefficient of 1×10^{-3}, 2×10^{-3}, 3×10^{-3}, 4.5×10^{-3}, and 6×10^{-3}; there are six lines for each colour in (b), corresponding to the quadratic drag coefficient of 1×10^{-3}, 2×10^{-3}, 3×10^{-3}, 4×10^{-3}, 5×10^{-3}, 6×10^{-3} (Table 3.2).

is much lower than that in the diffusive case even when we exclude the transitional region is because we do not adjust the restoring temperature profile to be the same as the northern temperature in the diffusive case. We argue that, even though adopting a temperature profile from the diffusive case would match the transport in the reference experiment of two cases, the sensitivity of the baroclinic transport to the increasing drag coefficient would not be altered in the restoring case because there is still very limited freedom of the isopycnals in the vertical direction in the sponge layer. This hidden and suppressed increase in the baroclinic transport in the interior demonstrates that the dynamics governing of transport by bottom drag is taking place but kept down at a very low level by the restoring boundary condition. In contrast, when a diffusive boundary condition is used, the isopycnals do not experience

a change in the tilting direction (Fig. 3.14b); the baroclinic transport decreases when the northernmost 500 km is excluded (Fig. 3.13a).

The restoring and diffusive boundary conditions have been shown to produce different sensitivity of the ACC baroclinic transport to the increasing drag coefficient. The comparison between the restoring and diffusive cases shows the strong constraint from the restoring boundary condition on the sensitivity of the baroclinic transport to the increasing drag coefficient. However, the interior region in the restoring case follows the same dynamics discussed in section 3.2.2: the isopycnals tend to steepen and the baroclinic transport increases following the increase in the drag coefficient.

3.7 Summary

Before exploring the impact of lee wave parameterisation, we characterise the sensitivity of our model to bottom drag. We have extended Marshall et al. (2017) to investigate how the linear and quadratic bottom frictional drag control the Southern Ocean circulation and its sensitivity to changes in wind stress. Marshall et al. (2017) focused on the linear bottom frictional drag and showed that the ACC transport increases with increased linear drag coefficient and is nearly insensitive to wind stress.

Using a model configuration with a more complex topography than the one used in Marshall et al. (2017), we test their theory (section 3.2.1) and confirm an increasing ACC baroclinic transport with increased linear drag coefficient (section 3.4.1). The increase in the baroclinic transport is attributed to the steepening of the isopycnals, which results in a larger eddy energy generation rate that compensates the increased eddy energy dissipation rate associated with a larger drag coefficient. In this case, when we increase wind stress, the transport remains eddy saturated.

We extend their theory to consider an ocean damped by the quadratic bottom frictional drag and predict that the ACC baroclinic transport also increases with increased quadratic drag coefficient (section 3.2.2). Furthermore, we find that the baroclinic transport is no longer eddy saturated as the baroclinic transport is now also dependent on EKE and therefore on wind stress (section 3.2.2). When wind stress increases, the domain-averaged EKE increases less in the quadratic drag case than the linear drag case, which leads to a reduced flattening of the isopycnals by eddies and therefore steeper isopycnals. Steeper isopycnals give a larger vertical shear, through geostrophy, which then leads to a stronger baroclinic transport and a weaker lower overturning circulation.

We find that, while the governing dynamics that sets the ACC baroclinic transport and the lower overturning circulation holds, the use of a restoring northern boundary condition

strongly constrains the vertical displacement of the isopycnals that effectively constrain the baroclinic transport to increasing drag coefficient. We divide the model domain into two regions, the interior region and the transitional region, to understand the circulation. Once we exclude the transitional region, the baroclinic transport shows a slight increase with increased drag coefficient, implying that the interior region follows the dynamics described in section 3.2.2 and behaves consistently with that in the diffusive case.

Given the impact of bottom frictional drag on the ACC baroclinic transport and the lower overturning circulation, our results imply that the inclusion of lee wave drag in models will very likely lead to an increase in the ACC transport and a decrease in the strength of the lower overturning circulation. The impacts of lee wave drag on the ACC and the MOC predicted here are expected to hold independent of the formula used in parameterisation. However, the dependence of lee wave drag on velocity, whether linear or quadratic, will determine how lee wave drag regulates the sensitivity of the ACC transport to changes in wind stress.

Chapter 4

The role of lee waves for the Southern Ocean circulation and its sensitivity to winds

4.1 Introduction

Lee waves have been suggested to apply a drag on the time-mean Antarctic Circumpolar Current (ACC) and play an important role in the momentum balance of the flow in the Southern Ocean (Naveira Garabato et al., 2013). It is estimated that lee waves extract 0.2-0.4 TW of energy from the geostrophic flow in the Southern Ocean (Nikurashin and Ferrari, 2011; Scott et al., 2011). Yang et al. (2018) estimated that 75% of the energy in lee waves came from the transient eddy field, which implies that lee waves also apply a drag on the eddy field (chapter 2). The implication of the finding in chapter 2 is that lee wave parameterisation should include a lee wave drag to reflect the impact of lee waves on the momentum balance of the time-mean and eddy flow. In chapter 3, we investigate how the bottom frictional drag affects the ACC and Meridional Overturning Circulation (MOC). We find that a larger drag coefficient leads to a stronger ACC transport and a weaker lower overturning circulation due to the bottom drag effect on the eddy field. This finding suggests that lee wave drag, which acts against the eddy flow similar to bottom frictional drag, might also affect the ACC and the MOC. Motivated by the potential impacts of lee wave drag on the Southern Ocean circulation, in this chapter, we will parameterise lee wave drag and investigate its role in regulating the Southern Ocean circulation and its sensitivity to changes in wind stress.

The impact of lee waves on the large-scale circulation is not well understood and is not accurately represented in the eddy-resolving global ocean models. The generation and

subsequent radiation and breaking of lee waves extract momentum and energy from the large-scale flow. The removal of momentum from the flow by lee waves is similar to the effect of bottom drag, and therefore is expected to have similar effects as those shown in chapter 3. The breaking of lee waves dissipates their energy and drives turbulent mixing. The enhanced level of mixing associated with the breaking of lee waves leads to increased water mass transformation in the abyssal ocean and hence is a control on the overturning circulation (Meyer et al., 2015; Naveira Garabato et al., 2004; Nikurashin and Ferrari, 2013; Watson et al., 2013). Here, for the first time, we study the impact of both lee wave drag and lee-wave-driven mixing on the ACC and the MOC in the Southern Ocean by developing and implementing an energetically consistent parameterisation of lee waves in an eddy-resolving ocean model.

Lee-wave-driven mixing has been shown to affect the overturning circulation and its response to changing wind stress. Using a coarse-resolution climate model and a fixed energy input into lee waves, Melet et al. (2014) found that the lee wave-driven mixing led to a stronger lower overturning circulation (+2 Sv, an increase in intensity of 10%), a stronger stratification, and a higher diffusivity in the Southern Ocean. Melet et al. (2014) also showed the importance of the spatial distribution of the lee-wave-driven mixing with respect to internal tide-driven mixing on the modification of the stratification and diapycnal diffusivity; they concluded that the lee-wave-driven mixing can not be simply parameterised by a larger internal tide-driven mixing due to its unique spatial distribution. Using an idealised channel model and a lee-wave-driven mixing parameterisation dependent on the resolved flow, Broadbridge et al. (2016) found that both the strength of the lower overturning circulation and the warming of the deep ocean were closely related to the intensity of the lee-wave-driven mixing. In addition, Broadbridge et al. (2016) showed that the lower overturning circulation strengthened with wind stress in the presence of a lee-wave-driven mixing that was regulated by the flow. This modification on the sensitivity of the lower overturning circulation to changes in wind stress by lee-wave-driven mixing has also been implied by an earlier study: Stanley and Saenko (2014) found that the deep overturning increased with wind energy input when eddies were allowed to maintain diapycnal mixing. As lee wave generation is one of the processes that enables downscale energy transfer from eddies to mixing, it can be inferred that the lee-wave-driven mixing would also lead to the increase of the lower overturning circulation with wind, which is otherwise opposite if there is no link connecting eddy energy and diapyncal mixing (Saenko et al., 2012).

Compared with lee-wave-driven mixing, much less is known about the role of lee wave drag in regulating the Southern Ocean circulation and its sensitivity to changes in wind stress. Trossman et al. (2016) studied the impact of lee wave drag on the eddy field using

an eddy-resolving global ocean model with a parameterised lee wave drag that represents both the generation of lee waves and topographic blocking. With this drag parameterisation, Trossman et al. (2016) found that the presence of lee wave drag primarily modified the bottom flow: it increased the dissipation of bottom flow and reduced eddy kinetic energy (EKE) in the deep ocean and its global integral. They also suggested that the lee wave drag parameterisation should use a spatially varying vertical decay depth based on the comparison between their model results and observations. However, they did not assess the impact of lee waves on the Southern Ocean circulation and its sensitivity to changes in wind stress.

Various parameterisations have been used to examine the role of lee waves with most of them focusing on lee-wave-driven mixing; hence, these parameterisations do not fully represent all of the potential lee wave effects. For example, Stanley and Saenko (2014) proposed a parameterisation for coarse ocean models that allowed a fraction of energy in the parameterised eddy field to support diapycnal mixing in the deep ocean, however, their mixing parameterisation did not rely on the characteristics of small-scale topography, and therefore it was not entirely representative of lee wave dynamics. Melet et al. (2014) took a global estimate of energy flux into lee waves from Nikurashin and Ferrari (2011) and implemented it in an ocean-ice-atmosphere climate model, where the lee-wave-driven mixing was not regulated by the energy extracted from the bottom flow and the bottom flow was not affected by the generation of lee waves. Although Broadbridge et al. (2016) used a physically-based parameterisation of lee-wave-driven mixing and acknowledged that the energy transfer into the lee wave field was accompanied by a loss of energy from the resolved flow, through the work done by a wave drag, they did not include such a momentum term in their parameterisation.

Our understanding of the impact of lee waves on the ocean circulation is strongly dependent on and, to some extent limited by, the parameterisation of lee waves. Given the potential impact of lee waves on both momentum and energy balance of the flow, the parameterisation of lee waves should be energetically consistent. An energetically consistent full parameterisation includes both lee wave drag, representing a momentum loss from the resolved flow due to the generation of lee waves, and its associated lee wave-driven mixing, representing an energy source for turbulent mixing due to the breaking of lee waves. It is anticipated that the full parameterisation of lee waves will not only improve the momentum and energy balance of the flow by contributing to the eddy energy dissipation, but also add a temporal- and spatial-dependent energy source for turbulent mixing.

Here, we develop an energetically consistent lee wave parameterisation scheme for eddy-resolving ocean models, which establishes the links between the resolved flow and lee waves, and between lee waves and turbulent mixing. The former extracts the momentum

and energy of the resolved flow while the latter enhances the mixing. We implement this lee wave parameterisation in the idealised channel configuration of the Southern Ocean we use in chapter 3. We look into the impact of parameterised lee waves on the mean state of the ocean and the sensitivity of the ocean circulation to changes in wind stress. We also attribute the changes induced by the parameterisation of lee waves to the lee wave drag or the lee-wave-driven mixing components of the parameterisation and discuss the implication of our findings.

4.2 Lee wave parameterisation

4.2.1 Parameterisation formulation

Lee waves are not resolved by eddy-resolving ocean models, yet they are suggested to extract momentum and energy from the time-mean and eddy field in the ocean. Lee waves are generated when geostrophic flows interact with small-scale topography. As lee waves are generated and radiate away, the geostrophic flow loses a significant amount of momentum and energy (Naveira Garabato et al., 2013; Nikurashin and Ferrari, 2011; Scott et al., 2011) and this energy is used to drive turbulent mixing in the ocean interior (de Lavergne et al., 2016; Meyer et al., 2015; Nikurashin and Ferrari, 2013). To include the impact of lee waves in ocean models in an energetically consistent way, we add lee wave stresses to the momentum equations and then relate them to lee-wave-driven mixing by using the work done by lee wave stresses as an energy source to drive turbulent mixing when lee waves break.

Although there are limited attempts to implement a lee wave drag parameterisation into ocean models, previous studies have suggested formulas that could be adopted in an ocean model. The formula of lee wave drag predicted by linear theory (Bell, 1975) is an integration of the contribution of radiating lee waves in the wavenumber space, which is too expensive a calculation for a global ocean model. Thus a simplification of this formula is necessary to ensure the computational affordability.

Previous attempts have led to a range of options for the simplification. Bell (1975) suggested that the influence of lee wave generation on the mean flow near seafloor was analogous to a bottom friction effect. Recently, Trossman et al. (2013) suggested that lee wave drag cannot be mimicked by artificially increasing bottom drag because lee wave drag was spatial-dependent and non-local. Later, Trossman et al. (2015) implied that there would be no need to parameterise non-local effects according to the spatial average comparison between

models (averaging over an ocean model grid cell) and observations (DIMES[1]/SOFine[2] region). Depending on how the topography is simplified and assumptions made, lee wave drag could be rewritten in several simpler ways, which are also less computationally expensive if coded into models. When a 2D, horizontally periodic sinusodial topography is assumed, lee wave drag is quadratically proportional to the velocity; if the intrinsic frequency of lee waves is much smaller than the local buoyancy frequency, lee wave drag becomes linearly proportional to the velocity (e.g., Pedlosky, 2013). Nikurashin and Ferrari (2010a) derived lee wave drag to be linearly proportional to the velocity for a monochromatic topography and linearly dependent on $|\mathrm{U}|^{3/2}$ for a multichromatic topography. Naveira Garabato et al. (2013) proposed to represent depth-integrated lee wave drag by a quadratic law for mid- and high-latitude oceans under a nonblocking condition; a drag coefficient was introduced while the possibly significant misalignment between the internal wave drag and the near-bottom velocity was neglected. Here, as a first step towards parameterising lee wave drag, we use a linear form suggested by Pedlosky (2013) under the assumption that the intrinsic frequency of lee waves is small compared with the local buoyancy frequency.

Lee wave momentum stresses

If we decompose the flow, $\mathbf{u}$, into a resolved component, $\overline{\mathbf{u}}$, and an unresolved lee wave component, $\mathbf{u}'$, the momentum equation for $\overline{\mathbf{u}}$ takes the form of,

$$\frac{D\overline{\mathbf{u}}}{Dt} - f\mathbf{k}\times\overline{\mathbf{u}} = -\frac{\nabla\overline{\mathbf{p}}}{\rho_0} + \mathbf{R} - \frac{1}{\rho_0}\frac{\partial}{\partial z}\boldsymbol{\tau}_{\mathrm{LW}}, \tag{4.1}$$

where, on the right hand side, there is a body force acting on the resolved flow due to the generation, radiation, and breaking of lee waves, given by the vertical divergence of the wave stress

$$\boldsymbol{\tau}_{\mathrm{LW}} = \rho_0 \cdot \overline{\mathbf{u}'w'}, \tag{4.2}$$

in units of N m^{-2}; the term $\mathbf{R}$ represents the lateral redistribution of momentum due to the viscous stresses.

The wave stress $\boldsymbol{\tau}_{\mathrm{LW}}$ represents the generation, radiation, and breaking of lee waves; it is assumed to decay away from the topography following a vertical structure consistent with energy dissipation observations (e.g., St. Laurent et al., 2012; Waterman et al., 2013), which is expressed as

$$\boldsymbol{\tau}_{\mathrm{LW}}(z) = \boldsymbol{\tau}_{\mathrm{LW}}|_{z=-H} \cdot F(z), \tag{4.3}$$

[1] Diapycnal and Isopycnal Mixing Experiment in the Southern Ocean
[2] Southern Ocean Finestructure project

where H is the depth of the ocean.

To construct a vertical profile of wave stress, we need the bottom value of the wave stress, $\boldsymbol{\tau}_{\text{LW}}|_{z=-H}$, and the vertical structure that captures the radiation and breaking of lee waves, $F(z)$. The wave stress at the bottom (in units of N m^{-2}) associated with lee wave generation is based on a scaling predicted by linear theory (e.g., Cushman-Roisin and Beckers, 2011; Pedlosky, 2013) and takes the form of

$$\boldsymbol{\tau}_{\text{LW}}|_{z=-H} = \rho_0 \cdot \overline{\mathbf{u}'w'}|_{z=-H} = -\frac{1}{2}\rho_0 N_b h_0^2 k \cdot \bar{\mathbf{u}}_{\mathbf{b}}, \tag{4.4}$$

where N_b is the local bottom stratification, h_0 is the amplitude and k the horizontal wavenumber of topography, $\bar{\mathbf{u}}_{\mathbf{b}}$ is the horizontal velocity of the resolved flow at the bottom. This scaling is based on 2D lee wave theory with 1D sinusoidal topography oriented perpendicular to (wavenumber parallel to) the flow $\bar{\mathbf{u}}_{\mathbf{b}}$ (Nikurashin and Ferrari, 2010a). Note that, for the small-scale topography of various height and shape, h_0 refers to the roughness of the small-scale topography as described in section 2.3.2.

Lee wave stress is assumed to decay exponentially as waves radiate upward, and follows a vertical structure proposed for the tidal-mixing parameterisation (Simmons et al., 2004; St. Laurent et al., 2002) and then used for the lee-wave-driven mixing parameterisation (Melet et al., 2014) as

$$F(z) = \frac{e^{-(H+z)/\zeta}}{\zeta(1-e^{-H/\zeta})}, \tag{4.5}$$

where ζ is the vertical decay scale, H is the local depth of the ocean and z is the vertical coordinate (ζ, $H > 0$; $z < 0$). The vertical structure describes how the momentum (and energy) extracted by lee waves at the bottom is redistributed throughout the water column and satisfies $\int_{-H}^{0} F(z)dz = 1$. The vertical structure F(z) is fixed in time. Therefore we can get the final expression for the wave stress (in units of N m^{-2})

$$\boldsymbol{\tau}_{\text{LW}}(z) = -\frac{1}{2}\rho_0 N_b h_0^2 k \cdot \bar{\mathbf{u}}_{\mathbf{b}} \cdot F(z), \tag{4.6}$$

and the body force (in units of m s^{-2}) that would act on the resolved flow

$$\mathbf{F}_{\text{LW}} = -\frac{1}{\rho_0}\frac{\partial}{\partial z}\boldsymbol{\tau}_{\text{LW}} = -\frac{1}{\rho_0}\boldsymbol{\tau}_{\text{LW}}|_{z=-H} \cdot \frac{\partial}{\partial z}F(z) = -\frac{N_b h_0^2 k \cdot \bar{\mathbf{u}}_{\mathbf{b}}}{2\zeta} \cdot F(z). \tag{4.7}$$

To make an analogy with bottom drag in Chapter 3, we introduce a lee wave drag coefficient

$$\gamma_{\text{LW}} = \frac{1}{2}N_b h_0^2 k, \tag{4.8}$$

in units of m s^{-1}, so that the expression for the wave stress can be simplified as

$$\boldsymbol{\tau}_{\mathrm{LW}} = -\rho_0 \cdot \gamma_{\mathrm{LW}} \cdot \overline{\mathbf{u}}_{\mathbf{b}} \cdot F(z) \tag{4.9}$$

to show its dependence on velocity and its vertical structure. The drag coefficient includes the dependence of the lee wave stress and body force on unresolved topography and local stratification. Substituting $N_b = 10^{-3.5}$ s^{-1} (Fig. 3.3c), $h_0 = 100$ m, and $k = 2\pi/2000$ rad m^{-1} into Eq. (4.8), the characteristic magnitude of the lee wave drag coefficient is 5.0×10^{-3} m s^{-1}, which is comparable with the linear bottom frictional drag coefficient used in numerical studies (Abernathey et al., 2011; Marshall et al., 2017) to investigate the sensitivity of the Southern Ocean circulation to changes in wind stress. The form of wave stress [Equation (4.9)] is analogous to the form of linear bottom frictional drag; the distinguishing features of lee wave stress are its dependence on stratification and its vertical structure.

Our parameterisation of body force associated with the generation, radiation and breaking of lee waves captures its dependence on near-bottom flow velocity, stratification, and small-scale topography. This body force acts as a momentum sink to the resolved flow and therefore represents the momentum budget in a consistent fashion, which was overlooked in previous studies (Broadbridge et al., 2016; Melet et al., 2014) that parameterised lee-wave-driven mixing κ_v^{LW} only.

Lee wave-driven mixing

To make our parameterisation energetically consistent, we derive a diffusivity associated with the breaking of lee waves that will be used in tracer equations. We estimate the work done by the body force and assume this amount of energy is converted into lee waves, which lose energy via local turbulent energy dissipation, $\varepsilon^{\mathrm{LW}}$, and enhance diapycnal mixing, κ_v^{LW}, upon breaking.

We estimate the turbulent energy dissipation rate $\varepsilon^{\mathrm{LW}}$ as the work done by the body force on the resolved flow $\overline{\mathbf{u}}$,

$$\varepsilon^{\mathrm{LW}} = |\overline{\mathbf{u}} \cdot \mathbf{F}_{\mathrm{LW}}| = |\overline{\mathbf{u}} \cdot (-\frac{1}{\rho_0}\frac{\partial}{\partial z}\boldsymbol{\tau}_{\mathrm{LW}})|, \tag{4.10}$$

in units of W kg^{-1}.

The total energy dissipation is estimated by the integral of energy dissipation rate from the bottom to 2 km above the bottom

$$\begin{aligned}\int_{-H}^{-H+2000} \rho_0 \cdot \varepsilon^{\mathrm{LW}} dz &= \int_{-H}^{-H+2000} [\overline{\mathbf{u}} \cdot (-\frac{\partial}{\partial z} \boldsymbol{\tau}_{\mathrm{LW}})] dz \\ &\approx \int_{-H}^{-H+2000} \frac{\partial}{\partial z} [\overline{\mathbf{u}} \cdot (-\tau_{\mathrm{LW}})] dz \\ &= \overline{\mathbf{u}} \cdot \boldsymbol{\tau}_{\mathrm{LW}}|_{z=-H} - \overline{\mathbf{u}} \cdot \boldsymbol{\tau}_{\mathrm{LW}}|_{z=-H+2000} \\ &\approx \overline{\mathbf{u}} \cdot \boldsymbol{\tau}_{\mathrm{LW}}|_{z=-H},\end{aligned} \tag{4.11}$$

which is equivalent to the energy extraction by lee waves at the bottom. Here we assume that the horizontal velocity $\overline{\mathbf{u}}$ is depth-independent in the deep ocean (the bottommost 2 km) and the lee wave stress at 2 km above the bottom is zero.

The breaking of lee waves enhances turbulent mixing, which can be parameterised as κ_v^{LW}. The lee wave-driven mixing rate is

$$\kappa_v^{\mathrm{LW}} = \Gamma \frac{\varepsilon^{\mathrm{LW}}}{N^2}, \tag{4.12}$$

in units of $\mathrm{m}^2\ \mathrm{s}^{-1}$, based on Osborn relation (Osborn, 1980), where Γ is the mixing efficiency, N is the buoyancy frequency. We use a mixing efficiency Γ of 0.2. Here we assume that all the energy in lee waves is dissipated locally, i.e., within a model grid cell in the horizontal.

Compared with the tidal-mixing parameterisation adopted by Simmons et al. (2004) and Jayne (2009), our parameterisation replaces the fixed map of the energy flux with the work done by a wave stress (Eq. 4.9). The wave stress connects the large-scale geostrophic flow with the small-scale turbulent mixing; the wave stress regulates the energy extraction from the geostrophic flow and the energy input into the turbulent mixing.

4.2.2 Parameter choices

While the parameterisation depends on the resolved flow, it also requires information about the small-scale topography. For the idealised channel configuration used here, we choose the following parameters for the small-scale topography.

Topographic amplitude

The amplitude of small-scale topography h_0 represents the roughness of small-scale topography in the area, evaluated as the root-mean-square (rms) height of small-scale topography. Both energy extraction from the resolved flow (e.g., Nikurashin and Ferrari, 2010a) and lee

wave-driven mixing (Broadbridge et al., 2016) are sensitive to the choice of this height. It has been shown in an idealized configuration that the roughness of small-scale topography can modify the parameterised lee wave-driven mixing and therefore the strength of the lower overturning circulation in the Southern Ocean (Broadbridge et al., 2016).

Nikurashin and Ferrari (2010a) found h_0=305 m in the Drake Passage using observations. Sheen et al. (2013) found that the roughness of small-scale topography increases from 30 m in the southeast Pacific to over 100 m in western Drake Passage and the Phoenix Ridge, using multibeam bathymetry data. Brearley et al. (2013) obtained an rms topographic height of 179 m within their mooring region in the western Scotia Sea south of the Subantarctic Front. Meyer et al. (2016) estimated the topographic roughness to be approximately 122.5 m north of the Kerguelen Plateau Polar Front Zone where the mixing is the highest. To represent the observed rms height of rough small-scale topography, we use a topographic amplitude h_0 of 100 m.

We calculate the Southern Ocean-averaged roughness of small-scale topography using the topography datasets of Goff (2010), Goff and Arbic (2010), and Nikurashin and Ferrari (2011) to justify our choice of the amplitude of small-scale topography (Table 4.1). To focus on the roughness (rms height) of small-scale topography that contributes significantly to the generation of lee waves, we repeat the calculation of the Southern Ocean averages by only including the region where the lee wave generation is larger than 1 mW m^{-2}, 10 mW m^{-2}, and 100 mW m^{-2}. Our calculations show that the higher the lee wave generation rate, the larger the rms height of small-scale topography. The small-scale topography that contributes to the lee wave generation rate greater than 100 mW m^{-2} has the rms height of the order of 100 m.

Table 4.1 Southern Ocean-averaged small-scale roughness, m.

	Goff (2010)	Goff and Arbic (2010)	Nikurashin and Ferrari (2011)
All	9.3	9.1	2.1
$>$ 1 mW m^{-2}	20.2	24.3	4.0
$>$ 10 mW m^{-2}	37.0	47.2	3.3
$>$ 100 mW m^{-2}	95.8	88.2	1.7

Topographic wavenumber

As discussed in section 2.3.2, the generation of (radiating) lee waves is constrained by the horizontal wavenumber of small-scale topography. Nikurashin and Ferrari (2010a) found the

characteristic wavenumber of 2.3×10^{-4} m^{-1} and 1.3×10^{-4} m^{-1} along the principal axes of topography in the Drake Passage. Brearley et al. (2013) found the characteristic wavenumber of 5.1×10^{-4} m^{-1} and 1.9×10^{-4} m^{-1} along the principal axes of topography within their mooring region in the western Scotic Sea. Here, we use a topographic wavenumber k of $2\pi/2000$ rad m^{-1} (equivalent to 5.0×10^{-4} m^{-1}).

Vertical decay scale

Nikurashin and Ferrari (2013) have shown that the water mass transformation due to lee wave-driven mixing is sensitive to the choice of vertical decay scale; the smaller the vertical decay scale is, the greater the water mass transformation rate. Here, we use a vertical decay scale ζ of 500 m. This choice is made following Simmons et al. (2004).

Topographic criticality

Using the small-scale topographic parameters chosen above, the steepness parameter is estimated as,

$$s = \frac{NH}{U} = \frac{10^{-3.5} \times 100}{0.1} = 0.3,$$

which is smaller than 0.75, the critical steepness parameter commonly used for 2D flow, which indicates that the bottom flow is linear. In this regime, the correction based on the steepness parameter is not needed. Therefore we do not apply the correction based on the steepness parameter to the lee wave stress as in Eq. (2.3). However, to develop a lee wave parameterisation scheme for a more realistic case, the correction to linear theory needs to be considered.

4.2.3 Lee wave characteristics

To evaluate the parameterised lee wave field in an eddy-resolving configuration of the idealised channel model used in chapter 3, we examine lee wave generation and its subsequent radiation and dissipation from the experiment with lee wave parameterisations and wind stress of 0.2 N m^{-2}. Lee wave generation is evaluated using the bottom energy flux into lee waves (TKE) and lee wave drag coefficient (γ_{Lw}) (Figs. 4.1a-b). Lee wave dissipation is evaluated using the turbulent energy dissipation rate ($\varepsilon^{\mathrm{LW}}$) and lee-wave-driven mixing (Figs. 4.1c-d).

The bottom energy flux into lee waves has an average magnitude of 10 mW m^{-2} with a domain maximum value exceeding 100 mW m^{-2} (Fig. 4.1a), which is consistent with the offline estimate from an eddy-resolving global ocean model (used in chapter 2) where

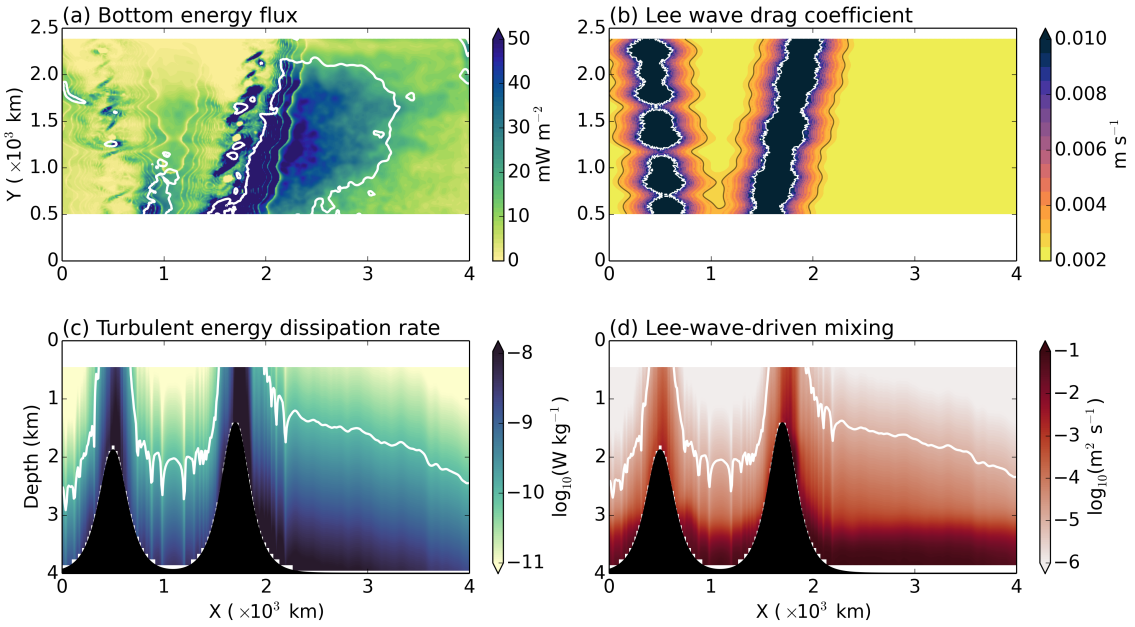

Fig. 4.1 Diagnostics of the lee wave field from the experiment with wind stress of 0.2 N m^{-2}. (a) Bottom energy flux into lee waves in units of mW m^{-2}. The white contour indicates the bottom-500m-averaged EKE of 30 cm^2 s^{-2}, inside which is a bottom EKE hotspot. (b) Lee wave drag coefficient in units of m s^{-1}. White contours indicate the lee wave drag coefficient of 0.01 m s^{-1} and grey contours 0.003 m s^{-1}. (c) Turbulent energy dissipation rate (log scale) associated with lee wave generation at Y=1255 km, in units of W kg^{-1}. The white contour indicates the value of 10^{-10} W kg^{-1}. (d) Diffusivity associated with lee-wave-driven mixing (log scale) at Y=1255 km, in units of m^2 s^{-1}. The white contour indicates the value of 10^{-5} m^2 s^{-1}. The shallowest depth shown in (c) and (d) is 1 km above the peak of the topography. The surface 500 m is masked to focus on the lee wave effects that radiate from the bottom. (a) and (b) are over the horizontal extent of the model domain, whereas (c) and (d) are the depth profiles for a transect at Y = 1255 km.

the characteristic lee wave generation rate in hotspots is on the order of 10-100 mW m^{-2} (Figs. 2.8a-c). The maximum bottom energy flux into lee waves in our sector model occurs downstream of the two meridional ridges and coincides with that of bottom EKE (Fig. 4.1a).

Lee wave drag is parameterised as a linear drag and has a spatially varying drag coefficient (Fig. 4.1b). The lee wave drag coefficient depends on bottom stratification (Eq. 4.8) and has an average of 0.005 m s^{-1} in the domain. Over the flat region, the lee wave drag coefficient ranges from 0.002 to approximately 0.003 m s^{-1}; over the topography, the lee wave drag coefficient increases up to 0.05 m s^{-1} due to strong bottom stratification over the topography (Fig. 4.1b). On average, the lee wave drag coefficient is about one order of magnitude larger than the linear drag coefficient we use in chapter 3, consistent with the finding in chapter 2

that lee wave drag contributes to more energy dissipation of the flow than bottom frictional drag.

The turbulent energy dissipation rate is intensified near the bottom (Fig. 4.1c). Turbulent energy dissipation rate decreases upward gradually within the water column from $O(10^{-8})$ W kg^{-1} to $O(10^{-10})$ W kg^{-1} at roughly 1-2 km off the bottom (Fig. 4.1c), which is consistent with observations (e.g., Naveira Garabato et al., 2004; St. Laurent et al., 2012; Waterman et al., 2013) and theoretical estimates (Nikurashin et al., 2013) in the Southern Ocean.

Consistent with the turbulent energy dissipation rate, the lee-wave-driven mixing is also strongly bottom-intensified, which leads to a diffusivity of up to 10^{-2} m^2 s^{-1} near the bottom (Fig. 4.1d). The diffusivity associated with lee-wave-driven mixing decreases away from the bottom reaching 10^{-5} m^2 s^{-1} at mid-depth. Overall, the spatial structure and magnitude of the bottom energy flux, lee wave drag coefficient, turbulent energy dissipation rate, and lee-wave-driven mixing are consistent with those in previous studies.

4.3 Impacts of lee waves on the ocean mean state

To investigate the impacts of lee waves on the mean state of the idealised channel model, we compare the ocean stratification, baroclinic transport, and lower overturning circulation in experiments with a lee wave parameterisation to those in the experiment without any lee wave parameterisation. The experiment without a lee wave parameterisation that we use for comparison is referred to as the reference case hereinafter. The reference case uses the model configuration described in section 3.3.1, with a peak surface wind stress of 0.2 N m^{-2} (Eq. 3.20), a diffusive boundary condition (Fig. 3.2b), and a quadratic bottom frictional drag ($C_d = 3 \times 10^{-3}$) (Eq. 2.7).

We conduct three sets of experiments: (1) a *lee wave drag only* experiment, where only lee wave drag is parameterised in the momentum equations to reflect the momentum loss from the resolved flow associated with lee wave generation; (2) a *lee-wave-driven mixing only* experiment, where only the diffusivity is modified to represent enhanced mixing effects due to the breaking of lee waves; and (3) a *lee wave full parameterisation* experiment, where both lee wave drag and its associated lee-wave-driven mixing are parameterised. The lee wave experiments are carried out using the same model configuration as that used in the reference case. Similar to the way the perturbation experiments are carried out in chapter 3, the lee wave experiments are run from a equilibrated state taken from the reference case for another 50 years, and the last 5 years of output are diagnosed and used for averaging.

4.3.1 Ocean stratification

To evaluate changes in the ocean stratification induced by the lee wave parameterisation, we examine the isopycnal slope and bottom stratification.

As discussed in chapter 3, changes in the isopycnal slope reflect the control of bottom drag on the EKE balance and lead to changes in the ACC and the MOC. To understand the impacts of lee waves on the ACC and the MOC, we compare the isopycnal slope from all lee wave parameterisation experiments with that from the reference case (Fig. 4.2). In the

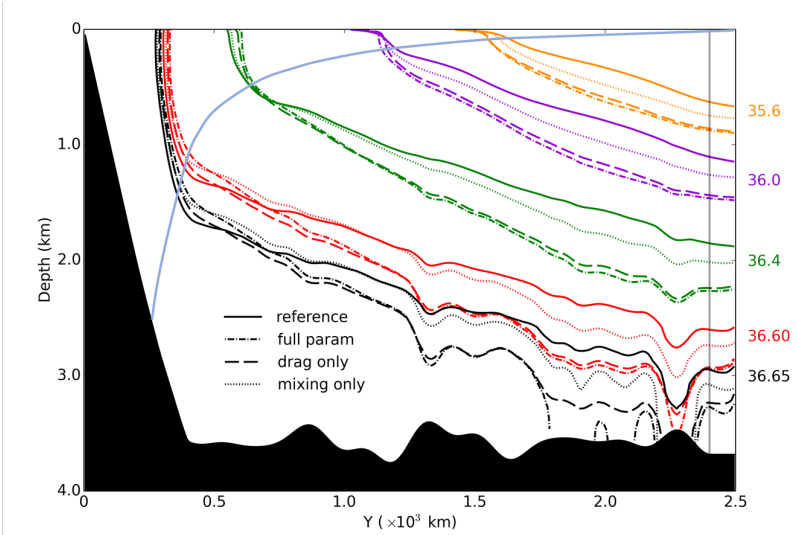

Fig. 4.2 Zonally averaged isopycnals in the experiments without any lee wave parameterisation (solid lines), with only lee-wave-driven mixing (dotted lines), with only lee wave drag (dashed lines), and full parameterisation (dash dotted lines). The colours represent different density levels; from top to bottom, orange, purple, green, red, and black lines represent the density level of 35.6 kg m^{-3}, 36.0 kg m^{-3}, 36.4 kg m^{-3}, 36.6 kg m^{-3}, and 36.65 kg m^{-3}, respectively. The blue solid line denotes the approximate position of the base of the mixed layer. The gray vertical line denotes the southern boundary of the northern sponge layer.

ocean interior, the isopycnals are steepened in all three cases of lee wave parameterisation compared with the reference case (Fig. 4.2). Isopycnals in the lee wave drag only experiment are steeper (Fig. 4.2) because the inclusion of lee wave drag acts against the flow analogous to the increase in the bottom frictional drag coefficient (Fig. 3.6); adding lee wave drag enhances the energy dissipation of the eddy field and requires steeper isopycnals to provide a larger eddy energy generation rate to balance. Isopycnals in the lee-wave-driven mixing only experiment are also steeper than the reference case (Fig. 4.2) because enhanced mixing diffuses more heat downward and therefore transforms denser waters into lighter waters. Isopycnals are steeper in the lee wave full parameterisation experiment (Fig. 4.2) than in all

other cases; however, they are only slightly steeper than their counterparts in the lee wave drag only case (Fig. 4.2). This nonlinear increase in the isopycnal slope shown in the lee wave full parameterisation experiment indicates the coupling between lee wave drag and lee-wave-driven mixing, which will be explained in detail using bottom total kinetic energy (Fig. 4.4) and bottom stratification (Fig. 4.6).

Changes in isopycnal slope imply that the ocean stratification is also modified. Here we focus on the bottom-500m-averaged stratification, which is affected by bottom-intensified lee-wave-driven mixing and also determines the lee wave drag coefficient (Eq. 4.8). We calculate the bottom-500m-averaged stratification from three experiments with a lee wave parameterisation and compare them with that from the reference experiment (Fig. 4.3). Our results show that the lee wave parameterisation affects the bottom stratification (Fig. 4.3). The parameterisation strengthens the bottom stratification over the ridges in all three

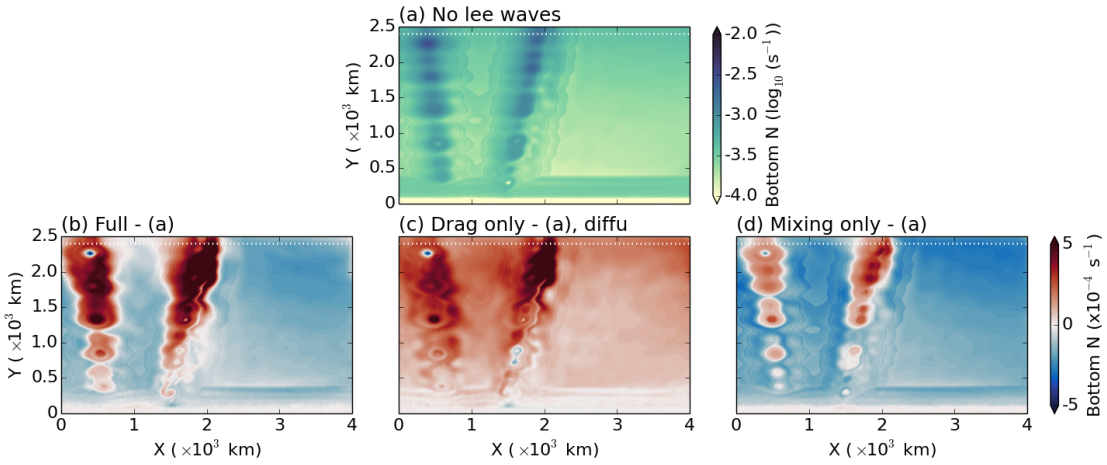

Fig. 4.3 (a) Bottom-500m-averaged stratification [$\log_{10}(s^{-1})$] in the quadratic drag case with the drag coefficient of $C_d = 0.003$. (b), (c), and (d) show the difference between the bottom-500m-averaged stratification in the lee wave full parameterisation case, lee wave drag only case, lee-wave-driven mixing only case and that shown in (a), respectively.

cases (Figs. 4.3b, c, d). However, over the flat bottom, the response is more complicated; the parameterisation of lee wave drag strengthens the bottom-500m-averaged stratification, whereas the parameterisation of lee-wave-driven mixing weakens the bottom-500m-averaged stratification (Fig. 4.3). The combined effect of lee wave drag and lee-wave-driven mixing leads to a weakening of the bottom stratification over the flat bottom (Fig. 4.3b). The weakening of the bottom stratification in the lee wave full parameterisation experiment is slightly weaker that in the lee-wave-driven mixing only experiment (Figs. 4.3b, d).

Both lee wave drag and lee-wave-driven mixing affect the bottom stratification but in opposite ways and for different reasons. The strengthening of the bottom stratification in

the lee wave drag only case results from the adiabatic redistribution of densities. Bottom stratification over the flat bottom is stronger in the lee wave drag only case because the isopycnals are steepened and are displaced deeper into the ocean in the north of the domain (Fig. 4.2). Accompanied by this steepening and displacement (deepening) of isopycnals, the weak stratification in the abyss is replaced with a slightly stronger stratification at depth. The strengthening of the bottom stratification is therefore intensified in the northern part of the domain. The increase in the bottom stratification and its intensification in the north are also found in chapter 3 when increasing the linear and quadratic bottom frictional drag coefficient (not shown). By contrast, the weakening of the bottom stratification in the lee-wave-driven mixing only case results from the irreversible diabatic mixing of density in the vertical. The parameterisation of lee-wave-driven mixing increases the diapycnal mixing in the deep ocean and therefore weakens the bottom stratification.

When both lee wave drag and its associated lee-wave-driven mixing are parameterised, the weakening effect of bottom stratification due to diabatic lee-wave-driven mixing dominates over the strengthening effect due to adiabatic displacement of isopycnals (Fig. 4.3). However, the weakening of the bottom stratification in the lee wave full parameterisation case is not as significant as that in the lee-wave-driven mixing only case due to the superposition and coupling between lee wave drag and lee-wave-driven mixing. The coupling weakens the effect of lee-wave-driven mixing: the presence of lee wave drag reduces the energy in the deep ocean that can be provided for the lee-wave-driven mixing (Fig. 4.4). As a result, the

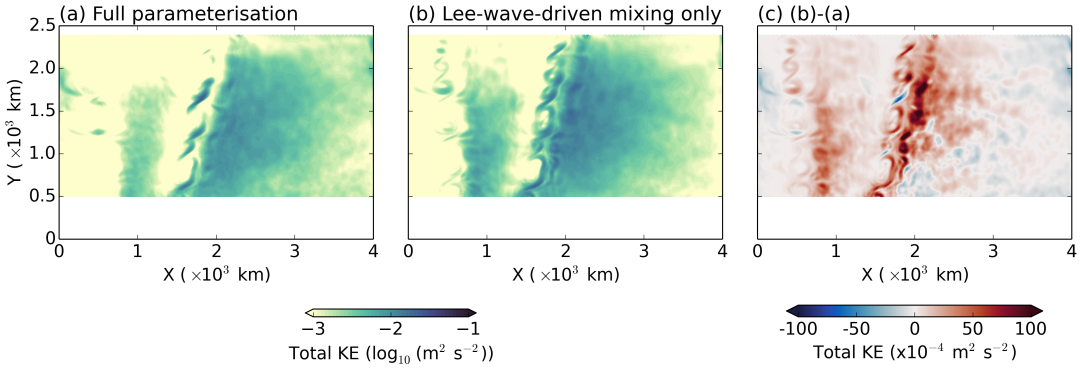

Fig. 4.4 Bottom-500m-averaged total kinetic energy is shown with a log scale in the (a) lee wave full parameterisation case and (b) lee-wave-driven mixing only case. The difference between (a) and (b) is shown in (c) with a linear scale.

diffusivity is larger in the lee-wave-driven mixing experiment than that in the lee wave full parameterisation experiment (Fig. 4.5).

4.3.2 Baroclinic transport and standing meanders of the ACC

The impact of lee wave parameterisation on the isopycnal slope implies that the baroclinic transport of the ACC is also affected. To examine the impacts of lee wave parameterisation on the ACC transport, we calculate the baroclinic transport for three sets of experiments with a lee wave parameterisation and compare them with the reference case. The baroclinic

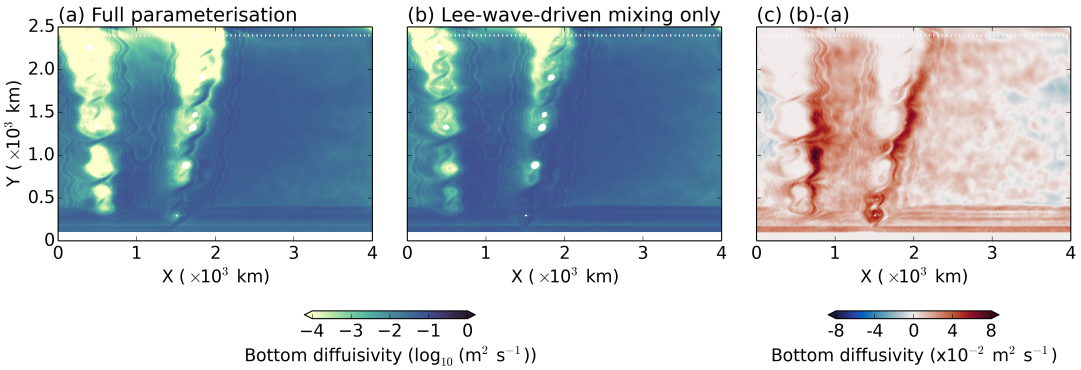

Fig. 4.5 Bottom-500m-averaged diffusivity associated with lee-wave-driven mixing is shown with a log scale in the (a) lee wave full parameterisation case and (b) lee-wave-driven mixing only case. The difference between (a) and (b) is shown in (c) with a linear scale.

transport increases from 144 Sv in the reference case, to 168 Sv, 202 Sv, and 207 Sv, in the lee-wave-driven mixing only, lee wave drag only, and lee wave full parameterisation cases, respectively. In the presence of lee waves, the increase in baroclinic transport is as large as 20% to 40% of that of the reference experiment. The increase in the baroclinic transport is consistent with the steeper isopycnals shown in all three experiments with a lee wave parameterisation (Fig. 4.2).

Both lee wave drag and lee-wave-driven mixing increase the baroclinic transport, but to varying extent and for different reasons. The parameterisation of lee wave drag leads to an increase in the baroclinic transport because it acts against the bottom flow similar to bottom frictional drag. Baroclinic transport is also increased in the lee-wave-driven mixing only case through another mechanism; the enhanced mixing leads to increased water mass transformation and therefore also steepens the isopycnals (Fig. 4.2). However, when comparing the lee wave full parameterisation case with the reference case, we find that the increase in the baroclinic transport is not a linear combination of the increase in the lee wave drag only case and that in the lee-wave-driven only case.

The transport is only slightly stronger in the lee wave full parameterisation than in the lee wave drag only case because of the nonlinear coupling between lee wave drag and lee-wave-driven mixing. This nonlinear coupling arises from the dependence of the lee-wave-driven

mixing on bottom kinetic energy (Figs. 4.4, 4.5), as well as from the dependence of the lee wave drag coefficient on bottom stratification (Eq. 4.8), which is regulated by the intensity of mixing. In the lee wave full parameterisation case, the bottom stratification is weaker than that in the lee wave drag only case due to lee-wave-driven mixing (Fig. 4.6). Weaker bottom

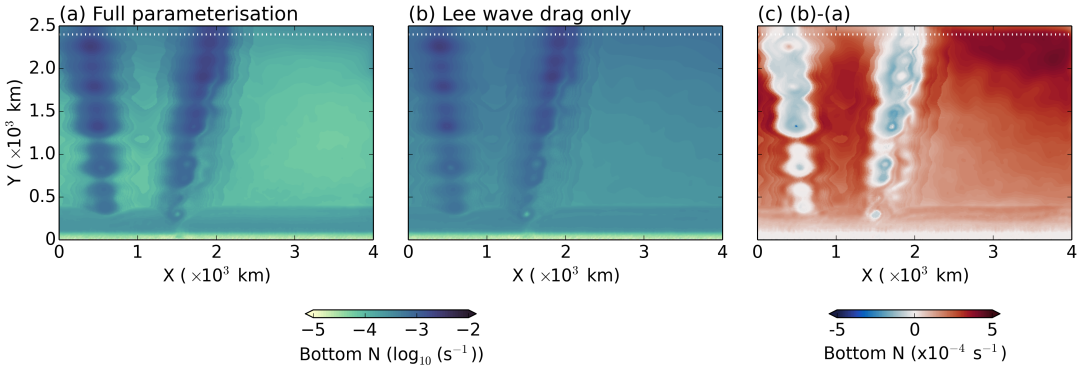

Fig. 4.6 Bottom-500m-averaged stratification is shown with a log scale in (a) the lee wave full parameterisation case and (b) lee wave drag only case. The difference between (a) and (b) is shown in (c) with a linear scale.

stratification in the lee wave full parameterisation case results in a lower lee wave drag coefficient and therefore a smaller increase of baroclinic transport associated with lee wave drag (Eq. 3.4). As explained in section 4.3.1, the lee-wave-driven mixing is weaker in the lee wave full parameterisation case than in the lee-wave-driven mixing only case. Therefore, the increase in the baroclinic transport due to the parameterisation of lee-wave-driven mixing is smaller in the lee wave full parameterisation case than that in the lee-wave-driven mixing only case. When the lee wave drag and lee-wave-driven mixing are parameterised together, the lee wave full parameterisation case produces a higher transport than the lee wave drag only case or the lee-wave-driven mixing only case; however, in the lee wave full parameterisation case, the contribution of each component to the increase in the baroclinic transport is reduced due to the coupling effect.

Lee wave parameterisation also modifies the structure of the standing meanders (Fig. 4.7). The position of the standing meanders are indicated by white streamlines. The curvature of the meanders downstream of both meridional ridges are significantly reduced in all three lee wave cases (Figs. 4.7b, c, d) compared with the reference case (Fig. 4.7a). The curvature of the meanders in the lee wave drag only and lee wave full parameterisation case is reduced because the presence of lee wave drag modifies the momentum balance of the mean flow. Zonally averaged bottom lee wave drag is shown to be as large as 0.05 N m^{-2} (Fig. 4.8b) in the lee wave full parameterisation case, which largely reduces the role of topographic form stress (not shown) in balancing the wind stress. The reduction in the topographic form

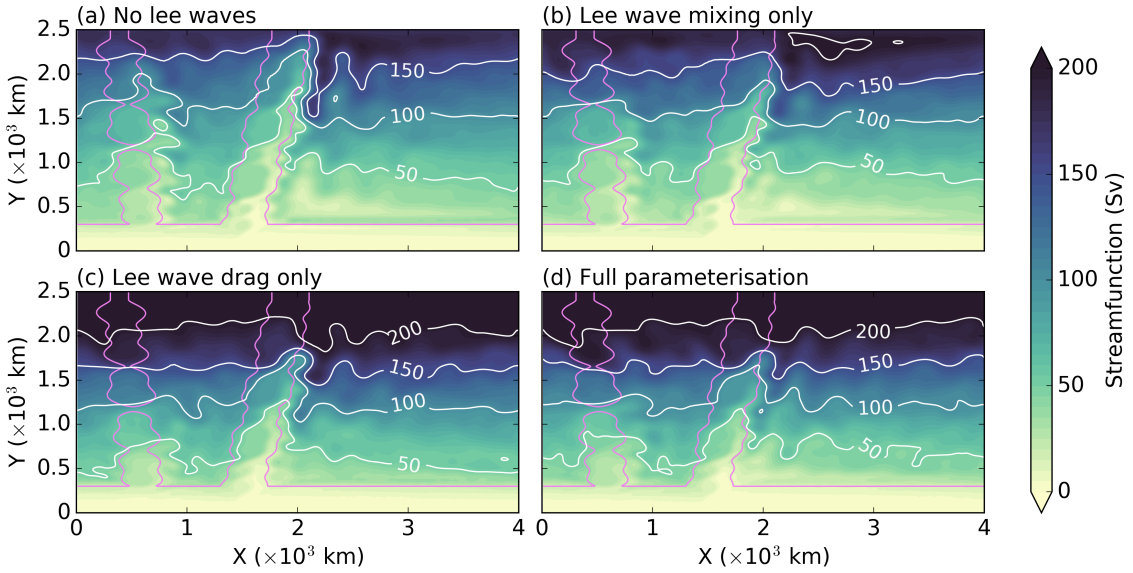

Fig. 4.7 Streamfunction in units of Sv for the experiments (a) without any lee wave parameterisation, (b) with only lee-wave-driven mixing, (c) with only lee wave drag, and (d) full parameterisation of lee wave drag and its associated lee-wave-driven mixing. White contours are streamlines. Violet contours indicate the topography at 3 km deep.

stress implies the pressure difference across the ridges is decreased, which is reflected by a smoother zonal flow (Fig. 4.7c, d).

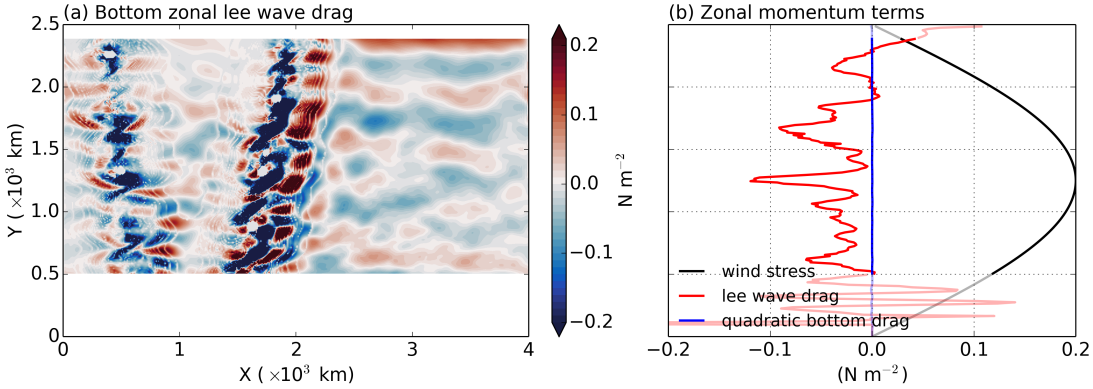

Fig. 4.8 Bottom zonal lee wave drag averaged over the final 5-year model output from the lee wave full parameterisation case. (a) Bottom zonal lee wave drag in units of N m^{-2}. (b) Zonal-mean wind stress (black line), bottom lee wave drag (red line), and quadratic bottom frictional drag (blue line) along latitude. Lighter parts of the lines are located in the northern sponge layer (2400 km $\leqslant$ Y $\leqslant$ 2500 km) and over the slope (0 km $\leqslant$ Y $\leqslant$ 500 km).

The parameterisation of lee-wave-driven mixing also modifies the structure of the standing meanders. Although lee-wave-driven mixing does not change the momentum balance of the

flow, it can change bottom pressure difference across the large-scale topography by regulating the strength of the lower overturning circulation, as suggested by Stewart and Hogg (2017). Modified bottom pressure will result in a different topographic form stress and therefore a change in the structure of the standing meanders.

4.3.3 MOC

The theory we discussed in chapter 3 suggests that the strength of the lower overturning circulation is controlled by both mixing intensity and isopycnal slope. We have shown that the breaking of lee waves enhances mixing and the parameterisation of lee wave drag increases the isopycnal slope. Thus, our results indicate that the parameterisation of lee waves is likely to modify the strength of the lower overturning circulation.

We compare the value of the lower overturning circulation from all three lee wave parameterisation experiments with that from the reference experiment to examine the changes in the lower overturning circulation (Fig. 4.9). The value of the lower overturning circulation

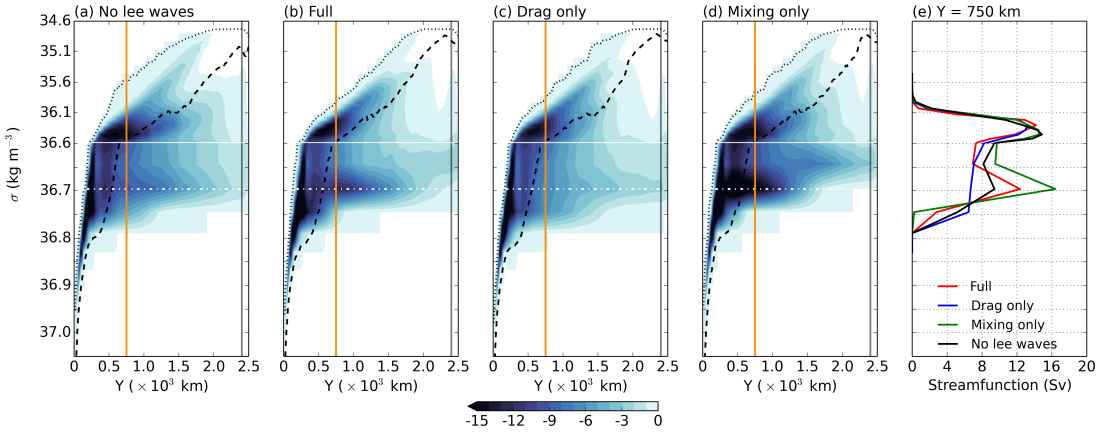

Fig. 4.9 Overturning circulation streamfunction in units of Sv in the (a) quadratic drag case with the drag coefficient of C_d = 0.003 (i.e., the reference case), (b) lee wave full parameterisation case, (c) lee wave drag only case, and (d) lee-wave-driven mixing only case. The values along Y = 750 km (marked by orange lines in a-d) are shown in (e). The dotted and dashed black lines represent the minimum and maximum density, respectively, that ever occurred at the surface. The grey vertical line indicates the location of the sponge layer. The density range below the white line is stretched. The white dashed dotted line marks the maximum lower overturning circulation streamfunction along the density axis.

is 9.4 Sv in the reference case (Fig. 4.9a). It reduces to 6.7 Sv in the lee wave drag only case (Fig. 4.9c) and increases to 12.4 Sv and 16.4 Sv, respectively, in the lee wave full parameterisation (Fig. 4.9b) and lee-wave-driven mixing only case (Fig. 4.9d).

The weakening of the lower overturning circulation due to the parameterisation of lee wave drag (Figs. 4.9a, c) is attributed to the increase in the isopycnal slope (Fig. 4.2) and is consistent with the theory and results found in chapter 3; introducing the lee wave drag leads to an increase in the isopycnal slope so that the eddy energy balance can be reestablished, and as a result, the residual lower overturning circulation decreases (Eq. 3.16).

In the lee-wave-driven mixing only case, the lower overturning circulation is strengthened compared with the reference case (Figs. 4.9a, d), which is consistent with the findings in previous studies (e.g., Melet et al., 2014). Despite a slight increase in the isopycnal slope (Fig. 4.2), which tends to weaken the lower overturning circulation, the increase in the diffusivity is more significant and therefore leads to an overall stronger lower overturning circulation. Lee-wave-driven mixing also enhances water mass transformation, which leads to a decrease in the density in the northern part of the domain (roughly 1500 to 2500 km) from 36.7 kg m^{-3} to 36.65 kg m^{-3} (Fig. 4.9d).

In the lee wave full parameterisation case, the strength of the lower overturning circulation is increased compared with the reference case, however not as strongly as that in the lee-wave-driven mixing only case (Figs. 4.9a, b, d). This smaller net increase in the lee wave full parameterisation case again reflects the non-linear coupling between lee wave drag and lee-wave-driven mixing. The presence of lee wave drag in the lee wave full parameterisation case weakens the strengthening effect of lee-wave-driven mixing on the lower overturning circulation through the bottom total kinetic energy field (Fig. 4.4).

4.4 Impacts of lee waves on the sensitivity of the Southern Ocean circulation to winds

To examine the impact of lee waves on the response of the Southern Ocean circulation to increasing wind stress, we compare the sensitivity shown in the lee wave full parameterisation experiment with that in the linear bottom drag experiment ($r_b = 3 \times 10^{-4}$ m s^{-1}). Here, we choose the linear bottom drag experiment as the reference experiment because the flow is influenced predominantly by linear drag dynamics in the lee wave full parameterisation experiment, given that lee wave drag has a larger impact on the flow than quadratic bottom frictional drag. For comparison, we also run the reference experiment and lee wave full experiment under the wind stress of 0.1 N m^{-2} and 0.3 N m^{-2}. We define the sensitivity of the baroclinic transport and the lower overturning circulation streamfunction to changes in wind stress as their relative change (in %) compared with their values in the experiments with wind stress of 0.2 N m^{-2}.

4.4.1 Sensitivity of the baroclinic transport to winds

In section 3.4.3 we show that the baroclinic transport is sensitive to changes in wind stress when quadratic bottom drag is used in contrast to the eddy saturation in the linear bottom drag case. Here, we parameterise lee wave drag as a linear drag with a drag coefficient dependent on the bottom stratification and small-scale topographic parameters (Eq. 4.8). Lee wave

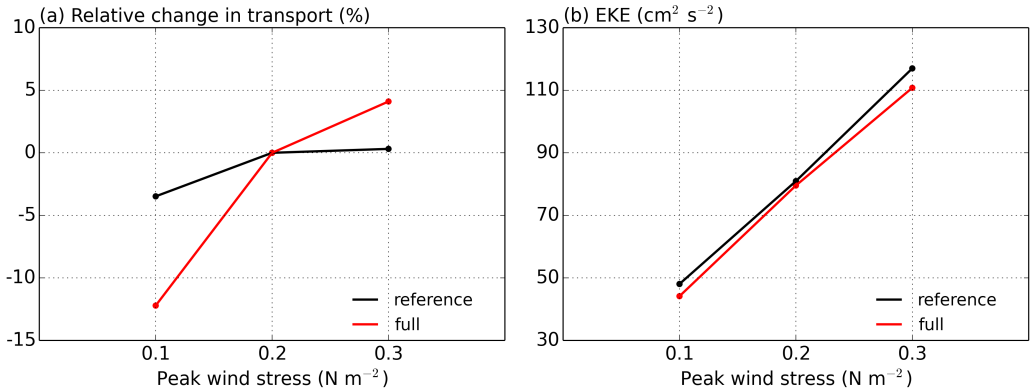

Fig. 4.10 Relative changes in the (a) baroclinic transport and (b) domain-averaged EKE as a function of wind stress. The black and red lines represent the linear bottom drag only (reference) case and lee wave full parameterisation case, respectively.

drag is linearly dependent on the velocity and is therefore expected to follow the linear drag dynamics discussed in section 3.2.1. However, lee wave drag is also a function of bottom stratification. In addition, the lee-wave-driven mixing also controls the baroclinic transport and potentially its sensitivity to changes in wind stress. We therefore seek to understand whether and why the baroclinic transport is sensitive to changes in wind stress when both lee wave drag and lee-wave-driven mixing are parameterised.

We compare the sensitivity of the baroclinic transport to changes in wind stress in the lee wave full parameterisation experiment to that in the reference experiment (Fig. 4.10a). Our results show that the parameterisation of lee waves leads to a more sensitive baroclinic transport to changing wind stress (Fig. 4.10a). In the reference case, the baroclinic transport reaches an eddy saturation limit where it becomes insensitive to the increase in wind stress (Fig. 4.10a, black line). This insensitivity agrees with the theoretical prediction of the baroclinic transport in the linear drag case (Eq. 3.4) and is consistent with the unchanged isopycnal slope with increasing wind stress (Fig. 4.11a). As explained in chapter 3, this insensitivity occurs because the increase in EKE with wind leads to a flattening of isopycnals that perfectly cancels the wind steepening of isopycnals. Consequently, the isopycnals retain their slope (Fig. 4.11a) and leave the baroclinic transport nearly unchanged (Fig. 4.10a).

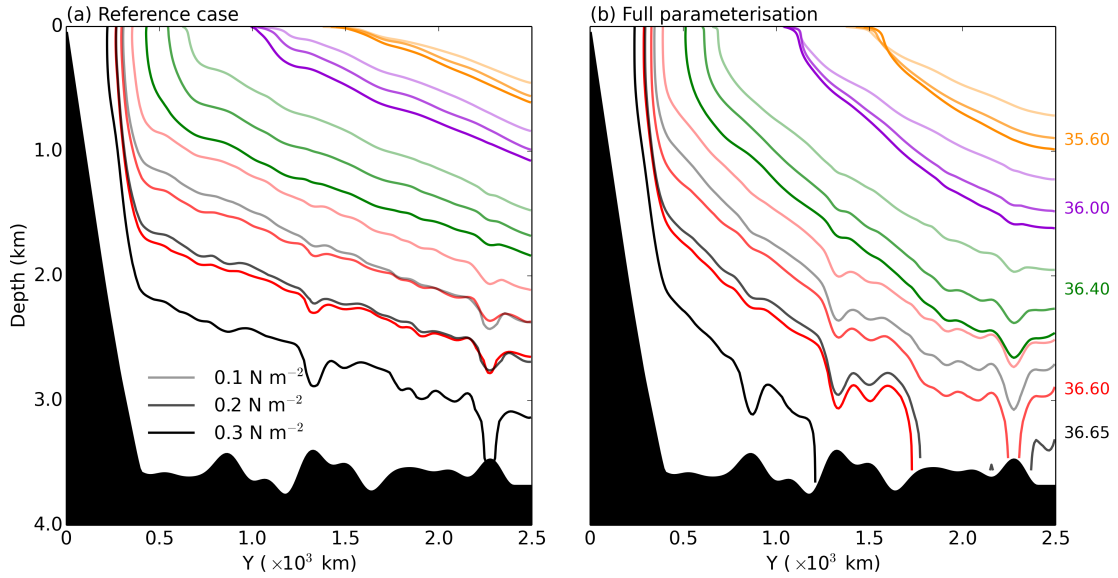

Fig. 4.11 Time- and zonal-mean isopycnals in the (a) reference and (b) lee wave full parameterisation cases. The colours represent different density levels; from top to bottom, orange, purple, green, red, and black colours represent the density level of 35.60 kg m^{-3}, 36.00 kg m^{-3}, 36.40 kg m^{-3}, 36.60 kg m^{-3}, and 36.65 kg m^{-3}, respectively. For each colour, the darker the line, the larger the wind stress. There are three lines for each colour in corresponding to peak wind stress of 0.1 N m^{-2}, 0.2 N m^{-2}, and 0.3 N m^{-2}.

In the lee wave full parameterisation case, the baroclinic transport increases with wind stress and is more sensitive to changes in wind stress than the reference case. This increased sensitivity in the lee wave case is consistent with the steepening of isopycnals (Fig. 4.11b). The sensitivity found in the lee wave case is attributed to both lee wave drag and lee-wave-driven mixing. As the parameterised lee wave drag is linearly dependent on the velocity, its control on the baroclinic transport follows the linear drag dynamics discussed in section 3.2.1: the baroclinic transport is linearly proportional to the lee wave drag coefficient (Eq. 3.4). Different from the linear bottom drag case, lee wave drag varies with wind stress through its dependence on bottom stratification, which is increased as the isopycnals steepen (Fig. 4.11b). On the other hand, the lee-wave-driven mixing can also regulate the sensitivity of the baroclinic transport to changes in wind stress because the strength of the lee-wave-driven mixing and its steepening effect on the isopycnal slope are sensitive to changes in wind stress. As wind stress increases, the lee-wave-driven mixing becomes stronger, as indicated by the bottom-500m-averaged diffusivity (Fig. 4.12), and further tilts the isopycnals. We therefore

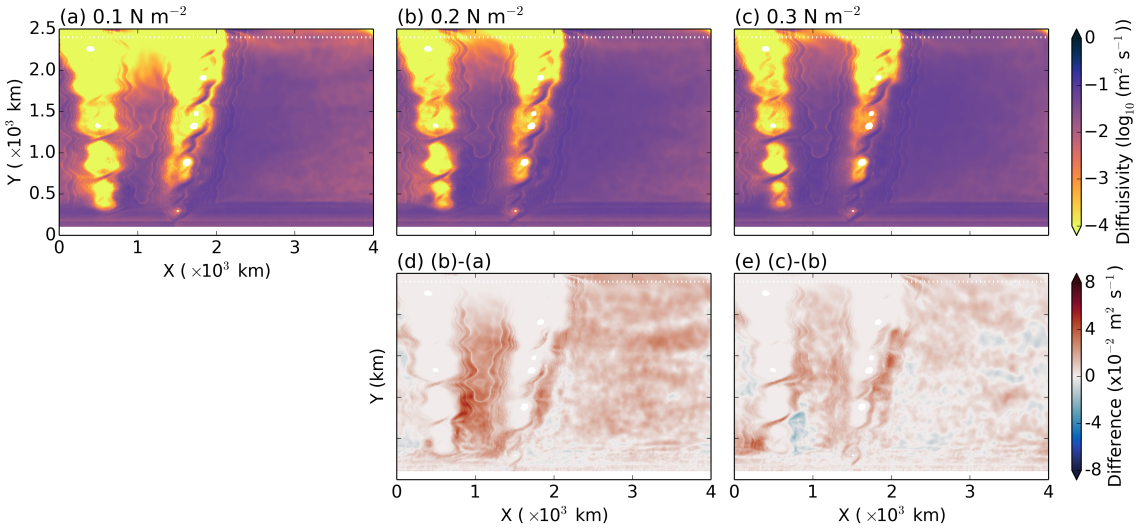

Fig. 4.12 Bottom-500m-averaged diffusivity corresponding to the peak wind stress of (a) 0.1 N m^{-2}, (b) 0.2 N m^{-2}, and (c) 0.3 N m^{-2}, from the lee wave full parameterisation experiment. The difference between (b) and (a) is shown in (d) with a linear scale. The difference between (c) and (b) is shown in (e) with a linear scale.

conclude that both lee wave drag and lee-wave-driven mixing increase with wind stress and contribute to the increase in the baroclinic transport with increasing wind stress.

4.4.2 Sensitivity of the MOC to winds

The sensitivity of the isopycnal slope to changes in wind stress (Fig. 4.11) in the lee wave full parameterisation case implies that the lower overturning circulation should also be sensitive to changes in wind stress. Here, we compare the sensitivity of the lower overturning circulation from the lee wave full parameterisation experiment to that from the reference experiment and investigate the impact of lee waves on the response of the lower overturning circulation to changes in wind stress.

In the absence of lee waves, the strength of the lower overturning circulation is sensitive to, and decreases with, wind stress (black line in Fig. 4.13, Fig. 4.14a-c). This sensitivity is consistent with changes in the isopycnal slope (Fig. 4.11a), and agrees with previous studies that predict the sensitivity of the lower overturning circulation to changes in wind stress using theories or ocean models that do not include lee waves (Ito and Marshall, 2008; Nikurashin and Vallis, 2011). Apart from changes in magnitude, the maximum overturning circulation streamfunction occurs at the same depth, but at lower densities, as wind stress increases (not shown). This shift of the maximum overturning circulation streamfunction in density space is due to the deepening of isopycnals in depth as wind stress increases, as shown in Fig. 3.9.

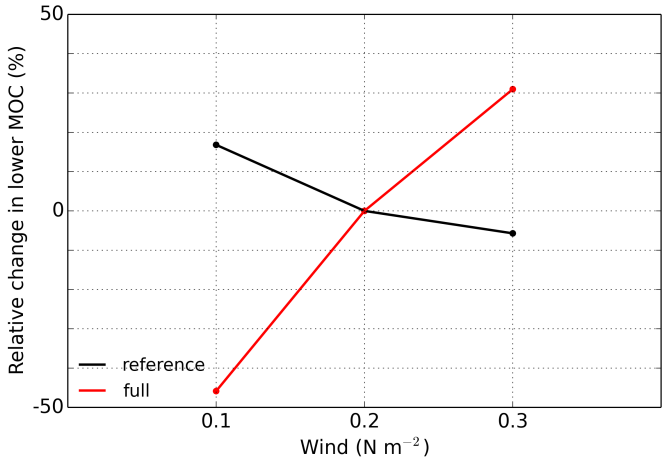

Fig. 4.13 Relative changes in the lower overturning circulation streamfunction as a function of wind stress. The black and red lines represent the linear bottom drag only (reference) case and lee wave full parameterisation case, respectively.

As discussed in section 4.3.3, the strength of the lower overturning circulation is affected by both lee wave drag, which regulates the isopycnal slope, and lee-wave-driven mixing, which increases the deep ocean diapycnal diffusivity. We expect that lee wave drag and lee-wave-driven mixing also affect the sensitivity of the lower overturning circulation to changes in wind stress. According to Eq. (3.16), the response of the isopycnal slope to increasing wind stress indicates that the lower overturning circulation should decrease with wind stress, if the diffusivity κ is constant (Fig. 4.11b). However, the lee-wave-driven mixing enhances the diapycnal diffusivity κ and opposes the effect of the isopycnal slope on the lower overturning circulation. Furthermore, the lee-wave-driven mixing strengthens with wind stress (Fig. 4.12). When both lee wave drag and lee-wave-driven mixing are parameterised, the strength of the lower overturning circulation increases with wind stress (Fig. 4.13, Fig. 4.14d-f). The sensitivity shown in the lee wave full parameterisation experiment implies that the sensitivity of the lower overturning circulation to changes in wind stress is controlled primarily by the lee-wave-driven mixing, but slightly offset by lee wave drag. The increasing lower overturning circulation to wind stress is consistent with the theoretical prediction proposed in Saenko et al. (2012), which demonstrates the importance of building the energy link between the eddy field and turbulent mixing.

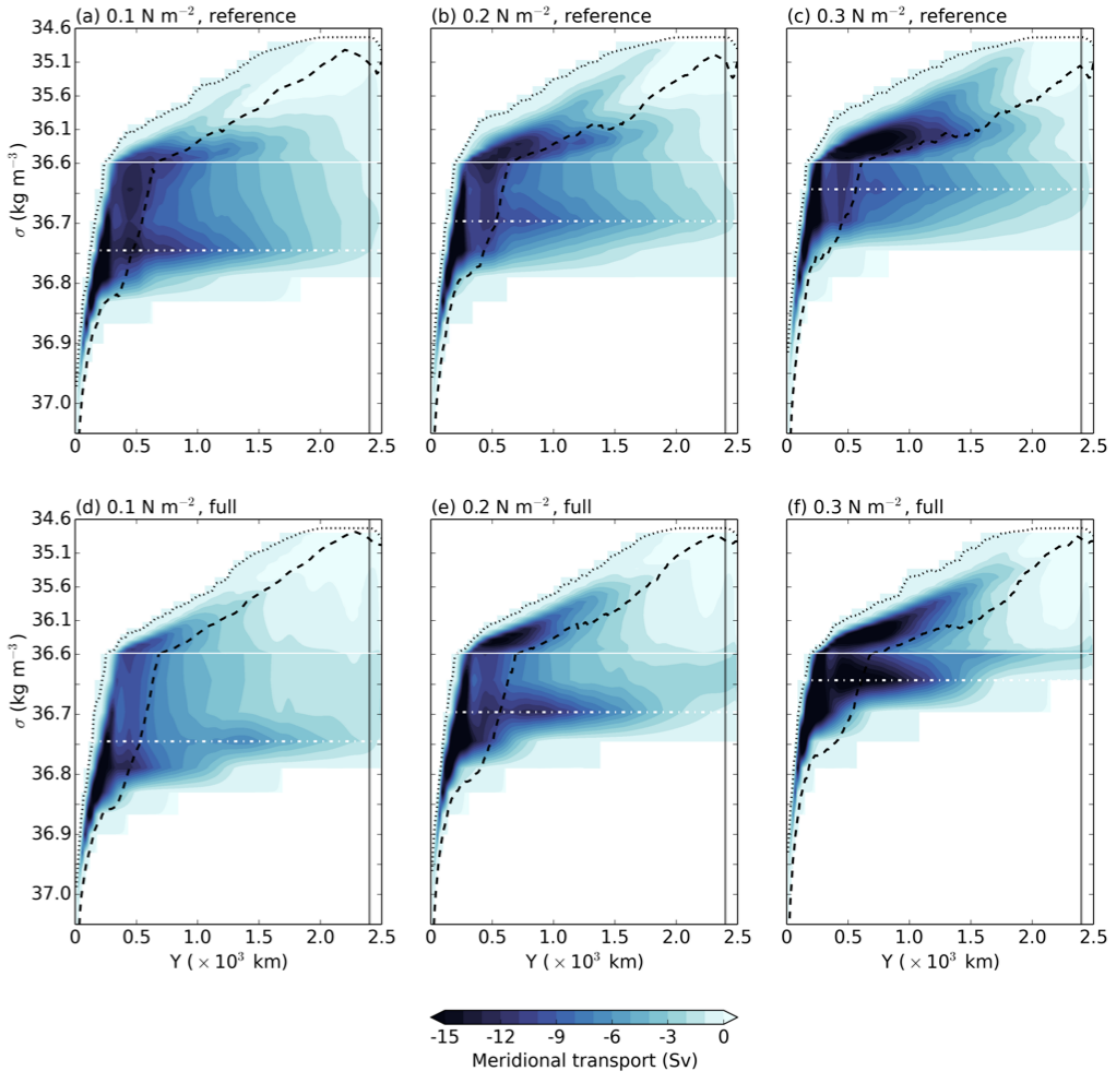

Fig. 4.14 Overturning circulation shown for the peak wind stress of (a) 0.1 N m^{-2}, (b) 0.2 N m^{-2}, and (c) 0.3 N m^{-2} in the linear bottom drag only case, where lee wave parameterisation is absent, and the peak wind stress of (d) 0.1 N m^{-2}, (e) 0.2 N m^{-2}, and (f) 0.3 N m^{-2} in the lee wave full parameterisation case. The dotted and dashed black lines represent the minimum and maximum density, respectively, that ever occurred at the surface. The grey vertical line indicates the location of the sponge layer. The density coordinate is stretched below the white solid line. The white dash dotted lines indicate the density level where the maximum overturning circulation streamfunction occurs.

4.5 Summary

Lee wave drag plays an important role in the energy budget of the eddy field in the Southern Ocean (Yang et al., 2018, chapter 2) and, as a bottom drag, it can potentially modify the ACC and the MOC through the EKE balance and isopycnal slope (chapter 3). However, to our knowledge, none of the current lee wave parameterisation schemes included both lee wave drag and its associated lee-wave-driven mixing. Furthermore, it remains unclear how lee wave drag affects the strength of the ACC and the MOC and their sensitivity to increasing wind stress. Motivated by these gaps in our understanding, we develop and implement an energetically consistent parameterisation of lee waves that takes both lee wave drag and lee-wave-driven mixing into account. We use this parameterisation to investigate the impact of lee waves on the mean state of the Southern Ocean circulation and its response to changes in wind stress.

We find that both lee wave drag and lee-wave-driven mixing have an impact on the ocean stratification. Lee wave drag steepens the isopycnals and strengthens the bottom stratification through the adiabatic displacement of the isopycnals controlled by the EKE balance. Lee-wave-driven mixing steepens the isopycnals and weakens the bottom stratification through the irreversible diabatic mixing and downward diffusion of heat.

Consistent with the steepening of isopycnals, we find that the parameterisation of lee waves leads to an increase (up to 40%) in the baroclinic transport of the ACC. Both lee wave drag and lee-wave-driven mixing leads to an increase in the baroclinic transport. Lee wave drag acts against the bottom flow similar to bottom frictional drag and modifies the EKE balance, which leads to the adiabatic adjustment of the isopycnal slope and the increase in the baroclinic transport. Lee-wave-driven mixing steepens the isopycnals through its diabatic effect on the stratification. When lee wave drag and lee-wave-driven mixing are parameterised together, the increase in the baroclinic transport is higher than that in the lee wave drag only case and the lee-wave-driven mixing only case. However, the increase in the baroclinic transport in the lee wave full parameterisation experiment is not a linear combination of that in the lee wave drag only experiment and that in the lee-wave-driven mixing only experiment. The nonlinear combination is due to the coupling between lee wave drag and lee-wave-driven mixing. We find that the parameterisation of lee waves modifies the structure of the standing meanders. The parameterisation of lee wave drag reduces the curvature of the standing meanders because the topographic form stress is largely reduced in the presence of a new momentum sink of the time-mean flow (i.e., lee wave drag).

We also find that the parameterisation of lee waves strengthens the lower overturning circulation. Both lee wave drag and lee-wave-driven mixing change the strength of the lower overturning circulation. When the diffusivity is constant, we show that the parameterisation

of lee wave drag leads to the steepening of isopycnals and therefore a reduction in the lower overturning circulation. However, the weakening effect of lee wave drag on the lower overturning circulation is much smaller than the strengthening effect of lee-wave-driven mixing. As a result, the lower overturning circulation is stronger in the lee wave full parameterisation case than in the reference case. The implication of our result is that the impact of lee waves on the lower overturning circulation might not be as significant as predicted by previous studies that only consider the lee-wave-driven mixing.

We find a coupling effect between lee wave drag and lee-wave-driven mixing that weakens one another in the lee wave full parameterisation experiment, when compared with the lee wave drag only and the lee-wave-driven mixing only experiment. In the lee wave full parameterisation experiment, lee wave drag is weaker than in the lee wave drag only experiment, and the lee-wave-driven mixing is smaller than that in the lee-wave-driven mixing only experiment. The coupling arises from two aspects; the dependence of the lee wave drag coefficient on bottom stratification (Eq. 4.8), which is regulated by the intensity of mixing; and the dependence of the lee-wave-driven mixing on bottom total kinetic energy, which is affected by lee wave drag. The coupling leads to a nonlinear combination of the effect of lee wave drag and that of lee-wave-driven mixing on the ocean stratification, baroclinic transport, lower overturning circulation.

The parameterisation of lee waves also alters the response of the ACC and the lower overturning circulation to changes in wind stress. In the presence of lee waves, the baroclinic transport is no longer eddy saturated and also becomes more sensitive to changes in wind stress compared with the reference case. The increase in the baroclinic transport responding to increasing wind stress is consistent with the steepening of the isopycnals. Both lee wave drag and lee-wave-driven mixing contribute to this sensitivity. Lee wave drag has a contribution because its drag coefficient depends on bottom stratification, which increases with wind stress. Lee-wave-driven mixing also has a contribution because it is intensified with wind and leads to steeper isopycnals. The parameterisation of lee waves has an impact on the response of the lower overturning circulation to changes in wind stress. Compared with a slight decrease with wind stress shown in the reference case, the parameterisation of lee waves leads to a highly sensitive lower overturning circulation that increases with wind stress. When wind stress increases, the steepening of the isopycnals tends to weaken the lower overturning circulation, however, the intensified lee-wave-driven mixing considerably strengthens the lower overturning circulation. Our finding is consistent with the results in Stanley and Saenko (2014) and Broadbridge et al. (2016), where the authors found that the lower overturning circulation increased with wind when a fraction of eddy energy was allowed to sustain diapycnal mixing. Our results suggest that the lee-wave-driven mixing

has a larger impact on the lower overturning circulation than lee wave drag, and the energy transfer from the eddy field to turbulent mixing is important for predicting the response of the lower overturning circulation to changing wind stress, as suggested by Saenko et al. (2012).

By using the parameterisation scheme in an idealised channel configuration, we have shown that lee waves significantly change the ACC transport and the lower overturning circulation and their response to increasing wind stress.

Chapter 5

Conclusions

5.1 Main findings

This research has provided an improved understanding of the impact of lee waves on the Southern Ocean circulation and new insight on its sensitivity to changes in wind stress. Previous studies have shown that, lee waves are important in the Southern Ocean for their regulation of the lower overturning circulation through lee-wave-driven mixing. Recently, it has also been suggested that lee waves can play an important role in the momentum balance of the time-mean Antarctic Circumpolar Current (ACC) through lee wave drag. Here, we find that lee waves are also important for setting the ACC transport and controlling the response of the Southern Ocean circulation to changes in wind stress, through both their drag and mixing effects. In addition, lee waves affect the Southern Ocean circulation and its sensitivity to changes in wind stress through both their drag and mixing effects. Due to the complex interaction between lee wave drag and lee-wave-driven mixing, through bottom eddy energy and bottom stratification, the response of the Southern Ocean circulation to lee wave parameterisations is not a linear combination of each component. Thus the simultaneous representation of both must be included in the parameterisation of lee waves employed in numerical models.

The first important finding of this thesis is that the parameterisation of lee waves significantly increases the baroclinic transport of the ACC by 60 Sv (over 40%). Lee waves control the strength of the ACC mainly through their drag effect on the transient eddy field. Lee wave drag acting on the eddy field extracts energy from the transient eddy field and thereby leads to a significant eddy energy dissipation in the Southern Ocean (chapter 2). Similar to the frictional drag control of the ACC found in Marshall et al. (2017), the parameterisation of lee wave drag acts to increase the eddy energy dissipation rate and requires a larger eddy energy generation rate to balance. The eddy energy generation rate is primarily governed

by baroclinic instability, which is dependent on the vertical shear of the horizontal velocity of the ACC, or equivalently (through the thermal wind relation) on the slope of isopycnals. Therefore, the presence of lee wave drag leads to steeper isopycnals and a larger baroclinic transport (chapter 4). Lee-wave-driven mixing is also found to steepen the isopycnals and enhance the baroclinic transport of the ACC, but to a smaller extent compared with the effect of lee wave drag.

The second important finding is that lee waves are also found to modulate the sensitivity of the ACC and the lower overturning circulation to changes in wind stress. The parameterisation of lee waves reduces the degree of eddy saturation (i.e., makes the ACC transport more sensitive to wind stress) and leads to a strengthening of the lower overturning circulation with increasing wind stress. The former is due to the effect of lee wave drag and the latter the effect of lee-wave-driven mixing. As the wind increases, it further tilts isopycnals, and hence strengthens the bottom stratification and results in a larger lee wave drag coefficient. As discussed in chapter 3, in the linear drag case, the baroclinic transport is proportional to the drag coefficient. Therefore, an increase in the lee wave drag coefficient with wind leads to an increase in the baroclinic ACC transport. Different from the eddy saturation reproduced in the linear drag case, the sensitivity shown in the lee wave case arises from the modulation of lee wave drag coefficient by wind stress through bottom stratification. Note that we parameterise lee wave drag as a linear drag. However, in case of multi-scale abyssal hill topography, it might be nonlinearly dependent on the velocity as suggested by Nikurashin and Ferrari (2010a) and Naveira Garabato et al. (2013). If a nonlinear form is used to parameterise lee wave drag, we show in chapter 3 that the sensitivity of the baroclinic transport to changes in wind stress can be further increased because the baroclinic transport will be regulated by wind stress through eddy kinetic energy (EKE) in addition to the drag coefficient.

The parameterisation of lee-wave-driven mixing also leads to an increase of the lower overturning circulation with wind stress. As the wind increases, more energy is supplied into the ocean and transferred to the bottom to dissipate. Through the work done by lee wave drag, this energy can then be used to power the lee-wave-driven mixing. As a result, the lee-wave-driven mixing gets stronger with the wind, and therefore the lower overturning circulation increases.

Lee wave drag and its associated lee-wave-driven mixing are coupled to each other: the presence of lee wave drag weakens the bottom kinetic energy, thereby reducing the energy available for the lee-wave-driven mixing; whereas the presence of lee-wave-driven mixing weakens the bottom stratification and therefore reduces the lee wave drag coefficient. This coupling is key to understanding the response of the Southern Ocean circulation to the

parameterisation of lee waves; It is not a simple linear superposition of the effect of lee wave drag and the effect of lee-wave-driven mixing.

Our estimates show that the generation of lee waves is an important eddy energy dissipation mechanism in the Southern Ocean. The generation of lee waves dissipates 0.12 TW of energy from the transient eddy field in the Southern Ocean, which exceeds the eddy energy dissipation of 0.04 TW in the turbulent bottom boundary layer (TBBL). The generation of lee waves is distinguished spatially from the frictional processes in the TBBL for its dependence on the small-scale roughness in addition to the local EKE. It is also shown that lee wave generation by the eddy field is sensitive to the anisotropy in the small-scale topography, likely through the anisotropy of the eddy field (Stewart et al., 2015). Lee waves are shown to extract 75% of their energy from the transient eddy field and the rest 25% from the time-mean field. The eddy field also contributes to the energy dissipation of the time-mean flow due to lee wave generation. The eddy contribution arises from the nonlinear dependence of lee wave drag on the velocity.

The parameterisation of lee waves affects the sensitivity of the Southern Ocean circulation to changes in wind stress through modifying eddy energy dissipation. Previous studies have demonstrated that a higher horizontal resolution of a model produces a less sensitive ACC to increasing wind stress and therefore is better at reproducing the eddy saturation limit (e.g., Munday et al., 2013); this finding indicates the importance of eddy energy generation to the simulation of the response of the Southern Ocean circulation to changes in wind stress. Here, we show that lee wave generation, as one of the eddy energy dissipation mechanisms in the deep ocean, can also regulate the sensitivity of the ACC to changes in wind stress. Given that the current computational capacity can not support a lee-wave-resolving global realistic configuration, the impact of lee waves has to be parameterised to better simulate the Southern Ocean circulation and predict its response to changing climate.

5.2 Implications

We have demonstrated that lee waves are important for the Southern Ocean circulation and its response to changing wind stress. The main implication of this study is that lee waves, both their drag and mixing effects, should be parameterised in eddy-resolving global ocean models to improve the simulation of the Southern Ocean circulation and its sensitivity to changes in wind stress.

One of the motivations of this study is that the eddy-resolving global ocean models lack physical representation of eddy energy dissipation mechanisms. We show that lee waves extract a significant amount of energy from the eddy field in the Southern Ocean

(chapter 2), but have not yet been represented in eddy-resolving global ocean models. This result implies that, as a physical mechanism of eddy energy dissipation, lee waves should be parameterised, in particular their drag effects, in the eddy-resolving ocean models to improve the representation of the eddy field. This improvement on the eddy field is extremely important for the Southern Ocean, especially in the latitude band of the Drake Passage where there is no meridional boundary to support a western boundary current. Here, the eddy field transports heat across the ACC fronts, transfers momentum downward, and regulates how the ACC and the Meridional Overturning Circulation (MOC) responds to changing climate (Olbers et al., 2004; Rintoul et al., 2001).

The reshaping of the standing meanders due to the parameterisation of lee waves implies that the parameterisation of lee waves will modify the momentum balance of the mean flow. As suggested by Naveira Garabato et al. (2013), lee wave drag is a significant momentum sink of the time-mean ACC and its presence in the model is likely to reduce the topographic form stress, given the same wind stress. Although the lee-wave-driven mixing does not affect the momentum of the flow directly, it leads to changes in the structure of the standing meanders, which implies that the lee-wave-driven mixing exerts a control on the momentum balance of the flow. The control of the lee-wave-driven mixing is achieved likely through its regulation on the bottom pressure via the lower overturning circulation (Fig. 1d in Stewart and Hogg, 2017).

We find that the parameterisation of lee waves largely enhances the baroclinic transport of the ACC. The implication of this finding is that there will be more interbasin exchange of heat, salt, and carbon allowed by the ACC in the presence of lee waves. We also find that lee waves significantly increase the sensitivity of the ACC to changes in wind stress, which moves the Southern Ocean further away from the eddy saturation regime. This finding implies that the Southern Ocean might reach the eddy saturation limit at a stronger wind stress if lee waves are parameterised in the model, compared with the case where the lee wave parameterisation is absent.

The lower overturning circulation produced in the full parameterisation of lee waves is weaker than that in the lee-wave-mixing only parameterisation. This reduction in the lower overturning circulation indicates an overestimation of the lower overturning circulation in the case where only the lee-wave-driven mixing is parameterised, as in Broadbridge et al. (2016), and therefore highlights the importance of parameterising both the drag and mixing effects of lee waves. Although reduced, the lower overturning circulation is still stronger when lee waves are parameterised compared with the case where lee waves are absent. In the presence of lee waves, the lower overturning circulation increases considerably with wind stress, in contrast to the previous theoretical prediction that it decreases with wind

stress (Ito and Marshall, 2008; Nikurashin and Vallis, 2011). This finding is consistent with the results in Broadbridge et al. (2016), and demonstrates that the importance of a flow-dependent lee-wave-driven mixing to the simulation of the sensitivity of the lower overturning circulation to changes in wind stress. However, the coupling effect between lee wave drag and lee-wave-driven mixing implies that the presence of lee wave drag is likely to alter the sensitivity of the lower overturning circulation to wind stress produced with only mixing parameterisation quantitatively.

The sensitivity of the Southern Ocean circulation to changes in wind stress is significantly altered by the parameterisation of lee waves and it has huge implications for the global climate. The intensifying wind stress observed for the past few decades might lead to a stronger mixing field through lee waves, which weakens the stratification in the deep Southern Ocean. The weakened stratification in the deep ocean leads to less efficient trapping of carbon, changes the internal wave field properties, and increases the deep-ocean temperature. Thus the parameterisation of lee waves might improve the ocean models by reproducing a more realistic carbon storage capacity, the self-regulating effect of the internal wave field, and the observed abyssal warming (Purkey and Johnson, 2010; Talley et al., 2016). The strengthening lower overturning circulation with increasing wind stress indicates a stronger upwelling branch, which might lead to more outgassing of carbon to the atmosphere then previously modelled. The parameterisation of lee waves is thus likely to improve the model simulation of the lower overturning on ocean carbon storage. The volume change of the lower overturning circulation also influences the upper overturning circulation, for example, through diapycnal mixing in the interior (Naveira Garabato et al., 2007) and the interaction with the sloping bathymetry (Ruan et al., 2017). Thus lee waves might affect the strength of the upper overturning circulation indirectly. The upper overturning circulation, a large sink of anthropogenic carbon, has been predicted to increase with wind stress (e.g., Farneti et al., 2015). The strength of the upper overturning circulation controls the uptake of anthropogenic carbon and the release of natural carbon, the combined effect and its time variability largely determine the amount of carbon in the atmosphere and its control on the global temperature (Gruber et al., 2019, and references therein). Furthermore, a stronger overturning rate allows more upwelling of the circumpolar deep water, which might accelerate the melting of the ice shelves and lead to sea level rise.

In addition to the impact of lee waves on the large-scale circulation, the parameterisation of lee waves is likely to improve the simulation of local dynamics. As shown in chapter 2, the generation of lee waves occurs at several hotspots in the Southern Ocean, as a result of the uneven distribution of EKE (localised downstream of large-scale topographic features on the scale of 100-1000 km) and small-scale abyssal hills. These hotspots are found in

the vicinity of major large-scale topographic features, which have been shown to provide pathways for the upwelling of deep waters in the Southern Ocean (Tamsitt et al., 2017). The vigorous lee waves there might lead to the localised intensified mixing and water mass transformation. As shown, we find that the parameterisation of lee waves leads to a smoother structure of the standing meanders (chapter 4), which implies that the role of the standing meanders might be overestimated in the absence of lee waves, for example, their contribution to compensate the wind-driven overturning circulation under the changing climate proposed in Bishop et al. (2016). Recent studies (Rintoul, 2018; Thompson and Naveira Garabato, 2014; Thompson et al., 2016) have shown the importance of local dynamics in the Southern Ocean, such as flow-topography interaction, which is not fully accounted for in a 2D zonal-mean theoretical framework. Thus the future addition of a complete (drag and mixing) lee wave parameterisation in global ocean and coupled models is expected to improve the representation of hotspots in the Southern Ocean and the establishment of their role in the Southern Ocean circulation.

5.3 Future work

We have used an idealised channel configuration in this study, which is representative of the Southern Ocean circulation albeit a lot simpler. The simplicity allows us to focus on the key governing processes through which lee waves exert a control on the ACC and the lower overturning circulation. This is a key step towards understanding the more complex dynamics that operate in the ocean. However, we acknowledge that more investigation needs to be done in the future because of the limitations of this configuration. The idealised configuration we use spans roughly 40° in longitude, whereas the Southern Ocean has an unblocked circumpolar structure. Therefore, this idealised configuration is only representative of a sector in the Southern Ocean. Another limitation of this idealised configuration is that it adopts a northern sponge layer to represent the ocean basins north of the Southern Ocean, which restricts how the Southern Ocean can interact with the northern ocean basins. Similarly, the restoring boundary condition used at the surface assumes that the atmospheric temperature above is as prescribed and steady, which is likely not justified when the wind stress is increasing. In addition, the salinity is set to be constant in the domain, whereas in the real ocean it can change density.

In this study, we used a simple sinusoidal small-scale topography representation throughout the domain; however, in the real ocean, small-scale topographic features display a variety of shapes and orientations and their spatial distribution, described by a spectrum, also makes a difference to the generation of lee waves (chapter 2). Following the sinusoidal topography

assumption, we also assume a linear dependence of lee wave drag on the velocity; however, this dependence can be nonlinear for the multi-scale topography. Another assumption we make is that the lee wave field has the same vertical structure througout the entire domain. However, Trossman et al. (2016) suggested that vertical decay depth of lee wave drag should be spatially dependent. Furthermore, we do not apply the finite topography correction to the parameterisation of lee wave drag. To generalise the parameterisation of lee waves for its use in a variety of cases and its inclusion in eddy-resolving global ocean models, we recommend the addition of steepness parameter is considered to avoid the overestimation of lee wave drag and lee-wave-driven mixing.

As an extension to this study, we recommend that the limitations mentioned above regarding the lee wave parameterisation be addressed in the future and an improve lee wave parameterisation be implemented into an eddy-resolving global configuration. Using the global configuration and realistic forcing conditions, our findings on the impact of lee waves on the Southern Ocean circulation can be tested and their climate implications can be investigated. Specifically, the research questions that arise out of this thesis include: the impact of lee waves on (1) the eddy field, its strength, and its vertical structure, (2) the stratification and water mass transformation, (3) the ACC transport and the structure of the standing meanders, (4) the upper and lower overturning circulation, and (5) the sensitivity of the ACC transport, the MOC, heat and carbon uptake of the Southern Ocean to the increasing and poleward-shifted wind stress. Moreover, it is still an open question that whether lee waves have an impact on the upwelling pathways of deep waters and on the northward pathways of the Antarctic Bottom Water (AABW). In the future, a lee wave parameterisation for non-eddy-resolving configurations can also be developed and used for coarse global ocean models to project future climate.

References

Abernathey, R., J. Marshall, and D. Ferreira, 2011: The Dependence of Southern Ocean Meridional Overturning on Wind Stress. *J. Phys. Oceanogr.*, **41 (12)**, 2261–2278, doi:10.1175/JPO-D-11-023.1.

Allison, L. C., H. L. Johnson, and D. P. Marshall, 2011: Spin-up and adjustment of the Antarctic Circumpolar Current and global pycnocline. *J. Mar. Res.*, **69 (2-3)**, 167–189, doi:10.1357/002224011798765330.

Allison, L. C., H. L. Johnson, D. P. Marshall, and D. R. Munday, 2010: Where do winds drive the antarctic circumpolar current? *Geophys. Res. Lett.*, **37 (12)**, doi:10.1029/2010GL043355.

Arbic, B. K., and R. B. Scott, 2008: On Quadratic Bottom Drag, Geostrophic Turbulence, and Oceanic Mesoscale Eddies. *J. Phys. Oceanogr.*, **38 (1)**, 84–103, doi:10.1175/2007jpo3653.1.

Arbic, B. K., and Coauthors, 2009: Estimates of bottom flows and bottom boundary layer dissipation of the oceanic general circulation from global high-resolution models. *J. Geophys. Res.*, **114 (C2)**, C02 024, doi:10.1029/2008JC005072.

Barthel, A., A. McC. Hogg, S. Waterman, and S. Keating, 2017: Jet–Topography Interactions Affect Energy Pathways to the Deep Southern Ocean. *J. Phys. Oceanogr.*, **47 (7)**, 1799–1816, doi:10.1175/JPO-D-16-0220.1.

Bell, T. H., 1975: Topographically generated internal waves in the open ocean. *J. Geophys. Res.*, **80 (3)**, 320, doi:10.1029/JC080i003p00320.

Bishop, S. P., P. R. Gent, F. O. Bryan, A. F. Thompson, M. C. Long, and R. Abernathey, 2016: Southern Ocean Overturning Compensation in an Eddy-Resolving Climate Simulation. *J. Phys. Oceanogr.*, **46 (5)**, 1575–1592, doi:10.1175/JPO-D-15-0177.1.

Böning, C. W., A. Dispert, M. Visbeck, S. R. Rintoul, and F. U. Schwarzkopf, 2008: The response of the Antarctic Circumpolar Current to recent climate change. *Nat. Geosci.*, **1**, 864, doi:10.1038/ngeo362.

Brearley, J. A., K. L. Sheen, A. C. Naveira Garabato, D. A. Smeed, and S. Waterman, 2013: Eddy-Induced Modulation of Turbulent Dissipation over Rough Topography in the Southern Ocean. *J. Phys. Oceanogr.*, **43 (11)**, 2288–2308, doi:10.1175/JPO-D-12-0222.1.

Broadbridge, M. B., A. C. Naveira Garabato, and A. J. Nurser, 2016: Forcing of the overturning circulation across a circumpolar channel by internal wave breaking. *J. Geophys. Res. Oceans*, **121 (8)**, 5436–5451, doi:10.1002/2015JC011597.

Bühler, O., and M. E. McIntyre, 2005: Wave capture and wave-vortex duality. *J. Fluid Mech.*, **534**, 67–95, doi:10.1017/S0022112005004374.

Cessi, P., 2019: The Global Overturning Circulation. *Ann. Rev. Mar. Sci.*, **11**, 249–270, doi:10.1146/annurev-marine-010318-095241.

Constantinou, N. C., 2018: A barotropic model of eddy saturation. *J. Phys. Oceanogr.*, **48 (2)**, 397–411, doi:10.1175/JPO-D-17-0182.1.

Cushman-Roisin, B., and J.-M. Beckers, 2011: *Introduction to geophysical fluid dynamics: physical and numerical aspects*, Vol. 101. Academic press.

de Lavergne, C., G. Madec, J. Le Sommer, A. J. G. Nurser, and A. C. Naveira Garabato, 2016: On the Consumption of Antarctic Bottom Water in the Abyssal Ocean. *J. Phys. Oceanogr.*, **46 (2)**, 635–661, doi:10.1175/JPO-D-14-0201.1.

de Lavergne, C., G. Madec, F. Roquet, R. M. Holmes, and T. J. McDougall, 2017: Abyssal ocean overturning shaped by seafloor distribution. *Nature*, **551 (7679)**, 181, doi:10.1038/nature24472.

Dufour, C. O., L. L. Sommer, J. D. Zika, M. Gehlen, J. C. Orr, P. Mathiot, and B. Barnier, 2012: Standing and transient eddies in the response of the Southern Ocean meridional overturning to the Southern annular mode. *J. Climate*, **25 (20)**, 6958–6974, doi:10.1175/JCLI-D-11-00309.1.

Farneti, R., and T. L. Delworth, 2010: The Role of Mesoscale Eddies in the Remote Oceanic Response to Altered Southern Hemisphere Winds. *J. Phys. Oceanogr.*, **40 (10)**, 2348–2354, doi:10.1175/2010JPO4480.1.

Farneti, R., T. L. Delworth, A. J. Rosati, S. M. Griffies, and F. Zeng, 2010: The Role of Mesoscale Eddies in the Rectification of the Southern Ocean Response to Climate Change. *J. Phys. Oceanogr.*, **40 (7)**, 1539–1557, doi:10.1175/2010JPO4353.1.

Farneti, R., and P. R. Gent, 2011: The effects of the eddy-induced advection coefficient in a coarse-resolution coupled climate model. *Ocean Model.*, **39 (1-2)**, 135–145, doi:10.1016/j.ocemod.2011.02.005.

Farneti, R., and Coauthors, 2015: An assessment of Antarctic Circumpolar Current and Southern Ocean meridional overturning circulation during 1958-2007 in a suite of interannual CORE-II simulations. *Ocean Model.*, **93**, 84–120, doi:10.1016/j.ocemod.2015.07.009.

Ferrari, R., L.-P. Nadeau, D. P. Marshall, L. C. Allison, and H. L. Johnson, 2017: A Model of the Ocean Overturning Circulation with Two Closed Basins and a Reentrant Channel. *J. Phys. Oceanogr.*, **47 (12)**, 2887–2906, doi:10.1175/jpo-d-16-0223.1.

Ferrari, R., and C. Wunsch, 2009: Ocean Circulation Kinetic Energy: Reservoirs, Sources, and Sinks. *Annu. Rev. Fluid Mech.*, **41 (1)**, 253–282, doi:10.1146/annurev.fluid.40.111406.102139.

Frölicher, T. L., J. L. Sarmiento, D. J. Paynter, J. P. Dunne, J. P. Krasting, and M. Winton, 2015: Dominance of the Southern Ocean in anthropogenic carbon and heat uptake in CMIP5 models. *J. Climate*, **28 (2)**, 862–886, doi:10.1175/JCLI-D-14-00117.1.

Garner, S. T., 2005: A topographic drag closure built on an analytical base flux. *J. Atmos. Sci.*, **62 (7)**, 2302–2315, doi:10.1175/JAS3496.1.

Gent, P. R., 2015: Effects of Southern Hemisphere Wind Changes on the Meridional Overturning Circulation in Ocean Models. *Ann. Rev. Mar. Sci.*, **8**, 79–94, doi:10.1146/annurev-marine-122414-033929.

Gent, P. R., and G. Danabasoglu, 2011: Response to increasing Southern Hemisphere winds in CCSM4. *J. Climate*, **24 (19)**, 4992–4998, doi:10.1175/JCLI-D-10-05011.1.

Gent, P. R., W. G. Large, and F. O. Bryan, 2001: What sets the mean transport through Drake Passage? *J. Geophys. Res. Oceans*, **106 (C2)**, 2693–2712, doi:10.1029/2000JC900036.

Gent, P. R., and J. C. McWilliams, 1990: Isopycnal Mixing in Ocean Circulation Models. *J. Phys. Oceanogr.*, **20 (1)**, 150–155, doi:10.1175/1520-0485(1990)020<0150:IMIOCM>2.0.CO;2.

Gill, A. E., 1968: A linear model of the Antarctic circumpolar current. *J. Fluid Mech.*, **32 (03)**, 465–488, doi:10.1017/S0022112068000868.

Gill, A. E., 1982: Atmosphere-ocean dynamics. 662 pp.

Gill, A. E., J. S. Green, and A. J. Simmons, 1974: Energy partition in the large-scale ocean circulation and the production of mid-ocean eddies. *Deep-Sea Res.*, **21 (7)**, 499–528, doi:10.1016/0011-7471(74)90010-2.

Gille, S. T., M. M. Yale, and D. T. Sandwell, 2000: Global correlation of mesoscale ocean variability with seafloor roughness from satellite altimetry. *Geophys. Res. Lett.*, **27 (9)**, 1251–1254, doi:10.1029/1999GL007003.

Gnanadesikan, A., 1999: A simple predictive model for the structure of the oceanic pycnocline. *Science*, **283 (5410)**, 2077–2079, doi:10.1126/science.283.5410.2077.

Goff, J. A., 2010: Global prediction of abyssal hill root-mean-square heights from small-scale altimetric gravity variability. *J. Geophys. Res. Solid Earth*, **115 (12)**, doi:10.1029/2010JB007867.

Goff, J. A., and B. K. Arbic, 2010: Global prediction of abyssal hill roughness statistics for use in ocean models from digital maps of paleo-spreading rate, paleo-ridge orientation, and sediment thickness. *Ocean Model.*, **32 (1-2)**, 36–43, doi:10.1016/j.ocemod.2009.10.001.

Goff, J. A., and T. H. Jordan, 1988: Stochastic Modeling of Seafloor Morphology: Inversion of Sea Beam Data for Second-Order Statistics. *J. Geophys. Res. Solid Earth*, **93 (B11)**, 13 589–13 608, doi:10.1029/JB093iB11p13589.

Goff, J. A., and T. H. Jordan, 1989: Stochastic modeling of seafloor morphology: A parameterized Gaussian model. *Geophys. Res. Lett.*, **16 (1)**, 45–48, doi:10.1029/GL016i001p00045.

Griffies, S. M., 2012: Elements of the Modular Ocean Model (MOM): 2012 release. GFDL Ocean Group Tech. Rep. 7, NOAA. *Geophys. Fluid Dyn. Lab. Princeton, NJ*.

Griffies, S. M., and Coauthors, 2015: Impacts on ocean heat from transient mesoscale eddies in a hierarchy of climate models. *J. Climate*, **28 (3)**, 952–977, doi:10.1175/JCLI-D-14-00353.1.

Gruber, N., P. Landschützer, and N. S. Lovenduski, 2019: The Variable Southern Ocean Carbon Sink. *Ann. Rev. Mar. Sci.*, **11 (1)**, 159–186, doi:10.1146/annurev-marine-121916-063407.

Hall, A., and M. Visbeck, 2002: Synchronous variability in the Southern Hemisphere atmosphere, sea ice, and ocean resulting from the annular mode. *J. Climate*, **15 (21)**, 3043–3057, doi:10.1175/1520-0442(2002)015<3043:SVITSH>2.0.CO;2.

Hallberg, R., and A. Gnanadesikan, 2001: An Exploration of the Role of Transient Eddies in Determining the Transport of a Zonally Reentrant Current. *J. Phys. Oceanogr.*, **31 (11)**, 3312–3330, doi:10.1175/1520-0485(2001)031<3312:AEOTRO>2.0.CO;2.

Hallberg, R., and A. Gnanadesikan, 2006: The Role of Eddies in Determining the Structure and Response of the Wind-Driven Southern Hemisphere Overturning: Results from the Modeling Eddies in the Southern Ocean (MESO) Project. *J. Phys. Oceanogr.*, **36 (12)**, 2232–2252, doi:10.1175/JPO2980.1.

Hausmann, U., and A. Czaja, 2012: The observed signature of mesoscale eddies in sea surface temperature and the associated heat transport. *Deep. Res. Part I Oceanogr. Res. Pap.*, **70**, 60–72, doi:10.1016/j.dsr.2012.08.005.

Heywood, K. J., A. C. Naveira Garabato, and D. P. Stevens, 2002: High mixing rates in the abyssal Southern Ocean. *Nature*, **415 (6875)**, 1011–1014, doi:10.1038/4151011a.

Hofmann, M., and M. A. Morales Maqueda, 2011: The response of Southern Ocean eddies to increased midlatitude westerlies: A non-eddy resolving model study. *Geophys. Res. Lett.*, **38 (3)**, doi:10.1029/2010GL045972.

Hogg, A. M., 2010: An Antarctic Circumpolar Current driven by surface buoyancy forcing. *Geophys. Res. Lett.*, **37 (23)**, doi:10.1029/2010GL044777.

Hogg, A. M., W. K. Dewar, P. Berloff, and M. L. Ward, 2011: Kelvin wave hydraulic control induced by interactions between vortices and topography. *J. Fluid Mech.*, **687**, 194–208, doi:10.1017/jfm.2011.344.

Hogg, A. M., M. Meredith, J. R. Blundell, and C. Wilson, 2008: Eddy heat flux in the Southern Ocean: response to variable wind forcing. *J. Climate*, **21 (4)**, 608–620, doi:10.1175/2007JCLI1925.1.

Hogg, A. M., M. P. Meredith, D. P. Chambers, E. P. Abrahamsen, C. W. Hughes, and A. K. Morrison, 2015: Recent trends in the Southern Ocean eddy field. *J. Geophys. Res. Oceans*, **120 (1)**, 257–267, doi:10.1002/2014JC010470.

Ito, T., and J. Marshall, 2008: Control of Lower-Limb Overturning Circulation in the Southern Ocean by Diapycnal Mixing and Mesoscale Eddy Transfer. *J. Phys. Oceanogr.*, **38 (12)**, 2832–2845, doi:10.1175/2008JPO3878.1.

Ivchenko, V., 1996: The dynamics of the Antarctic circumpolar current. *J. Phys. Oceanogr.*, **26 (5)**, 753–774, doi:10.1175/1520-0485(1996)026<0753:TDOTAC>2.0.CO%3B2.

Jansen, M. F., and L.-P. Nadeau, 2016: The effect of Southern Ocean surface buoyancy loss on the deep-ocean circulation and stratification. *J. Phys. Oceanogr.*, **46 (11)**, 3455–3470.

Jayne, S. R., 2009: The Impact of Abyssal Mixing Parameterizations in an Ocean General Circulation Model. *J. Phys. Oceanogr.*, **39 (7)**, 1756–1775, doi:10.1175/2009jpo4085.1.

Kamenkovich, I., and T. Radko, 2011: Role of the Southern Ocean in setting the Atlantic stratification and meridional overturning circulation. *J. Mar. Res.*, **69 (2-3)**, 277–308, doi:10.1357/002224011798765286.

Karsten, R., H. Jones, and J. Marshall, 2002: The role of eddy transfer in setting the stratification and transport of a circumpolar current. *J. Phys. Oceanogr.*, **32 (1)**, 39–54, doi:10.1175/1520-0485(2002)032<0039:TROETI>2.0.CO;2.

Karsten, R. H., and J. Marshall, 2002: Constructing the Residual Circulation of the ACC from Observations. *J. Phys. Oceanogr.*, **32 (12)**, 3315–3327, doi:10.1175/1520-0485(2002)032<3315:CTRCOT>2.0.CO;2.

Kunze, E., 2017: The Internal-Wave-Driven Meridional Overturning Circulation. *J. Phys. Oceanogr.*, **47 (11)**, 2673–2689, doi:10.1175/jpo-d-16-0142.1.

Kunze, E., E. Firing, J. M. Hummon, T. K. Chereskin, and A. M. Thurnherr, 2006: Global Abyssal Mixing Inferred from Lowered ADCP Shear and CTD Strain Profiles. *J. Phys. Oceanogr.*, **36 (8)**, 1553–1576, doi:10.1175/JPO2926.1.

Liang, X., and A. M. Thurnherr, 2012: Eddy-Modulated Internal Waves and Mixing on a Midocean Ridge. *J. Phys. Oceanogr.*, **42 (7)**, 1242–1248, doi:10.1175/JPO-D-11-0126.1.

Lumpkin, R., and K. Speer, 2007: Global Ocean Meridional Overturning. *J. Phys. Oceanogr.*, **37 (10)**, 2550–2562, doi:10.1175/jpo3130.1.

Marshall, D. P., M. H. Ambaum, J. R. Maddison, D. R. Munday, and L. Novak, 2017: Eddy saturation and frictional control of the Antarctic Circumpolar Current. *Geophys. Res. Lett.*, **44 (1)**, 286–292, doi:10.1002/2016GL071702.

Marshall, D. P., J. R. Maddison, and P. S. Berloff, 2012: A Framework for Parameterizing Eddy Potential Vorticity Fluxes. *J. Phys. Oceanogr.*, **42 (4)**, 539–557, doi:10.1175/JPO-D-11-048.1.

Marshall, D. P., and A. C. Naveira Garabato, 2008: A Conjecture on the Role of Bottom-Enhanced Diapycnal Mixing in the Parameterization of Geostrophic Eddies. *J. Phys. Oceanogr.*, **38 (7)**, 1607–1613, doi:10.1175/2007JPO3619.1.

Marshall, J., and T. Radko, 2003: Residual-Mean Solutions for the Antarctic Circumpolar Current and Its Associated Overturning Circulation. *J. Phys. Oceanogr.*, **33 (11)**, 2341–2354, doi:10.1175/1520-0485(2003)033<2341:RSFTAC>2.0.CO;2.

Marshall, J., and K. Speer, 2012: Closure of the meridional overturning circulation through Southern Ocean upwelling. *Nat. Geosci.*, **5 (3)**, 171–180, doi:10.1038/ngeo1391.

Mashayek, A., R. Ferrari, S. Merrifield, J. R. Ledwell, L. St Laurent, and A. N. Garabato, 2017: Topographic enhancement of vertical turbulent mixing in the Southern Ocean. *Nat. Commun.*, **8**, 14 197, doi:10.1038/ncomms14197.

Masich, J., T. K. Chereskin, and M. R. Mazloff, 2015: Topographic form stress in the Southern Ocean State Estimate. *J. Geophys. Res. Oceans*, **120 (12)**, 7919–7933, doi:10.1002/2015JC011143.

Melet, A., R. Hallberg, A. Adcroft, M. Nikurashin, and S. Legg, 2015: Energy flux into internal lee waves: Sensitivity to future climate changes using linear theory and a climate model. *J. Climate*, **28 (6)**, 2365–2384, doi:10.1175/JCLI-D-14-00432.1.

Melet, A., R. Hallberg, S. Legg, and M. Nikurashin, 2014: Sensitivity of the Ocean State to Lee Wave–Driven Mixing. *J. Phys. Oceanogr.*, **44 (3)**, 900–921, doi:10.1175/JPO-D-13-072.1.

Meredith, M. P., 2011: Cruise report: RRS James Cook JC054 (DIMES UK2) 30 Nov 2010 to 8 Jan 2011. *Br. Antarct. Surv. Cruise Rep*, **2593**, URL https://goo.gl/8gpcfN.

Meredith, M. P., and A. M. Hogg, 2006: Circumpolar response of Southern Ocean eddy activity to a change in the Southern Annular Mode. *Geophys. Res. Lett.*, **33 (16)**, doi:10.1029/2006GL026499.

Meredith, M. P., P. L. Woodworth, C. W. Hughes, and V. Stepanov, 2004: Changes in the ocean transport through Drake Passage during the 1980s and 1990s, forced by changes in the Southern Annular Mode. *Geophys. Res. Lett.*, **31 (21)**, doi:10.1029/2004GL021169.

Meredith, M. P., and Coauthors, 2011: Sustained monitoring of the Southern Ocean at Drake Passage: Past achievements and future priorities. *Rev. Geophys.*, **49 (4)**, doi:10.1029/2010RG000348.

Meyer, A., K. L. Polzin, B. M. Sloyan, and H. E. Phillips, 2016: Internal Waves and Mixing near the Kerguelen Plateau. *J. Phys. Oceanogr.*, **46 (2)**, 417–437, doi:10.1175/JPO-D-15-0055.1.

Meyer, A., B. M. Sloyan, K. L. Polzin, H. E. Phillips, and N. L. Bindoff, 2015: Mixing Variability in the Southern Ocean. *J. Phys. Oceanogr.*, **45 (4)**, 966–987, doi:10.1175/JPO-D-14-0110.1.

Molemaker, M. J., J. C. McWilliams, and I. Yavneh, 2005: Baroclinic Instability and Loss of Balance. *J. Phys. Oceanogr.*, **35 (9)**, 1505–1517, doi:10.1175/JPO2770.1.

Morrison, A. K., and A. M. Hogg, 2013: On the Relationship between Southern Ocean Overturning and ACC Transport. *J. Phys. Oceanogr.*, **43 (1)**, 140–148, doi:10.1175/JPO-D-12-057.1.

Munday, D. R., L. C. Allison, H. L. Johnson, and D. P. Marshall, 2011: Remote forcing of the Antarctic Circumpolar Current by diapycnal mixing. *Geophys. Res. Lett.*, **38 (8)**, doi:10.1029/2011gl046849.

Munday, D. R., H. L. Johnson, and D. P. Marshall, 2013: Eddy Saturation of Equilibrated Circumpolar Currents. *J. Phys. Oceanogr.*, **43 (3)**, 507–532, doi:10.1175/JPO-D-12-095.1.

Munk, W. H., and E. Palmén, 1951: Note on the Dynamics of the Antarctic Circumpolar Current. *Tellus*, **3 (1)**, 53–55, doi:10.3402/tellusa.v3i1.8609.

Naveira Garabato, A. C., 2009: RRS James Cook Cruise 29, 01 Nov-22 Dec 2008. SOFine cruise report: Southern Ocean Finestructure. URL https://eprints.soton.ac.uk/65884/1/nocscr035.pdf.

Naveira Garabato, A. C., 2010: RRS James Cook Cruise 41, 05-21 Dec 2009. UK DIMES1 Cruise Report: Diapycnal and Isopycnal Mixing Experiment in the Southern Ocean. URL https://eprints.soton.ac.uk/167561/1/nocscr056.pdf.

Naveira Garabato, A. C., A. J. G. Nurser, R. B. Scott, and J. A. Goff, 2013: The Impact of Small-Scale Topography on the Dynamical Balance of the Ocean. *J. Phys. Oceanogr.*, **43 (3)**, 647–668, doi:10.1175/JPO-D-12-056.1.

Naveira Garabato, A. C., K. L. Polzin, B. A. King, K. J. Heywood, and M. Visbeck, 2004: Widespread Intense Turbulent Mixing in the Southern Ocean. *Science*, **303 (5655)**, 210–213, doi:10.1126/science.1090929.

Naveira Garabato, A. C., D. P. Stevens, A. J. Watson, and W. Roether, 2007: Short-circuiting of the overturning circulation in the Antarctic Circumpolar Current. *Nature*, **447 (7141)**, 194–197, doi:10.1038/nature05832.

Nikurashin, M., and R. Ferrari, 2010a: Radiation and Dissipation of Internal Waves Generated by Geostrophic Motions Impinging on Small-Scale Topography: Application to the Southern Ocean. *J. Phys. Oceanogr.*, **40 (9)**, 2025–2042, doi:10.1175/2010JPO4315.1.

Nikurashin, M., and R. Ferrari, 2010b: Radiation and dissipation of internal waves generated by geostrophic motions impinging on small-scale topography: Theory. *J. Phys. Oceanogr.*, **40 (5)**, 1055–1074, doi:10.1175/2009JPO4199.1.

Nikurashin, M., and R. Ferrari, 2011: Global energy conversion rate from geostrophic flows into internal lee waves in the deep ocean. *Geophys. Res. Lett.*, **38 (8)**, doi:10.1029/2011GL046576.

Nikurashin, M., and R. Ferrari, 2013: Overturning circulation driven by breaking internal waves in the deep ocean. *Geophys. Res. Lett.*, **40 (12)**, 3133–3137, doi:10.1002/grl.50542.

Nikurashin, M., R. Ferrari, N. Grisouard, and K. Polzin, 2014: The Impact of Finite-Amplitude Bottom Topography on Internal Wave Generation in the Southern Ocean. *J. Phys. Oceanogr.*, **44 (11)**, 2938–2950, doi:10.1175/JPO-D-13-0201.1.

Nikurashin, M., and G. Vallis, 2011: A theory of deep stratification and overturning circulation in the ocean. *J. Phys. Oceanogr.*, **41 (3)**, 485–502, doi:10.1175/2010JPO4529.1.

Nikurashin, M., G. K. Vallis, and A. Adcroft, 2013: Routes to energy dissipation for geostrophic flows in the Southern Ocean. *Nat. Geosci.*, **6 (1)**, 48–51, doi:10.1038/ngeo1657.

Olbers, D., D. Borowski, C. VÖLker, and J.-O. WÖLff, 2004: The dynamical balance, transport and circulation of the Antarctic Circumpolar Current. *Antarct. Sci.*, **16 (4)**, 439–470, doi:10.1017/S0954102004002251.

Orsi, A. H., T. Whitworth, and W. D. Nowlin, 1995: On the meridional extent and fronts of the Antarctic Circumpolar Current. *Deep-Sea Res. Part I*, **42 (5)**, 641–673, doi:10.1016/0967-0637(95)00021-W.

Osborn, T. R., 1980: Estimates of the Local Rate of Vertical Diffusion from Dissipation Measurements. *J. Phys. Oceanogr.*, **10 (1)**, 83–89, doi:10.1175/1520-0485(1980)010<0083:EOTLRO>2.0.CO;2.

Patel, R. S., H. E. Phillips, P. G. Strutton, A. Lenton, and J. Llort, 2019: Meridional Heat and Salt Transport Across the Subantarctic Front by Cold-Core Eddies. *J. Geophys. Res. Oceans*, **124 (2)**, 981–1004, doi:10.1029/2018JC014655.

Pedlosky, J., 2013: *Waves in the ocean and atmosphere: introduction to wave dynamics*. Springer Science & Business Media.

Phillips, H. E., and S. R. Rintoul, 2000: Eddy Variability and Energetics from Direct Current Measurements in the Antarctic Circumpolar Current South of Australia. *J. Phys. Oceanogr.*,

30 (12), 3050–3076, doi:10.1175/1520-0485%282000%29030<3050%3AEVAEFD>2.0.CO%3B2.

Polzin, K. L., 2008: Mesoscale Eddy-Internal Wave Coupling. Part I: Symmetry, Wave Capture, and Results from the Mid-Ocean Dynamics Experiment. *J. Phys. Oceanogr.*, **38 (11)**, 2556–2574, doi:10.1175/2008JPO3666.1.

Polzin, K. L., J. M. Toole, J. R. Ledwell, and R. W. Schmitt, 1997: Spatial variability of turbulent mixing in the abyssal ocean. *Science*, **276 (5309)**, 93–96, doi:10.1126/science.276.5309.93.

Purkey, S. G., and G. C. Johnson, 2010: Warming of global abyssal and deep Southern Ocean waters between the 1990s and 2000s: Contributions to global heat and sea level rise budgets. *J. Climate*, **23 (23)**, 6336–6351, doi:10.1175/2010JCLI3682.1.

Purkey, S. G., and G. C. Johnson, 2012: Global contraction of Antarctic Bottom Water between the 1980s and 2000s. *J. Climate*, **25 (17)**, 5830–5844, doi:10.1175/JCLI-D-11-00612.1.

Rintoul, S. R., 2018: The global influence of localized dynamics in the Southern Ocean. *Nature*, **558 (7709)**, 209, doi:10.1038/s41586-018-0182-3.

Rintoul, S. R., C. Hughes, and D. Olbers, 2001: The Antarctic Circumpolar Current system. *Ocean Circ. Clim. Obs. Model. Glob. Ocean*, 77, chap. 4, 271–302.

Rintoul, S. R., and A. C. Naveira Garabato, 2013: Dynamics of the Southern Ocean circulation. *Ocean Circulation and Climate: A 21st Century Perspective*, G. Siedler, S. Grifiies, J. Gould, and J. Church, Eds., Vol 103 of International Geophysics, 2nd ed., Academic Press, chap. 18, 471–492, doi:10.1016/B978-0-12-391851-2.00018-0.

Ruan, X., A. F. Thompson, M. M. Flexas, and J. Sprintall, 2017: Contribution of topographically generated submesoscale turbulence to Southern Ocean overturning. *Nat. Geosci.*, **10 (11)**, 840–845, doi:10.1038/NGEO3053.

Saenko, O. A., A. S. Gupta, and P. Spence, 2012: On challenges in predicting bottom water transport in the Southern Ocean. *J. Climate*, **25 (4)**, 1349–1356, doi:10.1175/JCLI-D-11-00040.1.

Scott, R. B., B. K. Arbic, E. P. Chassignet, A. C. Coward, M. Maltrud, W. J. Merryfield, A. Srinivasan, and A. Varghese, 2010: Total kinetic energy in four global eddying ocean circulation models and over 5000 current meter records. *Ocean Model.*, **32 (3-4)**, 157–169, doi:10.1016/j.ocemod.2010.01.005.

Scott, R. B., J. A. Goff, A. C. Naveira Garabato, and A. J. Nurser, 2011: Global rate and spectral characteristics of internal gravity wave generation by geostrophic flow over topography. *J. Geophys. Res. Oceans*, **116 (9)**, doi:10.1029/2011JC007005.

Screen, J. A., N. P. Gillet, D. P. Stevens, G. J. Marshall, and H. K. Roscoe, 2009: The role of eddies in the Southern Ocean temperature response to the southern annular mode. *J. Climate*, **22 (3)**, 806–818, doi:10.1175/2008JCLI2416.1.

Sen, A., R. B. Scott, and B. K. Arbic, 2008: Global energy dissipation rate of deep-ocean low-frequency flows by quadratic bottom boundary layer drag: Computations from current-meter data. *Geophys. Res. Lett.*, **35 (9)**, doi:10.1029/2008GL033407.

Shakespeare, C. J., and A. M. Hogg, 2012: An analytical model of the response of the meridional overturning circulation to changes in wind and buoyancy forcing. *J. Phys. Oceanogr.*, **42 (8)**, 1270–1287, doi:10.1175/JPO-D-11-0198.1.

Sheen, K. L., and Coauthors, 2013: Rates and mechanisms of turbulent dissipation and mixing in the Southern Ocean: Results from the Diapycnal and Isopycnal Mixing Experiment in the Southern Ocean (DIMES). *J. Geophys. Res. Oceans*, **118 (6)**, 2774–2792, doi:10.1002/jgrc.20217.

Sheen, K. L., and Coauthors, 2014: Eddy-induced variability in Southern Ocean abyssal mixing on climatic timescales. *Nat. Geosci.*, **7 (8)**, 577–582, doi:10.1038/ngeo2200.

Simmons, H. L., S. R. Jayne, L. C. S. Laurent, and A. J. Weaver, 2004: Tidally driven mixing in a numerical model of the ocean general circulation. *Ocean Model.*, **6 (3-4)**, 245–263, doi:10.1016/S1463-5003(03)00011-8.

Sloyan, B. M., 2005: Spatial variability of mixing in the Southern Ocean. *Geophys. Res. Lett.*, **32 (18)**, 1–5, doi:10.1029/2005GL023568.

Sloyan, B. M., and S. R. Rintoul, 2001a: Circulation, Renewal, and Modification of Antarctic Mode and Intermediate Water*. *J. Phys. Oceanogr.*, **31 (4)**, 1005–1030, doi:10.1175/1520-0485(2001)031<1005:cramoa>2.0.co;2.

Sloyan, B. M., and S. R. Rintoul, 2001b: The Southern Ocean Limb of the Global Deep Overturning Circulation*. *J. Phys. Oceanogr.*, **31 (1)**, 143–173, doi:10.1175/1520-0485(2001)031<0143:tsolot>2.0.co;2.

Smith, W. H., and D. T. Sandwell, 1997: Global sea floor topography from satellite altimetry and ship depth soundings. *Science*, **277 (5334)**, 1956–1962, doi:10.1126/science.277.5334.1956.

Snow, K., A. M. Hogg, B. M. Sloyan, and S. M. Downes, 2016: Sensitivity of Antarctic bottom water to changes in surface buoyancy fluxes. *J. Climate*, **29 (1)**, 313–330, doi:10.1175/JCLI-D-15-0467.1.

Speer, K., S. R. Rintoul, and B. Sloyan, 2000: The Diabatic Deacon Cell*. *J. Phys. Oceanogr.*, **30 (12)**, 3212–3222, doi:10.1175/1520-0485%282000%29030<3212%3ATDDC>2.0.CO%3B2.

St. Laurent, L., A. C. Naveira Garabato, J. R. Ledwell, A. M. Thurnherr, J. M. Toole, and A. J. Watson, 2012: Turbulence and Diapycnal Mixing in Drake Passage. *J. Phys. Oceanogr.*, **42 (12)**, 2143–2152, doi:10.1175/JPO-D-12-027.1.

St. Laurent, L. C., H. L. Simmons, and S. R. Jayne, 2002: Estimating tidally driven mixing in the deep ocean. *Geophys. Res. Lett.*, **29 (23)**, 21–1, doi:10.1029/2002GL015633.

Stanley, G. J., and O. A. Saenko, 2014: Bottom-Enhanced Diapycnal Mixing Driven by Mesoscale Eddies: Sensitivity to Wind Energy Supply. *J. Phys. Oceanogr.*, **44 (1)**, 68–85, doi:10.1175/JPO-D-13-0116.1.

Stewart, A. L., and A. M. Hogg, 2017: Reshaping the Antarctic Circumpolar Current via Antarctic Bottom Water Export. *J. Phys. Oceanogr.*, **47 (10)**, 2577–2601, doi:10.1175/jpo-d-17-0007.1.

Stewart, A. L., and A. F. Thompson, 2012: Sensitivity of the ocean's deep overturning circulation to easterly Antarctic winds. *Geophys. Res. Lett.*, **39 (18)**, doi:10.1029/2012GL053099.

Stewart, K. D., A. M. C. Hogg, S. M. Griffies, A. P. Heerdegen, M. L. Ward, P. Spence, and M. H. England, 2017: Vertical resolution of baroclinic modes in global ocean models. *Ocean Model.*, **113**, 50–65, doi:10.1016/j.ocemod.2017.03.012.

Stewart, K. D., P. Spence, S. Waterman, J. L. Sommer, J. M. Molines, J. M. Lilly, and M. H. England, 2015: Anisotropy of eddy variability in the global ocean. *Ocean Model.*, **95**, 53–65, doi:10.1016/j.ocemod.2015.09.005.

Straub, D. N., 1993: On the Transport and Angular Momentum Balance of Channel Models of the Antarctic Circumpolar Current. *J. Phys. Oceanogr.*, **23 (4)**, 776–782, doi:10.1175/1520-0485(1993)023<0776:OTTAAM>2.0.CO;2.

Talley, L., and Coauthors, 2016: Changes in Ocean Heat, Carbon Content, and Ventilation: A Review of the First Decade of GO-SHIP Global Repeat Hydrography. *Ann. Rev. Mar. Sci.*, **8**, 185–215, doi:10.1146/annurev-marine-052915-100829.

Talley, L. D., 2013: Closure of the global overturning circulation through the Indian, Pacific, and Southern Oceans: Schematics and transports. *Oceanography*, **26 (1)**, 80–97, doi:10.5670/oceanog.2013.07.

Tamsitt, V., L. D. Talley, M. R. Mazloff, and I. Cerovecki, 2016: Zonal variations in the Southern Ocean heat budget. *J. Climate*, **29 (18)**, 6563–6579, doi:10.1175/JCLI-D-15-0630.1.

Tamsitt, V., and Coauthors, 2017: Spiraling pathways of global deep waters to the surface of the Southern Ocean. *Nat. Commun.*, **8 (1)**, 172, doi:10.1038/s41467-017-00197-0.

Tansley, C., and D. Marshall, 2001: On the Dynamics of Wind-Driven Circumpolar Currents. *J. Phys. Oceanogr.*, **31 (11)**, 3258–3273, doi:10.1175/1520-0485(2001)031%3C3258:OTDOWD%3E2.0.CO;2.

Taylor, G. I., 1922: Diffusion by continuous movements. *Proc. london Math. Soc.*, **2 (1)**, 196–212, doi:10.1112/plms/s2-20.1.196.

Thompson, A. F., and A. C. Naveira Garabato, 2014: Equilibration of the Antarctic Circumpolar Current by Standing Meanders. *J. Phys. Oceanogr.*, **44 (7)**, 1811–1828, doi:10.1175/JPO-D-13-0163.1.

Thompson, A. F., A. L. Stewart, T. Bischoff, A. F. Thompson, A. L. Stewart, and T. Bischoff, 2016: A Multibasin Residual-Mean Model for the Global Overturning Circulation. *J. Phys. Oceanogr.*, **46 (9)**, 2583–2604, doi:10.1175/JPO-D-15-0204.1.

Thompson, D. W., and S. Solomon, 2002: Interpretation of recent Southern Hemisphere climate change. *Science*, **296 (5569)**, 895–899, doi:10.1126/science.1069270.

Treguier, A. M., J. Le Sommer, J. M. Molines, and B. de Cuevas, 2010: Response of the Southern Ocean to the Southern Annular Mode: Interannual Variability and Multidecadal Trend. *J. Phys. Oceanogr.*, **40 (7)**, 1659–1668, doi:10.1175/2010JPO4364.1.

Trossman, D. S., B. K. Arbic, S. T. Garner, J. A. Goff, S. R. Jayne, E. J. Metzger, and A. J. Wallcraft, 2013: Impact of parameterized lee wave drag on the energy budget of an eddying global ocean model. *Ocean Model.*, **72**, 119–142, doi:10.1016/j.ocemod.2013.08.006.

Trossman, D. S., B. K. Arbic, J. G. Richman, S. T. Garner, S. R. Jayne, and A. J. Wallcraft, 2016: Impact of topographic internal lee wave drag on an eddying global ocean model. *Ocean Model.*, **97**, 109–128, doi:10.1016/j.ocemod.2015.10.013.

Trossman, D. S., S. Waterman, K. L. Polzin, B. K. Arbic, S. T. Garner, A. C. Naveira-Garabato, and K. L. Sheen, 2015: Internal lee wave closures: Parameter sensitivity and comparison to observations. *J. Geophys. Res. Oceans*, **120 (12)**, 7997–8019, doi:10.1002/2015JC010892.

Viebahn, J., and C. Eden, 2010: Towards the impact of eddies on the response of the Southern Ocean to climate change. *Ocean Model.*, **34 (3-4)**, 150–165, doi:10.1016/j.ocemod.2010.05.005.

Visbeck, M., 2007: Power of pull. *Nature*, **447 (7143)**, 383, doi:10.1038/447383a.

Waterhouse, A. F., and Coauthors, 2014: Global Patterns of Diapycnal Mixing from Measurements of the Turbulent Dissipation Rate. *J. Phys. Oceanogr.*, **44 (7)**, 1854–1872, doi:10.1175/JPO-D-13-0104.1.

Waterman, S., A. C. Naveira Garabato, and K. L. Polzin, 2013: Internal Waves and Turbulence in the Antarctic Circumpolar Current. *J. Phys. Oceanogr.*, **43 (2)**, 259–282, doi:10.1175/JPO-D-11-0194.1.

Waterman, S., K. L. Polzin, A. C. Naveira Garabato, K. L. Sheen, and A. Forryan, 2014: Suppression of Internal Wave Breaking in the Antarctic Circumpolar Current near Topography. *J. Phys. Oceanogr.*, doi:10.1175/JPO-D-12-0154.1.

Watson, A. J., J. R. Ledwell, M. J. Messias, B. A. King, N. Mackay, M. P. Meredith, B. Mills, and A. C. Naveira Garabato, 2013: Rapid cross-density ocean mixing at mid-depths in the Drake Passage measured by tracer release. *Nature*, **501 (7467)**, 408–411, doi:10.1038/nature12432.

Watts, D. R., K. L. Tracey, K. A. Donohue, and T. K. Chereskin, 2016: Estimates of Eddy Heat Flux Crossing the Antarctic Circumpolar Current from Observations in Drake Passage. *J. Phys. Oceanogr.*, **46 (7)**, 2103+2122, doi:10.1175/jpo-d-16-0029.1.

Wolfe, C. L., and P. Cessi, 2010: What sets the strength of the middepth stratification and overturning circulation in eddying ocean models? *J. Phys. Oceanogr.*, **40 (7)**, 1520–1538, doi:10.1175/2010JPO4393.1.

Wright, C. J., R. B. Scott, P. Ailliot, and D. Furnival, 2014: Lee wave generation rates in the deep ocean. *Geophys. Res. Lett.*, **41 (7)**, 2434–2440, doi:10.1002/2013GL059087.

Wu, L., Z. Jing, S. Riser, and M. Visbeck, 2011: Seasonal and spatial variations of Southern Ocean diapycnal mixing from Argo profiling floats. *Nat. Geosci.*, **4 (6)**, 363–366, doi:10.1038/ngeo1156.

Yang, L., M. Nikurashin, A. M. Hogg, and B. M. Sloyan, 2018: Energy Loss from Transient Eddies due to Lee Wave Generation in the Southern Ocean. *J. Phys. Oceanogr.*, **48 (12)**, 2867–2885, doi:10.1175/JPO-D-18-0077.1.

Youngs, M. K., A. F. Thompson, A. Lazar, and K. J. Richards, 2017: ACC Meanders, Energy Transfer, and Mixed Barotropic–Baroclinic Instability. *J. Phys. Oceanogr.*, **47 (6)**, 1291–1305, doi:10.1175/JPO-D-16-0160.1.